# SURFACE MODIFICATIONS OF InAs :EFFECT OF CHEMICAL PROCESSING ON ELECTRONIC STRUCTURE AND PHOTOLUMINESCENT PROPERTIES

**NASHWA ABO ALHASSANEASSA**

**SUBMITTED IN FULFILMENT OF THE REQUIREMENTS FOR THE DEGREE OF**

**PHILOSOPHIAE DOCTOR**

**IN THE FACULTY OF SCIENCE AT**

**NELSON MANDELA METROPOLITAN UNIVERSITY**

**(NMMU)**

**PROMOTER:** **PROFESSOR J. R. BOTHA** **SEPTEMBER 2012**

**CO-PROMOTER:** **PROFESSOR A. VENTER**

## *Dedications*

*I dedicate this thesis to the memory of my mother, FathiaAbdAlhamied (1960-2002), who is a constant source of inspiration*

*Acknowledgements*

This thesis would not have been possible without the guidance and the help of several individuals who in one way or another contributed and extended their valuable assistance in the preparation and completion of this study.

Foremost, I would like to express my sincere gratitude to my Promoter, Prof. Reinhardt Botha, for his continuous support, patience and motivation. His guidance helped me throughout the research and writing of this thesis.

My deep appreciation goes to my co-promoter, Prof. Andre Venter, for his significant contribution and his valuable comments and discussions throughout the course of this study.

My special thanks also go to:

- The Third World Organization for Women in Science (TWOWS) for their financial support.
- Dr Liza Coetsee and Prof. Hendrik Swart of the University of Free State, for welcoming me to their laboratory and assisting me with AES and XPS measurements presented in this thesis.
- Messrs Johan Wessels and ChrisMatshobongwana for technical assistance.
- Ms Jualine Ferreira, Ms Linda Kritzinger and Ms Carla Venter for administrative assistance.
- Dr ChantelleRadue, for editing and useful comments.
- My fellow graduate students, Julien, Cloud, Talla, Munyaradzi, Zola, Shura, Senzo, Mohit and Stephen, for their valuable discussions in physics and all aspects of life, and for all the fun we had in the last four years. Their kindness helped me overcome the hard times.
- Loshni, Neetha, Nobom, Tessnum, Marium and Maien for their true friendship, love and support.
- Rani (my three year old son) for giving me the strength; he literally wakes me up every morning by saying to me “Wakey, wakey, sunshine is here”.

Finally, I would like to express my sincere gratitude to my family, especially my sisters Nawal and Dalia, for their love and support and for being there for me no matter where and when.

*Abstract*

In this thesis, the effects of various chemical treatments on the surface modification of bulk InAs are investigated. The study focuses on the chemical processes that occur upon the exposure of the surface to sulphur-, chlorine- and bromine-containing solutions and oxygen, and the resulting changes to the electronic structure of the surface, as deduced from photoluminescence (PL) measurements, X-ray photoelectron spectroscopy (XPS), Auger electron spectroscopy (AES), Raman scattering and scanning electron microscopy (SEM). Three processing treatments were evaluated: i) treatment with sulphur-based solutions ($Na_2S{:}9H_2O$, $(NH_4)_2S$ + S, [$(NH_4)_2S$ / $(NH_4)_2SO_4$] + S); ii) etching in halogen-based solutions (bromine-methanol and HCl: $H_2O$); and iii) thermal oxidation.

A significant overall enhancement in PL response was observed after chemical treatment or thermal oxidation, which is associated with a reduction in surface band bending. These changes correlate with the removal of the native oxide, in addition to the formation of well-ordered layers of In-S (or In-As)O as a passivating layer, indicating that *electronic passivation* occurs at the surface. The passivating effect on sulphide treated surfaces is unstable, however, with an increase in band bending, due to re-oxidation, observed over periods of a few days. The lowest re-oxidation rate was observed for ([$(NH_4)_2S$ / $(NH4)_2SO_4$] + S). Etching in HCl**:**$H_2O$ and Br-methanol solutions of appropriate concentrations and for moderate times (1 min) resulted in smooth and defect-free InAs surfaces. Etching completely removed the native oxides from the surface and enhanced the PL response. The adsorption of bromine and chlorine onto the InAs surface led to the formation of As-$Br_x$ , In-$Br_x$, As-$Cl_x$ and In-$Cl_x$compounds (x = 1, 2, 3), as inferred from changes in the In $3d_{3/2;\ 5/2}$ and As *3d* core level binding energies. The etch rate was found to decrease because of strong anisotropic effects. The improvements in surface properties were reversed, however, if the concentrations of the etchants increased or the etch time was too long. In the worst cases, pit formation and inverted pyramids with {111} side facets were observed.

Surface treatments or thermal oxidisation significantly enhanced the PL intensity relative to that of the as-received samples. This was due to a reduction in the surface

state density upon de-oxidation, or in some cases, to the formation of a well ordered oxide layer on the surface. The overall increase in PL intensity after treatment is ascribed to a reduction in band bending near the surface. This allows several well-defined peaks not observed or reported previously for bulk InAs (with a carrier concentration $n \sim 2 \times 10^{16}$ $cm^{-3}$), to be studied. A combination of PL and XPS measurements before and after the various treatments was used to identify the chemical nature of the impurities giving rise to bound exciton recombination in InAs (111).

*Contents*

*List of publications emanating from this study*

Surface modification of InAs (111)A etched in bromine-methanol, N. Eassa, R. Betz, E. Coetsee, H.C. Swart, A. Venter and J.R. Botha, Current Applied Physics 13(2), 366-370.

Treatment for GaSb surfaces using a sulphur blended $(NH_4)_2S/(NH_4)_2SO_4$ solution, D.M. Murape, N.Eassa; R. Betz, E. Coetsee, H.C. Swart, J.R. Botha and A. Venter, Applied Surface Science 258 (18), 6753–6758.

Surface morphology and electronic structure of halogen etched InAs (111), N. Eassa, D.M. Murape, R. Betz, J.H. Neethling, A. Venter and J.R. Botha, Physica B: Condensed Matter 407(10), 1591–1594.

Improved GaSb surface using $[(NH_4)_2S$ / $(NH4)_2SO_4]$ solution, D.M. Murape, N. Eassa, C. Nyamhere, J.H. Neethling, R. Betz, E. Coetsee, H.C. Swart, J.R. Botha and A. Venter, Physica B: Condensed Matter 407(10), 1675 – 1678.

Chalcogen based treatment of InAs with $[(NH_4)_2S$ / $(NH_4)_2SO_4]$, N. Eassa, D.M. Murape, R. Betz, J.H. Neethling, E. Coetsee, H.C. Swart, A. Venter and J.R. Botha, Surface Science 605 (11-12), 994 – 999.

*List of Figures*

*List of Tables*

# Chapter 1

## Introduction

### 1.1 Background

InAs is a promising narrow band gap III-V semiconductor with very high electron mobility.For comparison, the typical room temperature electron mobility for InAs, GaAs and Si are 30000, 1000 and 1500 $cm^2/Vs$, respectively [1]. InAs has a room temperature band gap of 0.35 eVwhich makes it suitable for mid-infrared detection. It also has the potential for applications in both metal oxide semiconductor field effect transistors (MOSFETs) and metal semiconductor field effect transistors (MESFETs), which operate at very high speeds while using very little power. InAs (111) has received special interest as a promising substrate for the growth of low dimensional structuressuch as quantum dots [2-6].

Unlike most III-V semiconductors, *n*-type InAs exhibits an accumulation layer instead of a depletion layer at the surface, which was first observed using current-voltage (I-V)characterisation [7], and later confirmed with the use of ultraviolet photoemission spectroscopy, Kelvin probe measurements and electric field induced Raman spectroscopy [8,9]. The accumulation layer has been ascribed to native defects, as well as to the presence of native oxides on the surface[10,11].The surface is a common source of surfacestates. Electrons can be trapped at these surface states to create a localized charge layer at the surface, resulting in a large movement of the Fermi level into the conduction band. This Fermi level movement is accompanied by a downward bending of the conduction band edge at the surface, resulting in the formation of an accumulation layer.Since the active regions of most electronic devices use only the first few microns of the semiconductor, the surface properties of the material are critical to device performance. The surface accumulation layer in InAs strongly perturbs the electrical and optical properties of grown films, causing increased non-radiative recombination and strong reverse leakage currents in electronic devices [1,12,13]. Appropriate chemical etchants and surface passivation treatments are therefore essential to improve the surface quality of this semiconductor. These treatments are

commonly used to prepare high quality semiconductor surfaces. The ability to prepare a good quality surface requires the optimisation of conditions for both passivant and etchant.

## 1.2 Objectives

Considering the importance of InAs in infrared device technology, sustained research has been conducted on the epitaxial growth of high quality InAs using metal organic vapour phase epitaxy (MOVPE) and molecular beam epitaxy (MBE) [14-16].However, little is known of either the properties of the impurities orthe methods of their detection and characterisation. A clear understanding of the origin of the surface accumulation inInAs as well as the control of the surface electronic properties remains a subject of continued interest, and is essential to realise the full potential of this semiconductor. This thesis focuses on chemical treatments of InAsby sulphur-, chlorine- and bromine-containing solutionsin order to understand the relationship between the chemical reactions that occur inthe surface region upon treatment, and during thermal oxidation. The accompanying changes in surface electronic properties such as band bending and surface accumulation, and their impact on the luminescence properties of bulk *n*-InAswith orientations(111)A and (100), are investigated.

This thesis is organised as follows: Chapter 2 presents relevant background theory pertaining to the crystal structure, electronic band structure near the surface and other physical properties of InAs. Chapter 3 outlines the surface preparation techniques used in this work, while the characterisation techniques employed to study as-received bulk InAs and chemically treated/oxidised surfaces are discussed in Chapter 4. Chapters 5 to 8 provide details of the experimental results, and they are followed by a summary and conclusions in Chapter 9.

# Chapter 2

## Theoretical Background

In this chapter, emphasis is given to the crystal structure of InAs and the electronic band structure of the near-surface region of this semiconductor. Other physical concepts relevant to this study are also discussed.

### 2.1Crystal Structure

The most common crystal structure among frequently used semiconductors is the diamond lattice shown in Fig 2.1(a). Each atom in the diamond lattice is covalently bonded to four neighbouring atoms to form a regular tetrahedron. This lattice can also be viewed as two interpenetrating face-centred cubic (fcc) lattices, displaced by a quarter of the body diagonal of the conventional unit cell [17].

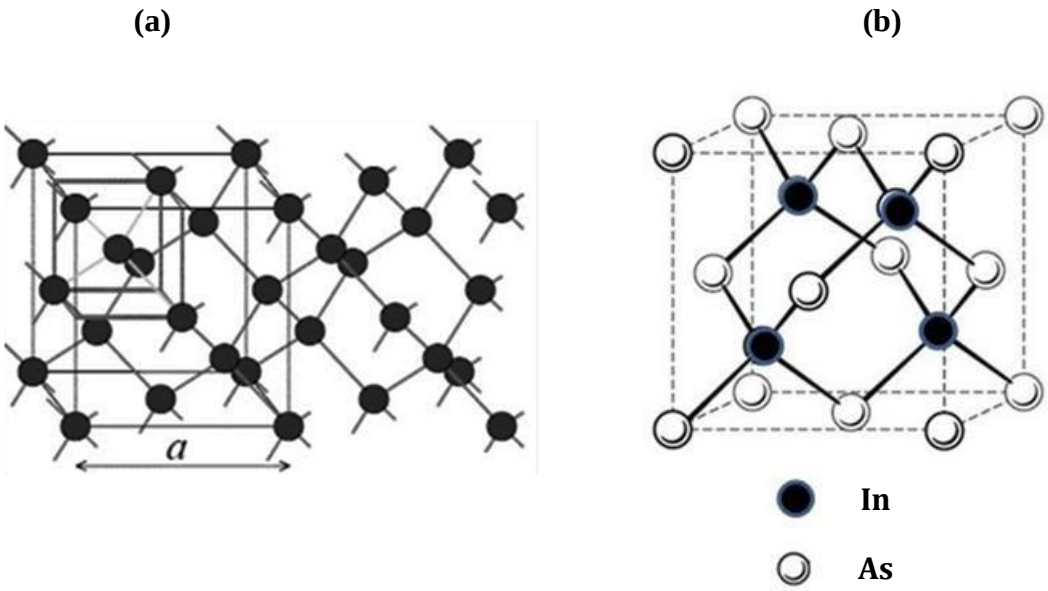


**Figure 2.1:**(a) The diamond crystal structure [18] and (b) the cubic zinc-blende structure of InAs[19].

Many III-V compound semiconductors (including InAs) crystallise in the zinc-blende structure, in which the lattice sites are occupied by two different types of atoms. Each group III atom is four-fold coordinated with group V atoms, and vice versa. The zinc-blende unit cell for InAs is shown in Fig. 2.1(b). The bonds are partially ionic and the lattice constant is 6.0584 Å[20].

## 2.2 Electronic Band Structure

Crystals form when atoms are brought together in a regular/periodic arrangement. In this configuration, the wave functions of adjacent atoms overlap, leading to a splitting of the discrete atomic energy levels, consistent with Pauli's Exclusion Principle. The splitting results in the formation of quasi-continuous energy bands interrupted by energy gaps. At 0 K, the valence band (VB) is the highest completely filled band of states. This is followed by a well-defined energy gap to the next band, the conduction band (CB), containing a range of quasi continuous empty states at 0 K. The energy difference between the minimum in the CB ($E_c$) and the maximum in the VB ($E_v$) is referred to as the band gap ($E_g = E_c - E_v$)[18].

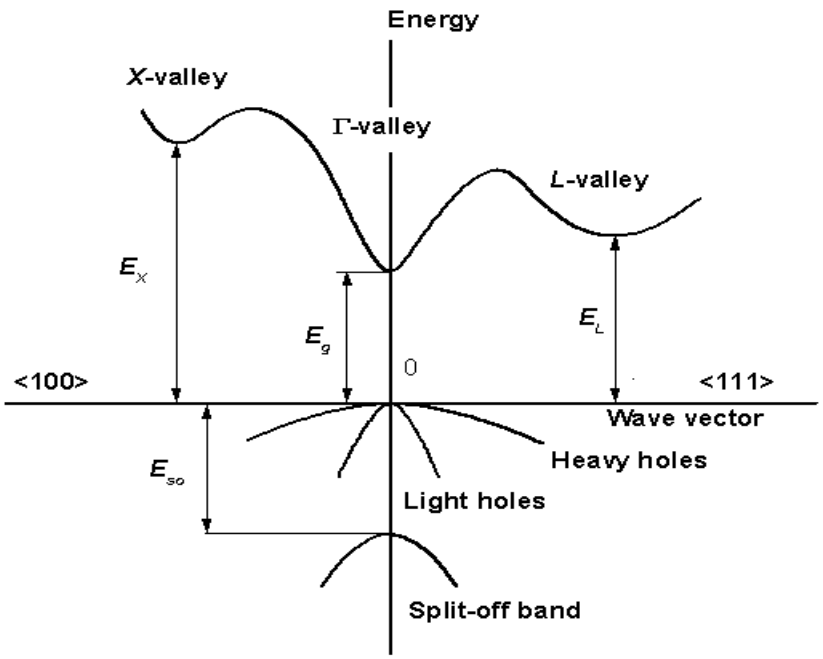


**Figure 2.2:** The band structure of InAs [21].

Figure 2.2 illustrates the energy band diagram (E versus k-vector) of InAsat 300 K [21]. The VB maximum and CB minimum occur at the same point in k-space (Γ), which is situated in the centre of the first Brillouin zone.In this case, absorption and emission of photons occur without requiring phonons for the conservation of momentum. Such semiconductors are called direct band gap semiconductors. This material is of interest for opto-electronic devices [22]. The energies of the symmetry points in the band structure relative to the top of the VB are presented in Table 2.1, along with other physical parameters for InAs.

**Table 2-1:** Energies of symmetry points of the band structure relative to the top of the valence band as well as other physical parameters of InAs.

| $\mathbf{E_g}$ 0.35 V | $\mathbf{E_L}$ 1.08 V | $\mathbf{E_x}$ 1.37 V | $\mathbf{E_{so}}$ - 0.41 eV |
|---|---|---|---|
| Effective electron mass [23, 24] | | $0.0265m_o$ (T= 4.2 K) | $0.0265m_o$ (T = 300 K) |
| Effective hole mass [23, 24] | | $m_{(100)}$ **:** $0.35m_o$ | $m_{(111)}$**:** $0.43m_o$ |
| Temperature dependence of the direct energy gap [25] | | $E_g = 0.415 - 2.76\cdot10^{-4}\cdot T^2/(T+83)$ (eV) | |
| Effective density of states in the conduction band [26] | | $N_c \approx 1.68\cdot10^{13}\cdot T^{3/2}$ ($cm^{-3}$) | |
| Effective density of states in the valence band [26] | | $N_v \approx 1.27\cdot10^{15}\cdot T^{3/2}$ ($cm^{-3}$) | |
| Free exciton binding energy [27] | | $E_b$ = 1.0 meV (T = 4.2 K) | |
| Ionisation energies of shallow donors [28, 29] | | ≥ 1 meV: Se, S, Te, Ge, Si, Sn, Cu | |
| Ionisation energies of shallow acceptors (meV) [28, 29] | | SnGe Si Cd Zn | |
| | | 10 14 20 15 10 | |

## 2.3 Fermi Energy

The Fermi level ($E_f$) defines the electrochemical potential of a system. At 0 K, all states below $E_f$ are occupied with electrons and all states above $E_f$ are empty. The minimum energy between the Fermi level at the surface of the solid, $E_{fs}$, and the vacuum level can be measured and is defined as the work function, $\phi_w$,of the material [18]. Localized surface states within the gap often occur in III-V semiconductors and lead to a near-surface electric field in the solid, represented by the bending of the energy band (in real space) at the surface and a surface potential, $\phi_s$.

The intrinsic Fermi energy,$E_i$,is located near the middle of the band gap andit canbe expressed as [18]:

$$E_i = \frac{1}{2}(E_C + E_v) + \frac{3}{4}kTln\frac{m_h^*}{m_e^*}, \tag{2-1}$$

where$m_h^*$and $m_e^*$are the effective masses of holes and electrons, respectively. Asemi-conductor can be doped by introducing electron*donors* orelectron*acceptors*,which correspondingly give rise to energy states $E_d$and $E_a$. Energy states located within the band gap at the surfacehave a surface energy,$E_{SS}$.

In *n*-type semiconductors, the mobile electrons in the conduction band are the majority charge carriers, with corresponding *holes* as the minority carriers. The numbers (density) of carriers are given by$n_o$ (electrons) and$p_o$ (holes). In bulk *n*-type material, electrons are majority carriers and $n_o$>$p_o$, while in *p*-type semiconductors the holes are the majority carriers and$p_o$>$n_o$.At equilibrium [30]:

$$n_o p_o = n_i^2 \tag{2-2}$$

where $n_i$is the electron density in the CB for an intrinsic semiconductor. If the energy bands are bent upwards or downwards near the surface, the electron and hole densities differ from those in the bulk. If a Boltzmann distribution is assumed, the surface electron density $n_s$isgiven by:

$$n_s = n_o exp\left(\frac{e\Delta\phi_x}{kT}\right), \quad (2\text{-}3)$$

and the surface hole density,$p_s$,is given by:

$$p_s = p_o exp\frac{e\Delta\phi_x}{KT}, \quad (2\text{-}4)$$

where$\Delta\phi_x$is a potential dropacross the space charge region. For a positive $\Delta\phi_x$, the bands are bent downward and for a negative$\Delta\phi_x$the bands are bent upward (see Fig. 2.3).

## 2.4 Surface Space Charge

In most III-V semiconductors, surface atoms relative to their bulk counterparts can lead to electronic states that are both spatially and energetically localized [31]. The wave functions corresponding to surface states have a maximum value at the surface, and they decay exponentially away from the surface to the regions both inside and outside the semiconductor bulk. When these surface states have energies within the band gap, they can have a great impact on the electronic properties of the semiconductor and on adsorption processes. Surface states can be either intrinsic or extrinsic in origin. Intrinsic surface states arise naturally from solutions to the Schrödinger equation by imposing boundary conditions to reflect the termination of the periodic lattice at the surface. Defects arising from surface reconstruction are also termed intrinsic [31, 32].Theoretical studies suggest that by occupying vacant coordination sites of surface atoms, adsorbates can induce surface atoms to adopt near-bulk coordination geometries; in some cases, this may even lead to the removal of intrinsic surface states. In contrast, extrinsic surface states are new states introduced by foreign adsorbed material. These new states correspond to dangling bonds of the adsorbate, which energetically may lie within the band gap or overlap with the continuum of bulk states.Oxide formation at the semiconductor surface, for example, is a common source of extrinsic surface states [8, 33].

The charge distribution within the space-charge region below the semiconductor surface is determined by the Poisson equation [30]:

$$-\frac{d^2\varphi_x}{dx^2} = \frac{\rho(x)}{\epsilon_r \epsilon_0} \tag{2-5}$$

where $\varepsilon = \varepsilon_r \varepsilon_0$is the permittivity, $\varepsilon_r$is the relative permittivity (dielectric constant) of the semiconductor,$\varepsilon_0$is the permittivity of vacuum and $\varphi_x$ is the electron potential. The charge density, $\rho$, depends on the distance from the surface and is given by:

$$\rho(x) = e[N_d^+ - N_a^- - n(x) + p(x)] \tag{2-6}$$

where $N_d^+$ and$d$ $N_a^-$ are the total densities of the charged donor and acceptor states, respectively. *n(x)* and *p(x)* representthe carrier densities which vary with distance *x* from the surface. The field strength, $E_s$,can be obtained by integration of equation (2-5):

$$-E_s = \frac{d\varphi_x}{dx} \|_{x=0} \tag{2-7}$$

The surface charge density produced in this field is given by:

$$\sigma_s = \varepsilon_r \varepsilon_0 E_s \tag{2-8}$$

Where$\sigma_s$ is positive for upward band bending and negative for downward band bending, as shown in Fig. 2.3.

Three situations are distinguishable for the space charge region, as shown for *n*-type semi-conductors in Fig 2.3:

(i) Accumulation: the energy bands are bent downwards and $n_s > n_0$and $p_s < p_0$.

(ii) Depletion: the energy bands are bent upwards and $n_s < n_o$.

(iii) Inversion: the energy bands are bent upwards and the Fermi level is located above $E_i$ at the surface, i.e.$p_s > n_s$.

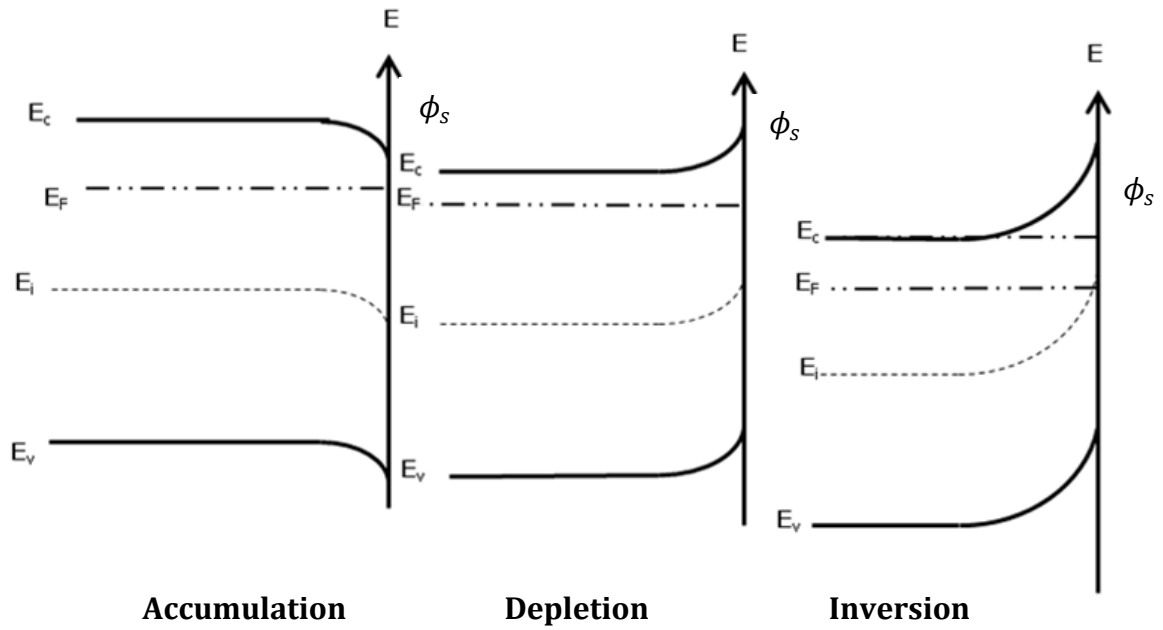


**Figure 2.3:** Formation of accumulation, depletion and inversion within the space charge layerfor *n*-type semiconductors [30].

The surface accumulation layer in InAs has been widely debated. Some studies ascribe this layer to intrinsic surface states or native defects [10], while others attribute it to the adsorption of impurities, since it has been shown that the surface Fermi level can be modulated in InAs by the incorporation of O, Cl, or metal atoms on the surface. This was observed by use of ultraviolet photoemission spectroscopy, Kelvin probe and electric field-induced Raman spectroscopy measurements [8, 34]. Watanabe *et al.* [35], using high resolution photoemission spectroscopy, reported that the adsorption of selenium on InAs(100) increased the downward band bending and located the Fermi level at 500 meV above the conduction band minimum. Sulphur-treated InAs (100) and (111)B surfaces also showed an increase in downward bending around 3 and 6 times greater than the untreated surface [36].

## 2.5 Surface Structure

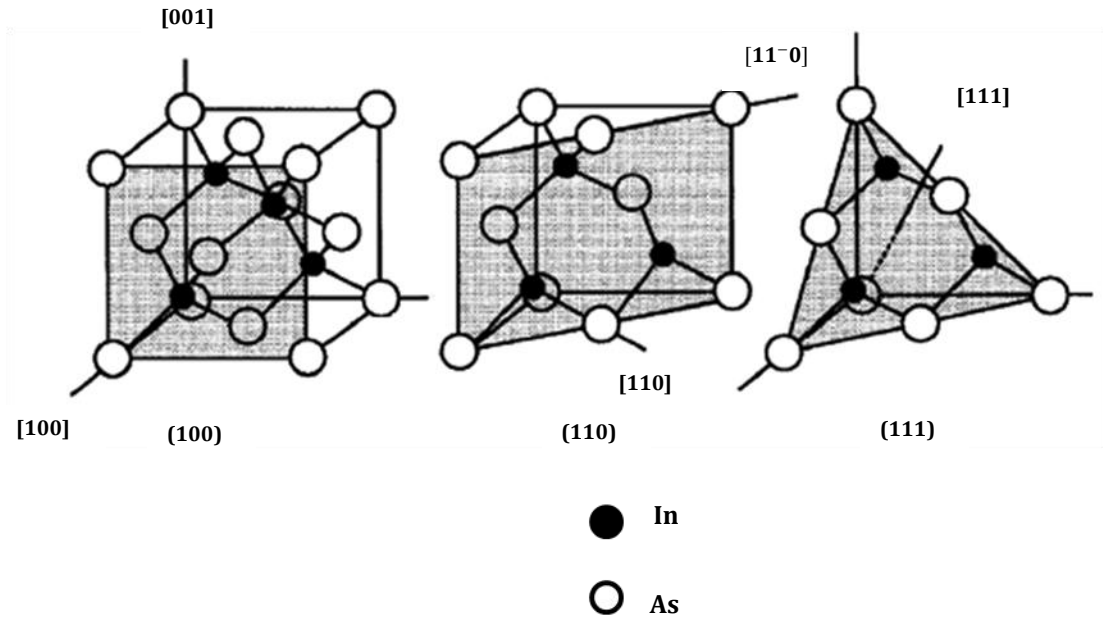


**Figure 2.4**:(100), (110) and (111) truncated surface structure [37].

The atomic arrangements on the (100), (110) and (111) planes in InAsare shown in Fig. 2.4.The (100) surface is obtained by cutting the *fcc* lattice parallel to the front surface of the conventional cubic unit cell. The (110) surface is obtained by cutting the unit cell in a manner that intersects the *x* and *y* axes, but not the *z*-axis. The (111) surface is obtained by cutting the unit cell in such a way that the surface plane intersects the *x*-, *y*- and *z*- axes at the same value [38]. The (110) surface consists of an equal number of anions and cations [39]. Both InAs (100) and (111) surfaces are terminated by either an anion or cation; only the atomic density is different. The (111)A surfaces are terminated by group III atoms when the (111)B surfacesare terminated by group V atoms[40].

The interaction of semiconductor surfaces with adsorbents critically depends on the stoichiometry of the surface. Berkovits *et al*. [41] used reflectance anisotropy spectroscopy (RAS) to investigate the oxidation of InAs (100) surfaces at low temperatures. They observed that the cation-rich surface oxidises more readily than the anion-rich one. Observations made by Sugiyma*et al*. [42] and Murphy *et*

*al.*[43]suggested that sulphur atoms adsorbed to Ga atoms on the GaAs (111)A surface, while they exchange As atoms on the (111)B surface. Similar observations were reported on sulphur adsorption on InAs (100) and (111)B. It has also been found that sulphurexchanges As atoms inInAs (111)A [44].

In this thesis,the surface modification of InAs (100) and (111)Aduring thermal oxidation, and the effect of chemical processing on the adsorption of sulphur-, chlorine- and bromine-containing solutions, will discussed further in Chapters 5 – 7.

# Chapter 3

## Surface Preparation

This chapter presents the general chemical reactions that occur between III-V semiconductors and either sulphur, halogens or oxygen. Emphasis is given to chemical reactions between InAs and $Na_2S.9H_2O$ or ([$(NH_4)_2S$ / $(NH_4)_2SO_4$] + S) or ($(NH_4)_2S$ + S). In addition, mechanisms related to etching InAs in HCl:$H_2O$ and bromine-methanol solutions, and the interaction of oxygen atoms with InAs upon thermal oxidation are investigated.

### 3.1 Sulphur Passivation

Sulphur passivation,using $Na_2S.9H_2O$ solutions, was first proposed by Sandroff*et al*. [45] as a method for improving the characteristics of AlGaAs/GaAs bipolar transistors. Treatment with aqueous solutions of inorganic compounds, including $(NH_2)_2S$, $(NH_2)_2S_x$, $P_2S_5/(NH_4)_2S_x$ and $P_2S_5/(NH_4)_2S$ yieldeddramatically reduced mid-gap surface state densities for most III/V materials. This reduction in surface state density was associated with an enhancement in photoluminescence (PL) intensity and an improvement in Schottky barrier diode quality[46-49]. Another promising direction for sulphur passivation is sulphurisation in alcohol solutions. Treatment in sodium sulphide and ammonium sulphide solutions in ethanol, isopropanol and butanol results in both a reduction of surface band bending and an increase in PL intensity, much higher than in the case of similar treatments in aqueous solutions [49, 50].

The passivation of a semiconductor surface can be broadly defined as the intentional deposition of an insulating layer on the surface with the purpose of providing electrical and chemical stability, by “isolating” the surface from the environment. It effectively renders the surface inert in the ambient, and eliminates or reduces surfacestates and non-radiative recombination centres. In addition, passivation should provide an adequate barrier against the transfer of electrons from the semiconductor bulk to the

surface layers. Fig. 3.1 depicts the three-step process which occurs during the formation of a sulphidecoating [49]. The three steps are:

(i) Breaking of bonds between group III and V atoms and removal of the oxide layer.
(ii) Transfer of electrons from the semiconductor to the solution.
(iii) Formation of chemical bonds between the semiconductor and sulphur atoms.

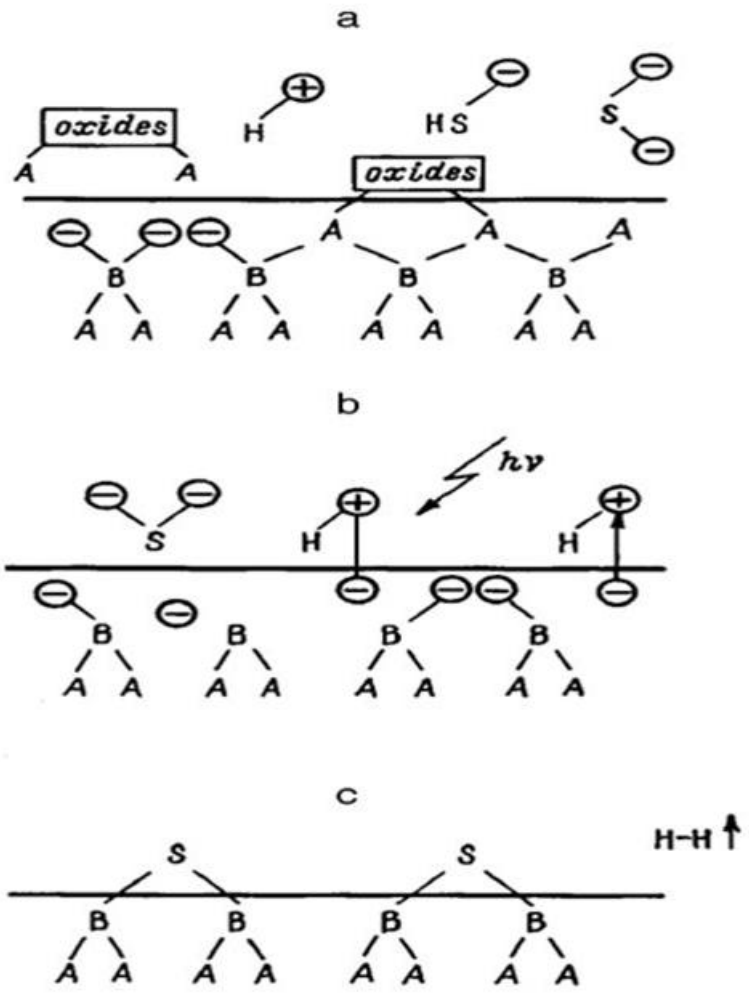


**Figure 3.1**: Schematic diagram illustrating the process occurring during the formation of a sulphidecoating layer on aIII-V semiconductor surface [49].

In this thesis, $Na_2S.9H_2O$ or ([$(NH_4)_2S$ / $(NH_4)_2SO_4$] + S) or ($(NH_4)_2S$ + S) solutions were used for surface passivation of InAs (111)A. The chemical reaction leading to the formation of a sulphide coating from a $Na_2S.9H_2O$ solution is well known [49, 51] andcan be written as:

$$Na_2S + H_2O \rightleftarrows 2Na^+ + HS^- + OH^- \quad (3\text{-}1)$$

$$A^{III}B^V + HS^- + H_2O \rightleftarrows A_xS_y + B_xS_y + OH^- + H_2(g) \quad (3\text{-}2)$$

where A and B are the group III and V elements, respectively, and *x* and *y* represent the stoichiometric coefficients. The chemistry related to the [$(NH_4)_2S$] and [$(NH_4)_2S$ / $(NH_4)_2SO_4$] treatments used in this work have been proposed to proceed as follows [44]:

$$(NH_4)_2S \rightarrow 2NH_{4_{aq}}^+ + S_{aq}^{2-} \quad (3\text{-}3)$$

$$S^{2-} + H_2O \longrightarrow HS^- + OH^- \quad (3\text{-}4)$$

$$NH_4^+ + H_2O \rightleftarrows \quad NH_3 + H_3O^+ \quad (3\text{-}5)$$

$$(NH_4)_2SO_4 \rightarrow 2NH_{4_{aq}}^+ + SO_{4_{aq}}^{2-} \quad (3\text{-}6)$$

$$SO_4^{2-} + H_2O \longleftarrow HSO_4^- + OH^- \quad (3\text{-}7)$$

$$(NH_4)_2S \rightarrow 2NH_{4_{aq}}^+ + S_{aq}^{2-} \quad (3\text{-}8)$$

$$NH_4^+ + H_2O \rightleftarrows NH_3 + H_3O^+ \quad (3\text{-}9)$$

The amount of $H_3O^+$ present through the hydrolysis reaction of $(NH_4)_2S$ and $(NH_4)_2SO_4$ according to equations (3-5) and (3-9) will facilitate the removal of $In_2O_3$, $As_2O_3$ and $As_2O_5$.Dissociation of $(NH_4)_2SO_4$ produces a higher amount of $H_3O^+$ in solution, according to equations (3-6 to 3-9). This enhances the solubility of the native oxide and should therefore be more effective in removal of the native indium and arsenic oxides.

## 3.2 Halogen Etching

Halogens and halogen-based compounds are commonly used as etchants in the fabrication of opto-electronic devices such as light emitting diodes (LED) and infrared (IR) detectors. Even though high performance devices require surfaces that are smooth and have low defect densities, many defects are often introduced during the etching process, and this can detrimentally affect the performance of these devices [52]. Halogen adsorption on most III-V semiconductors has been reported to yield an ordered or disordered layer as the material is etched, which will change the Fermi level position at the surface [53-55]. The exposure of GaAs (110) to iodine induces acceptor-like surfacestates. The energy positions of these surface state acceptors result in pinning of the Fermi level at ~0.3 eV above the valence band maximum (VBM). The adsorption of chlorine on GaAs (100) pins the Fermi level at 0.2 eV above the VBM, while the adsorption of chlorine on the InAs (110) surface induces donor-like surface states which pin the Fermi level at 0.52 eV above the VBM (i.e. inside the conduction band) [56, 57].

In this study, two halogen-based etchants were used to treat InAs (111)A, namely HCl: $H_2O$ and Br-methanol. The mechanism of surface etching is suggested as a complex, step-wise process. Firstly, hydrobromic/hydroiodic and hypobromic/hypoiodic acids are formed through the disproportionation reaction of bromine [58]:

$$Br_2^0 + H_2O \xleftrightarrow{\rightarrow} HBr^- + HOBr^+ \qquad (3\text{-}10)$$

The concentrations of the hydrobromic/hydroiodic acids depend on the concentrations of bromine or iodine in the solutions. At the first stage of the etching process, the halogen solutions dissociate the native oxides ($In_2O_3$, $As_2O_3$ and $As_2O_5$), forming $AsX_3$, $AsX_5$ and $InX_3$ (X= Cl, Br):

$$As_2O_3 + 6HX \leftrightharpoons 2AsX_3 + 3H_2O \quad \text{and} 2As_2O_5 + 20HX \leftrightharpoons 4AsX_5 + 10H_2O \qquad (3\text{-}11)$$

$$In_2O_3 + 6HX \xrightleftharpoons{\leftarrow} 2InX_3 + 3H_2O \qquad (3\text{-}12)$$

The removal of the oxide layer allows a multi-step reaction between the halogen atoms and the III-V surface. Firstly, halogen atoms break the III-V bond to form both III-halogen and V-halogen compounds:

$$2(A^{III}, B^{V}) + 3X_2 \longrightarrow 2A^{III}X_3 \text{ and } 2\mathrm{B^V}X_3 + \mathrm{HX} \quad (3\text{-}13)$$

where $\mathrm{A^{III}}$ represents group III atoms (In) and $\mathrm{B^V}$ represents group V atoms (As). Subsequently, the intermediate halogen compounds $(A^{III}B^{V})(\mathrm{OR})\mathrm{X}_2$ and $(A^{III}B^{V})(\mathrm{OR})_2X_2$form in the presence of water or alcohol, where R is either a hydrogen atom (for an aqueous solution) or an alkyl group (for an alcohol solution):

$$(A^{III}, B^{V})X_3 + R - OH \leftrightharpoons (A^{III}, B^{V})(OR)X_2 + HX \quad (3\text{-}14)$$

These intermediate halogen compounds yield the acids$H_3(A^{III}, B^{V})O_3$, which are soluble in water or alcohol and can lead to the breaking of the InAs bond. The extent of material removal depends on many factors, such as etching time, etchant concentration, and temperature and halogen solubility in alcohol or water.

## 3.3 Thermal Oxidation

Unlike silicon, III-V semiconductors do not form high quality native oxides. Moreover, oxidised surfaces are generally disordered and this has hampered the development of opto-electronic technology.

The interaction of oxygen with InAs surfaces has attracted much attention in the past few years, since knowledge of oxide properties is important in understanding the fundamental issues of material oxidation and also in developing various applications. The nature of oxygen reactions with In and As atoms on both (100) and (111) surfaces, and the chemical composition are well understood [59-61]. A huge amount of work has been undertaken to understand how the presence of the native oxide on InAs surfaces contributes to the Fermi-level pinning, and to preventing the formation of these oxides.

It has also been found that in the crystalline interface between the metal-oxide film and the III-V surface, no pinning occurs [62, 63].Very recently, a family of well-ordered, thermally oxidisedInAs, GaAs and InP defect-free surfaces were characterised using scanning tunnelling microscopy (STM) and photoemission measurements. The existence of a zinc-blende structured oxide on aIII-V surface was demonstrated and this was attributed to two factors: proper oxidisation temperature and oxygen pressure [64].

In this thesis, both InAs (100) and (111)A surfaces are thermally oxidised by exposing the InAs substrate to an oxygen rich atmosphere. The temperature was varied between 350°C and 550°C, producing oxide films. These experiments are discussed further in Chapters 4 and 7.

# Chapter 4

## Characterisation Techniques

This chapter describes the characterisation techniques used to evaluate the surface properties of bulk *n*-InAs before and after sulphur passivation, halogen etching or thermal oxidation. The sample properties were evaluated optically using Fourier Transform Infrared (FTIR) photoluminescence (PL) spectroscopy, whilethe surface electronic structure was investigated using Raman spectroscopy. The chemical compositions of the different samples were investigated using X-ray photoelectron spectroscopy (XPS) and Auger electron spectroscopy (AES), while surface morphologies were observed with a scanning electron microscope (SEM). The details of the procedures used for sample preparation are presented in the last section of this chapter.

### 4.1 Photoluminescence Spectroscopy

Photoluminescence is the spontaneous emission of light from a material under optical excitation. This process occurs when the difference in electron energy between the initial (excited) and the final (ground) state is emitted in the form of photons. The PL technique has been used in this study as an essential tool to evaluate the surface quality of InAs. The use of low temperature PL measurements provides information on both intrinsic and extrinsic material properties, such as the energy levels of impurities or defects, and the fundamental properties of semiconductors, such as the band gap.

In the bulk of a crystalline material, translational symmetry leads to the formation of electronic energy bands. Defects and impurities break the periodicity of the lattice and perturb the band structure locally. The perturbation can usually be characterised by a discrete energy level that lies within the band gap. Depending on the defect or impurity, the state acts as a donor or acceptor of excess electrons in the crystal. Electrons or holes are attracted to the excess or deficiency of local charge due to the impurity nucleus or defect, and Coulomb binding occurs. When the temperature is sufficiently low, carriers

will be trapped at these states. If these carriers recombine radiatively, the energy of the emitted light can be analysed to determine the energy of the defect or impurity level, but the sample temperature must be low enough to discourage thermal activation of carriers out of the traps [65, 66].Several intrinsic and impurity-related transitions are illustrated in Fig. 4.1.

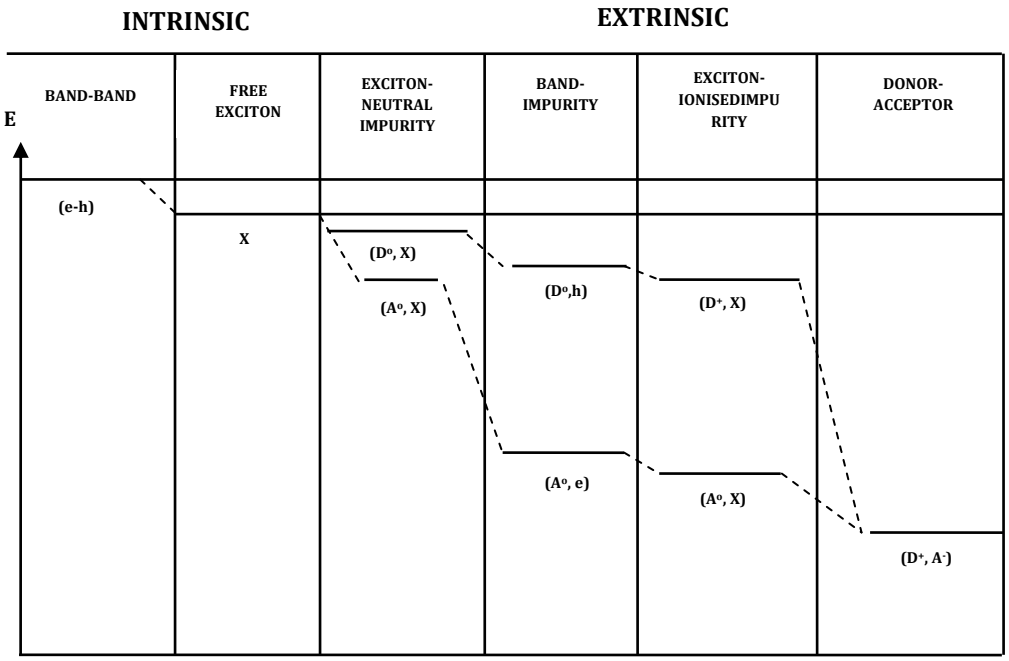


**Figure 4.1:** Energy level diagram showing several intrinsic and impurity-related optical transitions [67].

### *i) Band-to-band (B-B) transitions*

Band-to-Band (B-B) transitions involve the recombination of a free electron in the conduction band with a free hole in the valence band. These transitions dominate at high temperatures and can be used to estimate the band gap energy of the material. A band-to-band transition is most likely to occur in direct band gap semiconductors, since the electron-hole (e-h) pairs can recombine radiatively without the involvement of a phonon. The photon energies resulting from (B-B) transitions at finite temperatures occur at [68]:

$$E = E_g + \frac{1}{2}kT \tag{4-1}$$

where$E_g$ is the bandgap energy and the$\frac{1}{2}kT$ term results from the thermal distribution of free carriers in the bands.

***ii) Excitonic transitions***

Excitonic transitions are observed at low temperatures, such as at liquid helium temperature~4 K. Excitons are e-hpairs that are bound by coulomb interactions. The coulomb interaction results in a quasi-particle which is similar to the hydrogen atom. Electron-hole pairs bound by coulomb interaction are called *free excitons*if they don't interact with any other centre. The free exciton binding energy ($E_{FE}$) can be obtained using the hydrogen atom analogy, and is given by [68]:

$$E_{FE} = E_g - \frac{m_r^* e^4}{32\pi^2\varepsilon^2\hbar^2} \tag{4-2}$$

Where$\varepsilon$ is the permittivity of the semiconductor and $m_r^*$ is the reduced effective mass:

$$\frac{1}{m_r^*} = \frac{1}{m_e^*} + \frac{1}{m_h^*}\ . \tag{4-3}$$

Here, $m_e^*$ and $m_h^*$are the effective electron and hole masses, respectively. The effective Bohr radius of the exciton is given by:

$$a_B^* = \frac{4\pi\varepsilon\hbar^2}{m_r^* e^2} \tag{4-4}$$

Equations (4-2) and (4-3) can be expressed as:

$$E_{FE} = E_g - [\frac{\varepsilon_o}{\varepsilon}]^2 \frac{m_r^*}{m_o} E_{Ryd} \tag{4-5}$$

where the Rydberg energy $E_{Ryd}$ = 13.6 eV and theBohr radius $a_B^*$= 0.53 Å.

A free exciton can be localised at a neutral or ionised donor or acceptor, giving rise to an exciton impurity complex. An exciton bound to an ionised donor ($D^+$, X) is a complex of a donor ion and an electron and a hole. An exciton bound to a neutral donor ($D^o$, X) consists of the donor ion, two electrons and one hole. The descriptions of an exciton bound to an ionised acceptor ($A^-$, X) or to a neutral acceptor ($A^o$, X) are analogous.

***iii) Donor-acceptor pair (DAP) transitions***

The donor-acceptor pair (DAP) transition is an extrinsic transition which occurs in semiconductors with high compensation ratios, particularly when the concentration of donor and acceptor species is increased. The energy of aDAP transition is given by [68]:

$$E_{(DAP)} = E_g - E_d - E_a + \frac{e^2}{4\pi\varepsilon r} \tag{4-6}$$

where$E_{(DAP)}$, $E_g$, $E_d$, $E_a$, $e$, $\varepsilon$ and $r$ are the DAP transition energy, bandgap energy, donor ionisation energy, acceptor ionisation energy, elementary electrical charge, permittivity and donor-acceptor pair distance, respectively.

***iv) Free-to-bound (FB) transitions***

Free-to-bound (FB) transitions involve the recombination of a free electron with a hole localised on an acceptor ($e, A^o$) or the recombination of an electron localised on a donor and a free hole($D^o, h$). These processes give rise to emission at energy [68]:

$$E = E_g - E_i + \frac{1}{2}kT \tag{4-7}$$

where $E_g$is the band gap energy, $E_i$ is the impurity binding energy and the$\frac{1}{2}kT$term, as eluded to previously, results from the thermal distribution of free carriers in the conduction or valence bands.

***Fourier Transform Infrared PhotoluminescenceSpectroscopy***

A Fourier Transform Infrared (FTIR) spectrometer is a tool for acquiring near infrared and far infrared spectra. In an FTIR spectrometer, all the wave numbers/wavelengths are observed at once. This is in contrast to dispersive techniques which use grating monochromators or spectrographs where the wave numbers are observed sequentially as the grating is scanned. FTIR is a method of obtaining infrared spectra by first collecting an interferogram of the emission from a sample using an interferometer, and then performing a Fourier transform on the interferogram.In the following paragraphs, the basic principles of FTIR PL spectroscopy are described[69, 70].

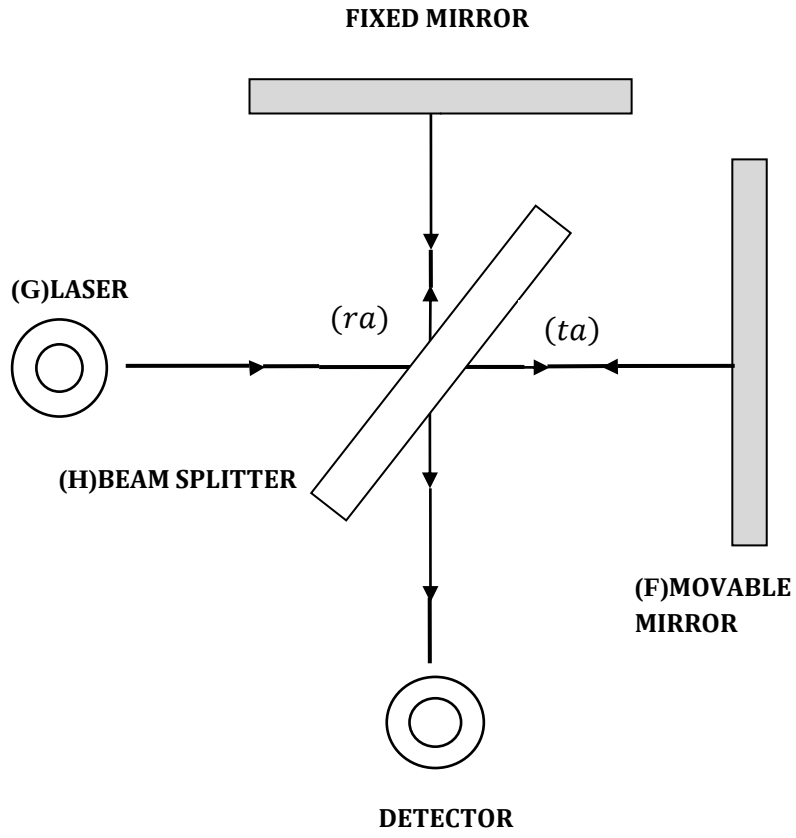


**Figure 4.2:** Schematic diagram of aMichelson interferometer [70].

Fig. 4.2 shows a schematic diagramof a Michelson interferometer. Consider the case of a monochromatic beam with amplitude $(a)$ and wave number $(v)$ passing through a beam splitter. The reflection coefficient is given by$(r)$and the transmission coefficient by$(t)$. The beam splitter splits the light into two parts: the reflected beam with amplitude $(ra)$,

and the transmitted beam with amplitude($ta$).The beam travels to the movable mirror and are then reflected back to the beam splitter and recombined. The motion of the movable mirror changes the path of the reflected beam, and the optical path difference between the two beams results in constructive and destructive interference. The signal amplitude collected by the detector is:

$$A_D = rat\left(1 + e^{-i\varphi}\right) \tag{4-8}$$

The intensity of this signal is given by:

$$I_D(x, v) = A_D A_D^* = 2RTB_o(v)(1 + cos\varphi) \tag{4-9}$$

where $R$ and $T$ are the reflectance and transmission ratios, respectively, of the beam splitter. The intensity of the incident beam is given by $B_o(v) = aa^*$, $x$ is the optical path difference, and $\varphi$is the phase difference between the two beams:

$$\varphi = 2\pi\frac{x}{\lambda} = 2\pi vx \tag{4-10}$$

When the incident beam has a random spectral distribution, $I_D(x, v) = dI_D(x)/dv$ is an integral with a spectral element of infinitely narrow line width $d(v)$:

$$I_D(x) = \int_0^\infty 2RTB_o\,(v)[1 + \cos(2\pi vx)]dv \tag{Z(4-11}$$

The final spectrum,$B_v$, is obtained by carrying out a Fourier transform of the interferogram.

The system used in this study is shown in Fig. 4.3. The excitation source for the PL spectra was the 532 nm line from a diode pumped YAG laser. The samples were mounted in a cold finger pulse tube cryostat that uses helium gas to reach low temperatures (~3.5 K) for the measurements. The PL signal was collected by a parabolic

mirror and sent to an MIR8025 Fourier Transform Interferometer, and a cooled (77 K) InSb detector.

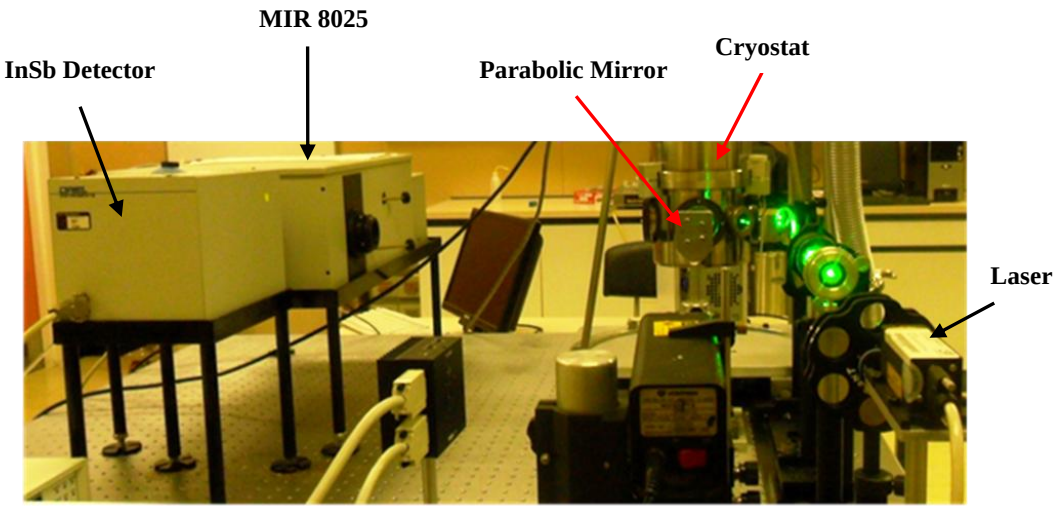


**Figure 4.3:** FTIR Photoluminescence Setup

## 4.2Raman Spectroscopy

Raman spectroscopy is a highly sensitive, non-destructive technique suitable for probing the surface and sub-surface region of a semiconductor.Both LO and TO modes are allowed for scattering from the InAs(111) surface in a pseudo-backscattering configuration, when all polarisations of the scattered light is collected. Scattering from the TO mode (through deformation potential scattering) will take place in the bulk and near the surface region. The efficiency of scattering from the bare LO phonon is also affected by the electric field present near a depleted/accumulated surface (the so-called electric fieldinduced Raman scattering or EFIRS) [9]. Note that this scattering appears even for configurations where deformation scattering is forbidden. The efficiency of LO mode scattering is influenced by band bending, because a change in the accumulation/depletion layer width implies a shift of the interface between the two regions, as well as a change in the surface electric field, which will both change the relative contributions from the two modes observed in the Raman spectrum.

Figure 4.5 shows the correspondence between band bending and Raman scattering modes from LO, TO and plasmon–LO phonon coupled modes (PLP). Band bending is plotted as a function of depth *z,* with the depletion depth indicated by $d_D$ on the horizontal axis. The upper part of Fig. 4.5 schematically shows the potential $V_{BB}(z)$, the electric field *Es(z)* and carrier concentration *n(z)*, while the lower part of Fig. 4.5 shows the depth dependence of the deformation potential induced LO phonon scattering($LO^{DP}$), the plasmon-LO phonon coupled mode scattering (PLP), the electric field induced LO phonon scattering ($LO^{EFIRS}$) and the TO phonon scattering. The last scattering mechanism is independent of depth, while the others are stronlgy influenced by the near-surface field.

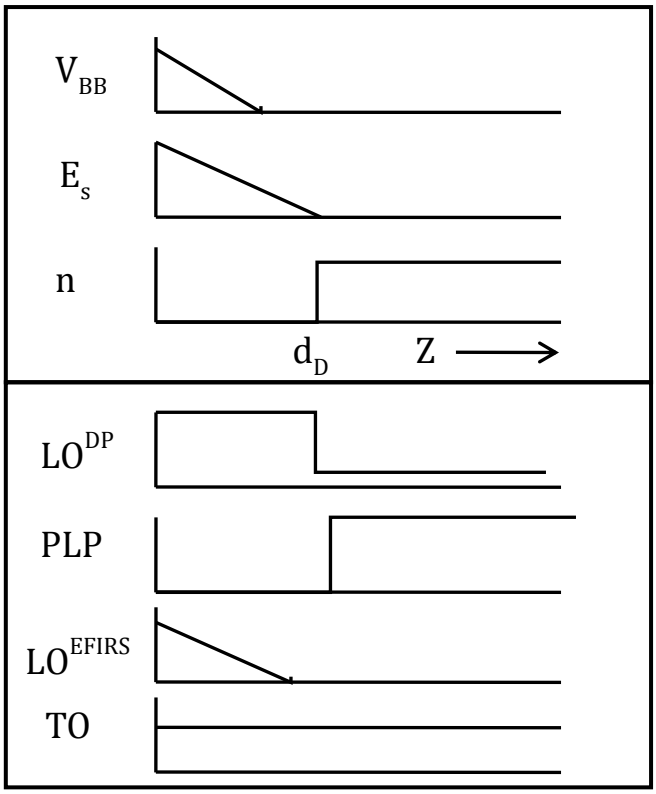


**Figure 4.4**: Raman features from different depth region. Upper part: dependence of the band bending $V_{BB}$ *(z)*, the surface field $E_s$ and the carrier concentration*(n)*. Lower part: local Raman-scattering modes of $LO^{DP}$, PLP, $LO^{EFIRS}$ and TO [9].

In theory,the measured Raman intensity ratio, $LO^{EFIRS}/\ I_{TO}$ can be related to the known surface band bending potential, $V_{BB}^{S}$, yielding a proportionality factor, $C^{EFIRS}$ [9]:

$$C^{EFIRS} = \left( \frac{I_{LO}^{EFIRS}}{(I_{TO})_{cal} \left[ \frac{1}{(V_{BB}^{S})_{cal}} \right]} \right) \tag{4-12}$$

$C^{EFIRS}$ can be determined empirically by using a sample with known band bending:

$$V_{BB}^{S} = \frac{\left( \frac{1}{C^{EFIRS}} \right) I_{LO}^{EFIRS}}{I_{TO}} \tag{4-13}$$

Raman spectroscopy was used in the present work to measure the effect of the adsorption of sulphur, halogen atoms, or oxygen on band bending and the associated surface accumulation width in InAs (111)A. Raman measurements were carried out at room temperature using the 488 nm and 514.5 nm lines of an argon ion laser with incident powers of 120 mW and 40 mW, respectively. Spectra were collected in a pseudo-backscattering configuration: no polariser was used in front of the monochromator. The general experiment for measuring Raman scattering is described elsewhere [71].

### 4.3 X-ray Photoelectron Spectroscopy

X-ray photoelectron spectroscopy (XPS) is a surface chemical analysis technique used to analyse the surface chemistry of a material [72].XPS spectra are obtained by irradiating a material with a beam of X-rays to eject photoelectrons from the surface. The binding energy of the emittedphotoelectrons isdetermined by:

$$E_{bin} = h\upsilon - E_{Kin} - \phi \tag{4-14}$$

where $E_{bin}$,$h\upsilon$, $E_{Kin}$ and $\phi$ are the binding energy of the electron in its initial state, the photon energy, the kinetic energy of the emitted electron and the work function of the

examined sample, respectively. This information can also be used to identify the compounds present on the surface.

In this study, XPS measurements were performed using a high resolution PHI 5000 Versaprobe ESCA (Electron Spectroscopy for Chemical Analysis) microprobe systemat a take-off angle of $45^{\circ}$. Survey scans were recorded using monochromatic Al $K_{\alpha}$ X-rays with a beam diameter of 100 μm. A pass energy of 11.75 eV was used for the high resolution XPS scans. The accelerating voltage was 15 kV and the beam power 25 W.

### 4.4 Auger Electron Spectroscopy

Auger electron spectroscopy (AES) [72] is a widely used technique for the surface analysis of semiconductors, sincethe energy of the emitted electron gives an indication of the specific elements present on the surface. The basic Auger process starts with the removal of a core electron to form a vacancy. The vacancy (hole) can be filled by a second electron from a higher shell with the simultaneous release of energy. The excess energy in this process is dissipated as kinetic energy transferred to a third electron, the Auger electron, which is emitted from the sample. The process of an excited ion decaying into a doubly charged ion by the ejection of an electron is called the Auger process.

AES measurements were performed in this study using a PHI 700 Scanning Auger Nanoprobe with a 20 kV, 10 nA electron beam. The base pressure of the system was $6 \times 10^{-10}$torr.

### 4.5 Scanning Electron Microscopy (SEM)

The surface morphologies of the samples were studied using a Jeol JSM-700 1F Field Emission Scanning Electron Microscope (FESEM). The microscope usesa beam of electrons to form an image, and is mainly used for surface topographic studies.

The basic principle in SEM is to scan a focused electron beam over the surface of the sample, and at the same time detect electrons emanating from every point on the

surface. To produce an image on the display, the beam must be scanned synchronously over the sample and the display tube. The magnification is the ratio between the area of display and the area of the scanned surface [73].

## 4.6 Sample Preparation

The InAs (111)A and (100) substrates used in this work were supplied by NewWay Semiconductor Ltd, China,with a carrier concentration n~$2\times10^{16}$ $cm^{-3}$. Thematerial was cleaned before use by removing organic contaminants as follows: successivelyboiling the samples in trichloroethylene, acetone and methanol, followed by rinsing in deionised (DI) water with a resistivity $\rho$ = 18.2 MΩ.cm. The samples were then blown dry with nitrogen gas, and subsequently treated as follows:

***i) Treatment insulphide solutions***

The three sulphide based solutions used in thiswork wereprepared as follows:

i) A 1molar solutionof sodiumsulphide was prepared at room temperature by dissolving 4.8 g of $Na_2S.9H_2O$ in 20 ml of DI water. The pH of the solution was 13.2.
ii) A $(NH_4)_2S$ + S solution (pH = 9.8) was prepared at 35°C by dissolving 0.2 g of sulphur in 15 ml of a 20% aqueous solution of $(NH_4)_2S$.
iii) The [$(NH_4)_2S$ / $(NH_4)_2SO_4$] + S solutionwas prepared by dissolving 0.2 g of sulphur in 15 ml of a 10% aqueous $(NH_4)_2S$ solution containing 4.7g/l of $(NH_4)_2SO_4$, resulting in a pH of 9.8.

Sampleswere immersed for 25 min in the above-mentioned solutions. For all treatments, solution concentrations and treatment time werechosen to produce a free-oxide or minimum residue oxide on InAs. The remaining oxideswere evaluated using XPS.

***ii) Halogen etching***

1% and 3% bromine-methanol solutionswere used to etch InAs (111)A surfaces.The etch times ranged from1 min to 30 min, while 37% HCl:$H_2O$ (1:1) and (2:1) solutions were used for etch times ranging between 1 and 10 minutes. The solution concentrations and etching time were chosen for relatively low LO intensity compared to that of the as-received surface.

***iii) Thermal annealing***

Thermal oxide films were formed between 350°C and 550°C for 45 min on both InAs (111)A and (100). The annealing time was chosen for a relatively low LO intensity compared to the as-received surface.

# Chapter 5

## SulphurTreatment of Bulk InAs (111)A

Results presented in this chapter aredetailed analysis of the surface properties of as-received and sulphurized bulk InAs (111)A. Sulphurization was achieved by exposing the material to various sulphur-containing chemicals, namely $Na_2S.9H_2O$, $(NH_4)_2S$ + S or $[(NH_4)_2S$ / $(NH_4)_2SO_4]$ + S,for 25 min. The surface properties were extensively studied using X-ray photoelectron spectroscopy (XPS), Auger electron spectroscopy (AES), scanning electron microscopy (SEM), Raman spectroscopy and photoluminescence (PL) spectroscopy.

### 5.1 Surface Morphology

The surface treatment of III-V semiconductors with sulphide solutions has received considerable attention. Many attempts have been made to improve the surface properties of InAs and reduce the effects of surface states on the electronic and optical properties. Treatment with sulphur-based solutions, including $(NH_2)_2S$, $(NH_2)_2S_x$, $P_2S_5$ /$(NH_4)_2S_x$ and $P_2S_5$/$(NH_4)_2S$,dramatically reduced mid-gap surface state densities for most III-V materials, accompanied by an enhancement in the PL intensity and an improvement in Schottky barrier diode quality [49].

Figure 5.1 shows typical SEM micrographs of the as-received and sulphurized InAs surfaces. Results from four samples are shown: Sample A was only degreased as described in Chapter 4, while samples B to D were degreased and then treated for 25 min in $Na_2S.9H_2O$, $(NH_4)_2S$ + S, or $[(NH_4)_2S/(NH_4)_2SO_4]$ + S. It can be seen that the surface of the reference sample (A) is relatively smooth, although randomly distributed etch pits and scratches of non-uniform density are visible in some areas. For the sample treated with $Na_2S.9H_2O$ (B), no significant change in morphology is observed. Sample C, treated with $(NH_4)_2S$ + S, displays uniformly distributed chemisorbed surface features

of varying size. This produces a significantly rougher surface compared to samples A, B and D. Sample D, treated with [$(NH_4)_2S$ / $(NH_4)_2SO_4$] + S, has an almost specular surface with no etch pits.

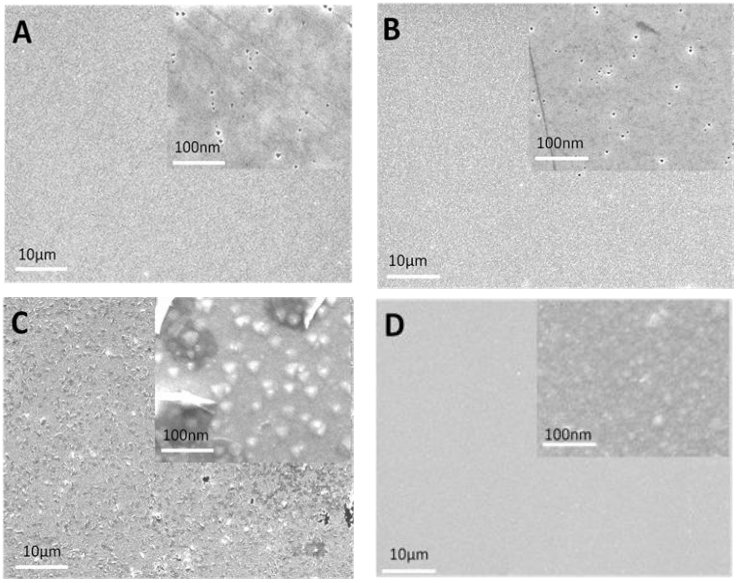


**Figure 5.1**: SEM micrographs of the as-received and sulphurized InAs surfaces: (A) as-received, and treated with (B) $Na_2S.9H_2O$, (C) $(NH_4)_2S$ + S and (D) [$(NH_4)_2S$ / $(NH_4)_2SO_4$] + S.

## 5.2 Auger Electron Spectroscopy and X-ray Photoelectron Spectroscopy

Figure 5.2 shows (a) AES and (b) XPS spectra for the reference sample (A), and the various sulphur treated samples (B – D). The AES and XPS spectra were normalised with respect to theIn (405 eV) and In *3d* transitions, respectively. Four Auger peaks at, 1 229 eV (As), 511 eV (O) 405 eV (In) and 272 eV (C), are clearly visible in the AES spectrum of sample A, while the O signal is absent for all the treated samples (B – D). XPS has a greater sensitivity than AES, and thus reveals the presence of oxygen after treatment, with the smallest O *1s* signal observed for sample D, i.e. [$(NH_4)_2S$ /

$(NH_4)_2SO_4$] + S. The presence of oxygen on the treated samples is also observed in the high resolution XPS spectra of the O *1s* core level for as-received and treated InAs, seen in Fig. 5.6 (to be discussed later). Furthermore, both the AES and XPS results in Fig. 5.2 indicate a more pronounced degree of sulphurization for sample C. This is seen in the higher intensities of the S-related signals, suggesting a thicker sulphide layer compared to samples B and D. This observation is reinforced by the depth profiles depicted in Fig 5.3.

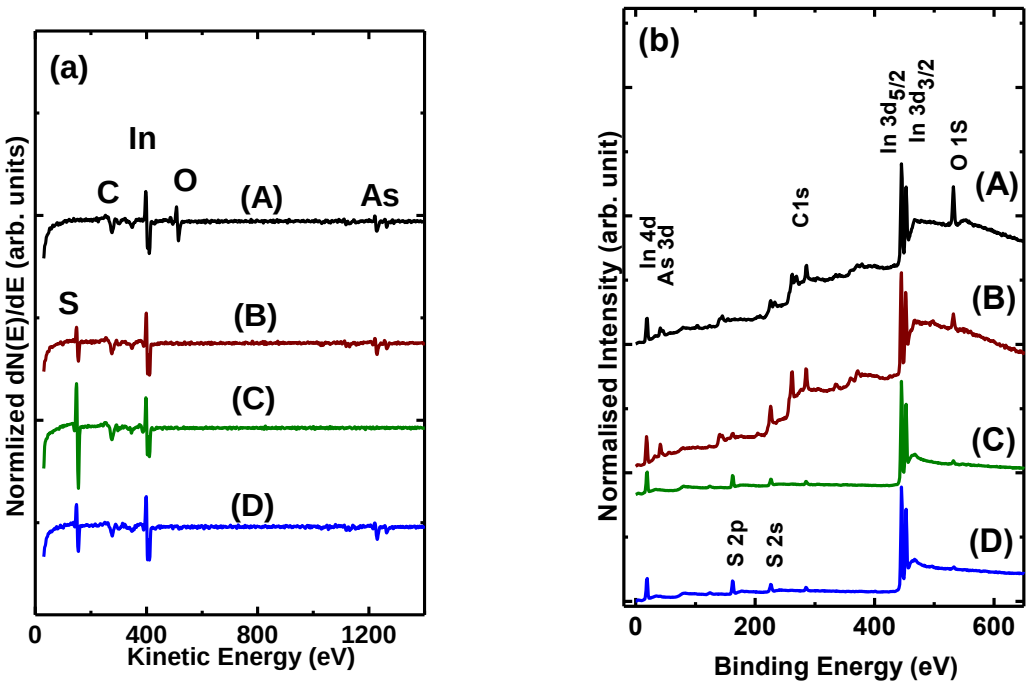


**Figure5.2:**(a) Differential Auger and (b) XPS spectra for the as-received sample (A), and the $Na_2S.9H_2O$ (B), $(NH_4)_2S$ +S (C) and [$(NH_4)_2S$ / $(NH_4)_2SO_4$] + S (D) treated bulk InAs samples.

AES depth profiles of the as-received and treated samples are presented in Fig. 5.3 on the next page. The results show that Ar ion sputtering for a period of 1 min results in the complete removal of O from all the surfaces. Similarly, S was removed after a sputtering

period of 1 min for samples B and D and after 2 min for sample C. The sputter rate in all cases was approximately8.5 nm/min. The persistent presence of adventitious carbon on the surface is attributed to the fact that the samples were not sputtered sufficiently long enough to completely remove the carbon contamination (presumably caused by exposure to the atmosphere prior to loading in the AES system).

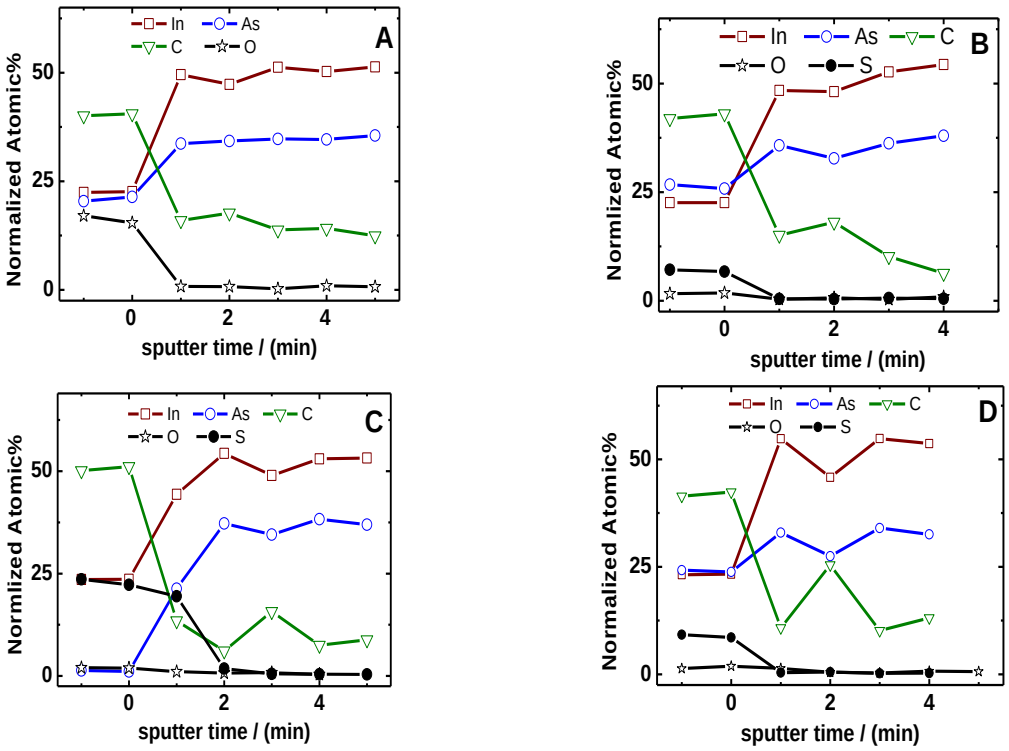


**Figure 5.3:**AES depth profiles for the reference sample (A) and the various treated sample (B), (C) and (D), respectively

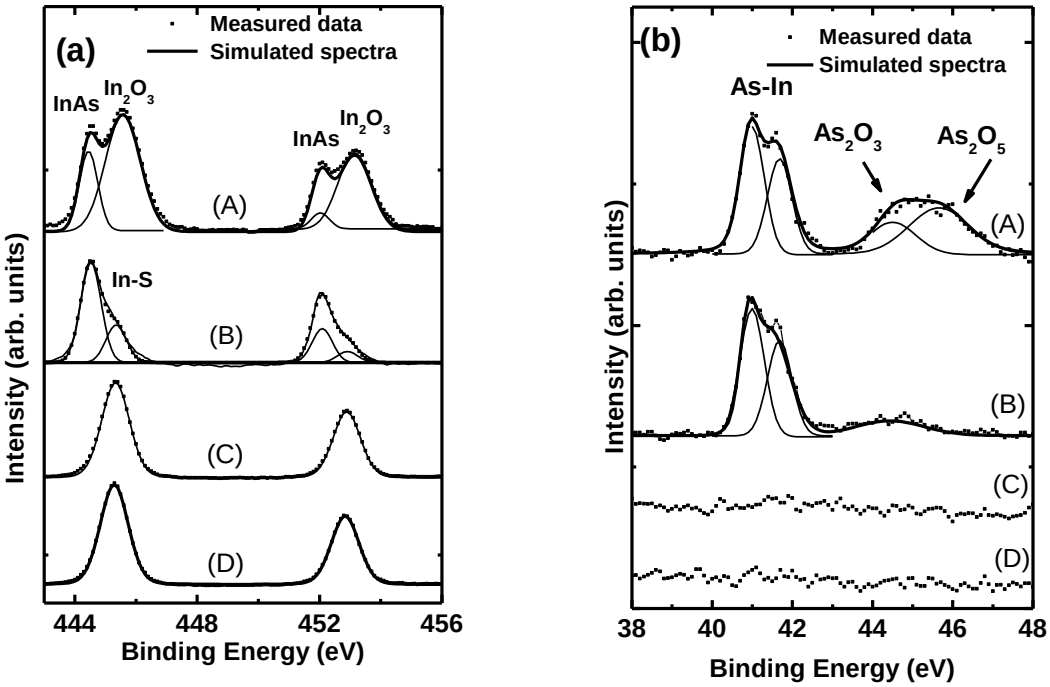


**Figure 5.4:** XPS spectra obtained from the (a) In $3d_{3/2}$ and In $3d_{5/2}$core levels, and (b) the As *3d* core levels for theas-received sample (A), and the various sulphurized samples (B), (C) and (D). The measured data are shown by symbols, while the simulated spectra and Gaussian/Lorentzian components used to simulate the spectra, are shown by thick and thin solid lines, respectively.

Figure 5.4(a) shows narrow XPS spectra of the In$3d_{5/2}$ and In $3d_{3/2}$ core level signals for the reference and treated InAs samples. Gaussian and Lorentzian functions were used to deconvolute the measured signals. The binding energies for the deconvoluted peaks and their possible chemical bonding relationships are listed in Table 5.1. The energies for all the elements and chemical components relevant to the results are presented in this table.

**Table 5-1**: Measured and reported binding energies (eV), and possible chemical components, of XPS core level data for as-received and treated InAs (111) samples.

| | Peak | Measured Binding Energy (eV) | Reported Binding Energy (eV) | Possible chemical component |
|---|---|---|---|---|
| **In *3d*** | $3d_{5/2}$ | 444.5 | 444.5 [46] | InAs |
| | $3d_{5/2}$ | 445.1 | 445.0 [46] | In-S |
| | $3d_{5/2}$ | 445.5 | 445.3 [46] | $In_2O_3$ |
| | $3d_{3/2}$ | 452.1 | | InAs |
| | $3d_{3/2}$ | 452.7 | | In-S |
| | $3d_{3/2}$ | 453.1 | | $In_2O_3$ |
| **As *3d*** | $3d_{5/2}$ | 41 | 41[74] | InAs |
| | $3d_{3/2}$ | 41.8 | 41.7 [74] | InAs |
| | $3d_{3/2}$ | 45.1 | 44.9 [51] | $As_2O_3$ |
| | $3d_{3/2}$ | 46.4 | 46.5 [51] | $As_2O_5$ |
| **O *1s*** | O *1s* | 530.9 | 530.2 [60] | $In_2O_3$ |
| | O *1s* | 531.8 | 531.9[60] | $As_2O_3$ |
| | O *1s* | 532.8 | 532.4[60] | $As_2O_5$ |
| **S *2p*** | S $2p_{3/2}$ | 162.1 | 161.8 [75] | S-In |
| | S $2p_{1/2}$ | 163.3 | 163.3 [76] | S?; S-In ? |

The XPS peaks observed for the as-received sample at a binding energy of 444.5 eV (In $3d_{5/2}$) and 452.1 eV (In $3d_{3/2}$) are assigned to In bonded to elemental As, while those at 445.5 eV (In $3d_{5/2}$) and 453.1 eV (In $3d_{3/2}$) are attributed to indium oxide ($In_2O_3$) [72, 77]. In addition to the InAs peaks, the sample immersed in $Na_2S.9H_2O$ (B) shows a

relatively weak $In_2O_3$ signal, suggesting partial removal of the native oxide for this treatment. Deconvolution of the XPS spectrum reveals the *possible* presence of a very thin In-S surface layer.

For samples C and D, no In-O peaks are observed. Instead, two peaks (In $3d_{5/2}$ and In$3d_{3/2}$ core level signals) shifted in energy by +0.6 eV relative to bulk InAs and ascribed to the In-S bond, are located at 445.1 eV and 452.7 eV, respectively. These results are in good agreement with the reported binding energies for In-S [74, 78].

Figure 5.4(b) depicts XPS spectra of the As*3d* core levels for as-received and treated samples. InAs (~41 eV) and As-O peaks weredetected (44.9 eV to 46.5 eV). The InAs contribution consists of a closely spaced doublet with spin-split energy of 0.80 eV. Deconvolution of the broad peak between 44 eV and 46 eV for the reference samples yielded peaks at ~45.1 eV and ~46.4 eV, which are ascribed to unresolved $3d_{5/2}$and $3d_{3/2}$transitions in $As_2O_3$ and $As_2O_5$.Partial removal (sample B) and complete removal (for samples C and D) of the oxides is evident after treatment. The latter result agrees with the earlier assertion that the surface is covered with S bonded to In for these two samples.

Figure 5.5 shows XPS spectra obtained from the S *2p* core levels for samples B – D. Here, deconvolution of the spectra confirmed the presence of two In-S related peaks, due to the S $2p_{3/2}$ and S $2p_{1/2}$ levelsbetween 161.8 eVand 163.3 eV. These are in good agreement with results reported by Fukuda *et al*. [74] and Ho *et al.*[76].Furthermore, the intensity of the In-S peaks for material treated with $Na_2S.9H_2O$ (B) and [$(NH_4)_2S$ / $(NH_4)_2SO_4$] + S (D) is about 45% lower than for the sample treated with $(NH_4)_2S$+ S (C).

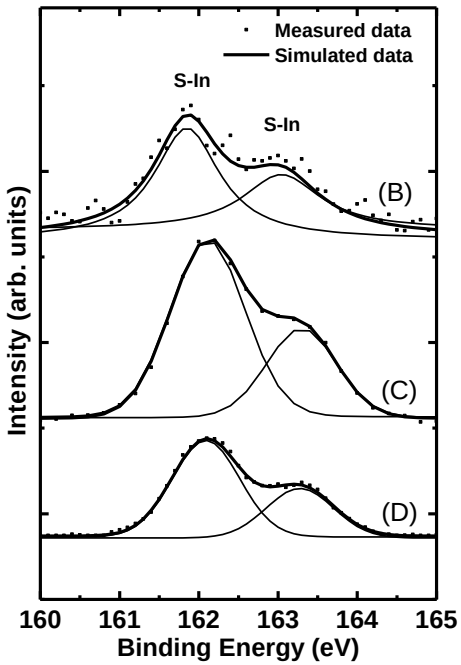


**Figure 5.5:** XPS spectra of the S *2p* core level. The figure shows the measured (symbols), simulated (thick line) and Gaussian/Lorentzian components (thin lines) used to simulate the spectra, for $Na_2S.9H_2O$ (B),( $NH_4)_2S$ + S (C) and [$(NH_4)_2S$ / $(NH_4)_2SO_4$] + S (D) treated samples.

Figure 5.6 depicts the O *1s* core levels for samples A – D. As pointed out earlier, AES (due to its lower sensitivity compared to XPS) did not reveal the presence of oxygen on samples C and D, whereas a broad band resulting from multiple native oxides (In-O and As-O) could still be detected by XPS from these samples. Three peaks at 530.9 eV ($In_2O_3$), 531.8 eV ($As_2O_3$) and 532.8 eV ($As_2O_5$) were detected for the as-received sample. The partial removal of the native oxides upon sulphurization is evident for samples B – D, with the smallest signal detected for the sample treated with [$(NH_4)_2S/(NH_4)_2SO_4$] + S (sample D). This sample also had the smoothest surface as observed by SEM (Fig. 5.1). The residual native oxides could not be detected in samples C and D from the narrow XPS spectra obtained for the In$3d_{5/2}$, In $3d_{3/2}$ and As *3d* core level signals.

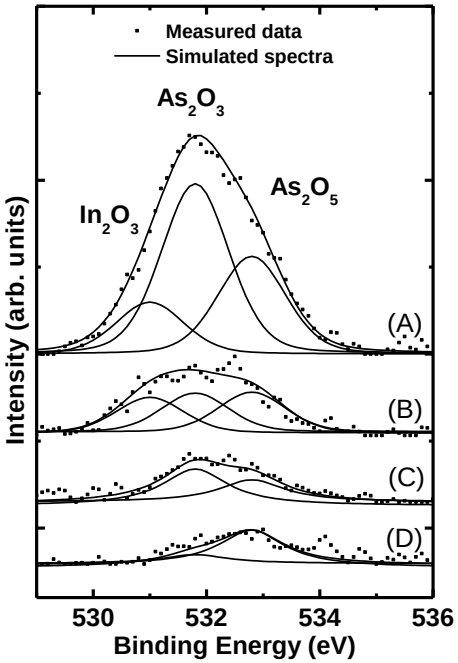


**Figure 5.6:**XPS spectra of O *1s* for the as-received sample (A), and the various treated samples (B – D).

Figures 5.7 and 5.8 show the XPS signal strengths of the O *1s* and S *2p* core levels for samples C and D, respectively. The data was collected over a period of 10 days in order to investigate the stability of the sulphur-terminated surface of these samples after treatment. The oxide-related signals progressively increase with time. In addition, the O and S present on the InAs surface seem to have an inverse relationship, i.e. an increase in O is accompanied by a decrease in S, suggesting that desorption of the S enhances re-oxidation. The amount of sulphur adsorbed onto sample C (see Fig. 5.5) is greater than for sample D, suggesting that a larger sulphur concentration after treatment does not imply more effective removal of the native oxide. The high amount of sulphur observed on sample C could also be due to the accumulation of sulphur atoms on the surface (see Fig. 5.1).

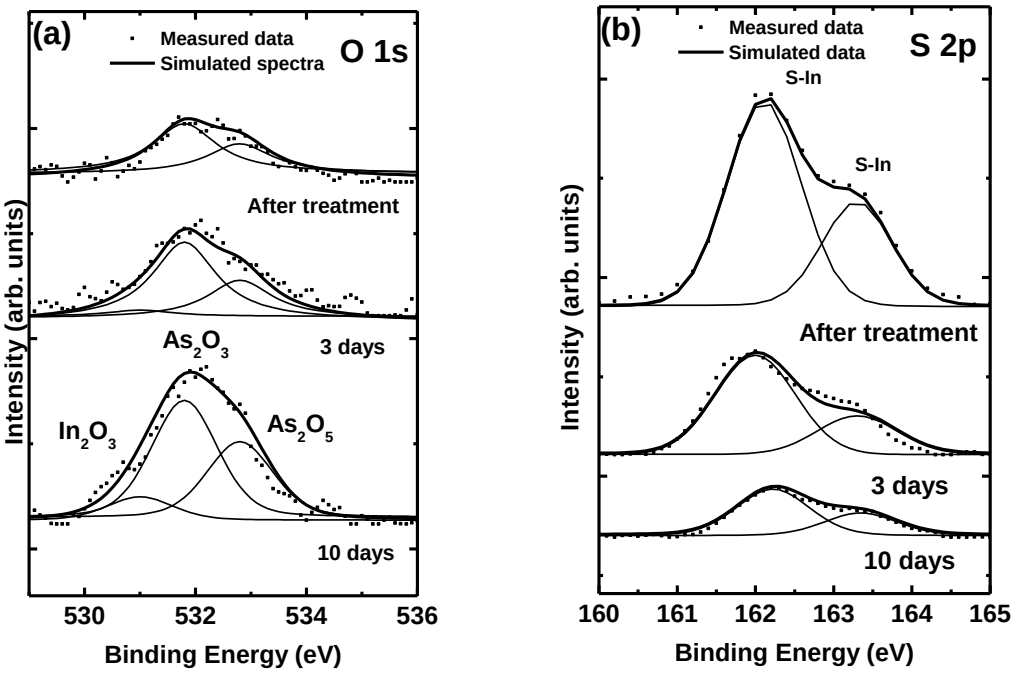


**Figure 5.7:**XPS spectra of (a) the O *1s* core level and (b) the S *2p* core level collected for sample C over a period of 10 days.

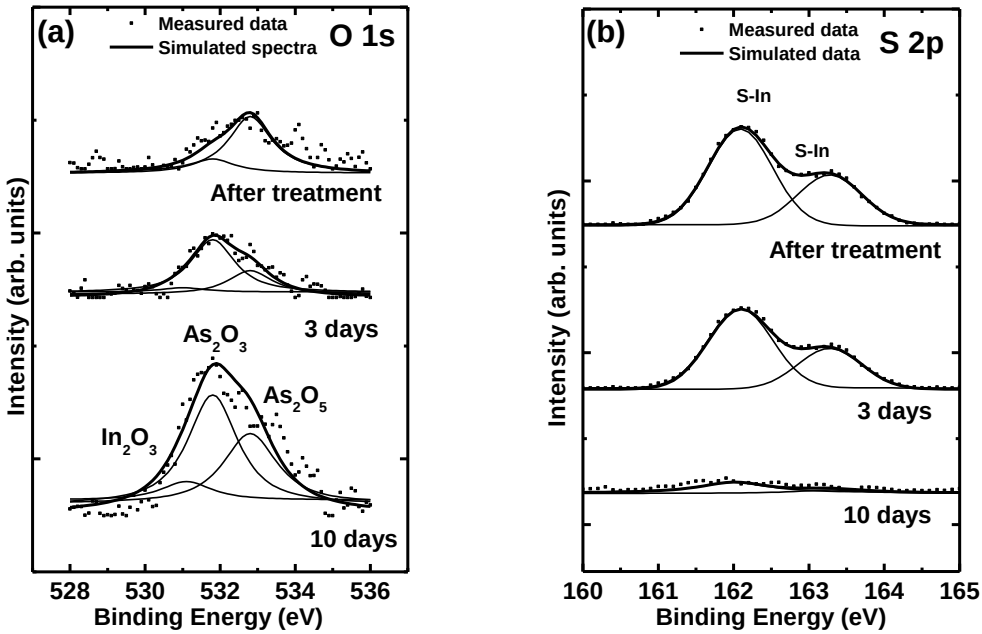


**Figure 5.8:**XPS signal strengths of (a) O *1s* core level (b) S *2p* core level collected for sample D over a period of 10 days.

The results presented in this chapter verify that treatment with unsaturated $Na_2S.9H_2O$ results in the partial removal of $In_2O_3$ fromsample B, as seen in Fig. 5.6. The small amount of $H_3O^+$ present through the hydrolysis reaction of $(NH_4)_2S$, according to equations (3-5) to (3-9), have facilitated the complete removal of $In_2O_3$ from sample C and D, as observed.

The removal of the native As-O from the InAs surface (as is evident from the XPS results shown in Fig. 5.6) is ascribed to the chemical reactions of the sulphur-based solutions (B – D) with the native oxides $As_2O_3$ and $As_2O_5$, whichresult in the formation of a number of ionic species of $As^{3+}O$, $As^{3+}S$, $As^{5+}O$ and $As^{5+}S$. These include:

$$AsO_3^{3-},\ AsO_2S_1^{3-},\ AsO_1S_2^{3-},\ AsS_3^{3-},\ AsO_4^{3-},\ AsO_3S_1^{3-},\ AsO_2S_2^{3-},\ AsO_1S_3^{3-} and AsS_4^{3-}.$$

These species are soluble in water and stable in alkaline media. It is clear from Fig. 5.6 that, in the case of treatments C and D, $As_2O_3$ was effectively removed from the surfaces of samples treated with $(NH_4)_2S$ + S (C) and $[(NH_4)_2S$ / $(NH_4)_2SO_4]$ + S (D), while for samples treated with $Na_2S.9H_2O$ (B), a noticeable amount of $As_2O_3$ still remained. This observation is attributed to the higher solubility of the As ion species in $[(NH_4)_2S]$ + S and $[(NH_4)_2S$ / $(NH_4)_2SO_4]$ + S solutions compared to $Na_2S.9H_2O$. Furthermore, the dissociation of $(NH_4)_2SO_4$ produces a higher amount of $H_3O^+$ in solution according to equation (3-9). This enhances the solubility of the native As-O together with the conversion of $As^{3+}$ to $As^{5+}$, as indeed observed from sample D.

## 5.3 Raman Spectroscopy

Both longitudinal optical (LO) and transverse optical (TO) phonon modes are allowed for scattering from the InAs (111)A surface in a pseudo-backscattering configuration. Scattering from the TO mode occurs in the bulk and near-surface regions, while the scattering from the bare LO phonon originates from the surface and is affected by the electric field present near an accumulated surface (the so-called electric field induced Raman scattering or EFIRS) [9]. The efficiency of the LO mode scattering is influenced by the accumulation layer as well as by a change in the surface electric field, which

changes the relative contributions from the two modes observed in the Raman spectrum.

Figure 5.9 shows Raman spectra obtained for InAs (111)Awith n ~ 2 × $10^{16}$ $cm^{-3}$before and after $(NH_4)_2S$ + S or $[(NH_4)_2S/(NH_4)_2SO_4]$ + S treatments. All the spectra show two Raman modes: the low frequency phonon-Plasmon mode (TO) near 219 $cm^{-1}$, and the unscreened LO phonon mode at ~239 $cm^{-1}$[79]. The spectra were normalised with respect to the mode at the lower wave numbers. It is clear that the intensity of the LO phonon signal decreases after chemical treatment. This reduction in the LO mode integrated intensity indicates a decrease in the width of the accumulation region, resulting in a smaller scattering volume for the LO phonons. The highest relative intensity related to the LO phonon signal is observed for untreated samples. XPS analysis indicated an oxygen concentration on the surface of ~34% for the untreated samples, compared to 11% and 5% for the samples treated with $(NH_4)_2S$+ S and $[(NH_4)_2S/(NH_4)_2SO_4]$ + S, respectively. Oxide removal seems to be most effective for samples treated with $[(NH_4)_2S$ / $(NH_4)_2SO_4]$ + S. The observed enhanced removal of the native oxide inthese cases is attributed to the availability of $H_3O^+$ through a hydrolysis reaction, as discussed previously.

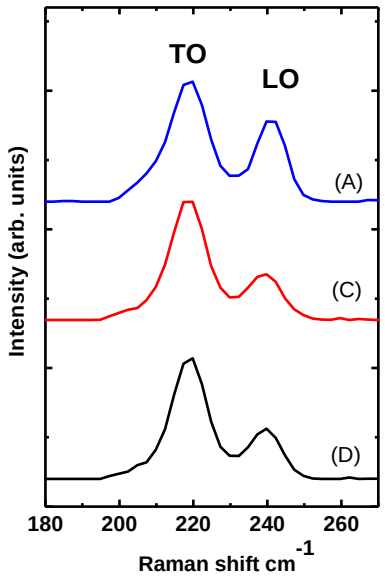


**Figure5.9:**Raman spectra of *n*-InAs (111)A collected before and after $(NH_4)_2S$ + S (sample C) or $[(NH_4)_2S/(NH_4)_2SO_4]$ + S (sample D) treatment. The spectra were normalised with respect to the transverse optical phonon (TO).

A combination of Raman scattering and XPS measurements were carried out in order to investigate the possible relation between surface band bending, as indicated by the reduction of $I_{LO}/I_{TO}$as described in equation (4-9), and the surface coverage of sulphur and oxygen. Figure 5.10 shows the intensity ratio of the LO and TO modes, $I_{LO}/I_{TO}$, for the treated and untreated samples versus (a) the residual oxygen atomic percentage and (b) the surface concentration of sulphur, obtained using XPS. A decrease in the $I_{LO}/I_{TO}$ ratio after chemical treatment, from 0.5 for the untreated sample to 0.36 and 0.28 for the samples treated in $(NH_4)_2S$+ S and $[(NH_4)_2S/(NH_4)_2SO_4]$ + S, respectively, is observed. It is clear that there is a correlation between the degree of band bending and the surface oxygen concentration, with the largest band bending (i.e. largest $I_{LO}/I_{TO}$ ratio) observed for the untreated sample, which also has the largest oxygen surface coverage (see also Figs.(5.4) and (5.6)). Although there is no clear correlation between the $I_{LO}/I_{TO}$ratio (i.e. amount of band bending) and sulphur coverage on the surface, it is tempting to ascribe the reduction in band bending to the removal of oxygen-related states, resulting from the replacement of In-O bonds with In-S bonds.

The results show that the degree of band bending is inversely proportional to the oxygen concentration. This suggests that the native oxide which results from exposure to air causes surface states and may enhance the accumulation of charge on the surface.

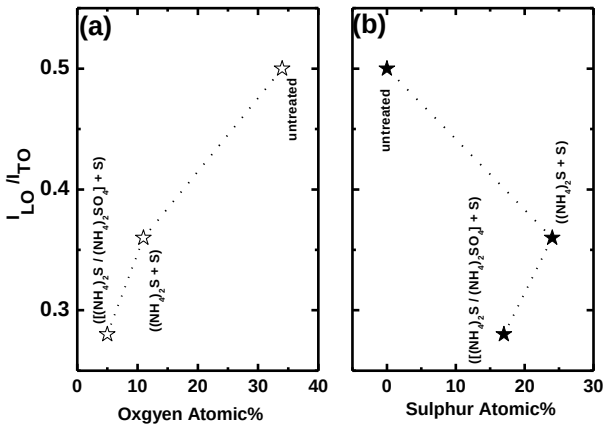


**Figure 5.10:** The $I_{LO}/I_{TO}$ ratio as a function of surface oxygen and sulphur atomic percentages for untreated bulk InAs (111)A and samples treated in $(NH_4)_2S$ + S (sample C) and $[(NH_4)_2S/(NH_4)_2SO_4]$ + S (sample D).

## 5.4 Photoluminescence Spectroscopy

Figure 5.11 shows the low temperature PL spectra of samples A, C and D. The PL spectra were obtained at 3.5 K with a laser power of 5 mW. All the PL spectra show five emission lines at 0.4185eV, 0.414 eV, 0.403 eV, 0.382 eV and 0.373eV. The line at 0.4185eV is ascribed to band-to-band transitions, while the emission lines at 0.414 eV and 0.403 eV are attributed to donor-bound exciton transitions. The low energy transitions at0.382eV and 0.373 eV are due to donor-acceptor pair recombination [80, 81].

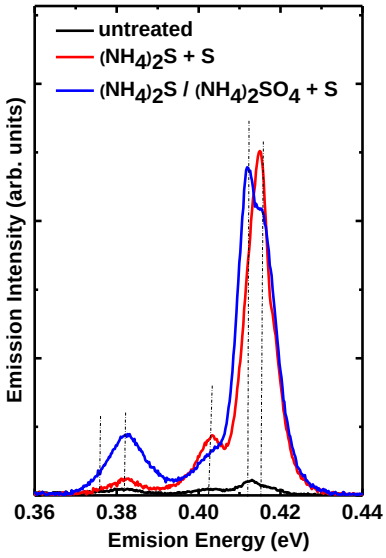


**Figure 5.11:**Photoluminescence spectra at 3.5 K (laser power of 5 mW) of samples A, C and D.

It is clear that both the $(NH_4)_2S$ + S and $[(NH_4)_2S/(NH_4)_2SO_4]$+ S treatments result in an increase in the PL intensity by a factor of ~20. The enhancement in PL intensity is ascribed to the removal of the native oxides on the surface, which reduces the surface statedensity and hence the accumulation layer width. Chang *et al*. [82] discussed the role of surface recombination velocity and band bending on the PL response of InP. They concluded that surface space-charge leads to a reduction in the radiative recombination caused when photo-excited electrons and holes are separated by the near-surface electric field. The PL intensity is enhanced if the magnitude of the band

bending (and hence the width of the accumulation layer) is decreased. It is also known that the surface recombination velocity is proportional to the density of surface states [82,83]. A high surfacestate density will consequently lower the overall PL intensity.

In conclusion, the treatment of InAs (111)Awith ([$(NH_4)_2S$ / $(NH4)_2SO_4$] + S) effected a significant improvement over other treatment procedures in the surface morphology of the as-received surface. From AES depth profiles, the native oxide was estimated to be less than 8.5 nm thick, as a sputter rate of 8.5 nm/min resulted in their complete removal from the surface. Treatment of the material in all the chalcogen-based solutions employed in this study resulted in partial ($Na_2S.9H_2O$) or complete removal ([$(NH_4)_2S$] + S) and ([$(NH_4)_2S$ / $(NH4)_2SO_4$] + S) of the indium oxide from the surface with minimal surface degradation. Regarding the latter two treatments, an In-S layer "replaced" the In-O instead, suggesting that chemisorbed S atoms substituted O (in In-O) to form a thin In-S layer. Oxide removal seems to be most effective for samples treated with ([$(NH_4)_2S$ / $(NH_4)_2SO_4$] + S). Finally, the treated surfaces, assessed over a period of 10 days, show poor short term stability with the lowest re-oxidation rate observed for ([$(NH_4)_2S$ / $(NH4)_2SO_4$] + S). The observed enhanced removal of the native oxide, $In_2O_3$ in the case of samples treated with ([$(NH_4)_2S$] +S) and ([$(NH_4)_2S$ / $(NH4)_2SO_4$] + S), is attributed to the availability of $H_3O^+$ through a hydrolysis reaction, while the efficient removal of As-O is accounted for by its higher solubility in the ([$(NH_4)_2S$ / $(NH4)_2SO_4$] + S) solution. From Raman scattering it could be deduced that these chemical changes on the surface result in a reduction in the band bending near the surface. The improvement in both the electronic properties and the enhancement of the PL intensity after treatment correlate with the surface de-oxidation.

# Chapter 6

## Halogen Etching of Bulk InAs (111)A

This chapter discusses the properties of bromine-methanol and HCl:$H_2O$-etched InAs (111)A surfaces, for different etching times and etchant concentrations. The chemical compositions of the surfaces were investigated using X-ray photoelectron spectroscopy (XPS) and the surface morphology was studied using scanning electron microscopy (SEM). Raman spectroscopy and photoluminescence (PL) spectroscopy were again used to evaluate the electronic/optical properties of the near-surface region of the material.

### 6.1 Surface Morphology

Surface modifications of halogen-etched III-V semiconductors have received considerable attention. Many authors have attempted to explain the surface modifications and the mechanisms responsible for these changes [52]. However, few studies have been conducted to understand the mechanism of surface etching, as well as the influence of etchant concentration and etching time of halogen-based etchants for InAs [84], particularly for PL obtained from as-grown and chemically etched InAs (111)A.

Figure 6.1 shows SEM micrographs for the as-received and halogen-etched InAs surfaces, using different etch times and etchant concentrations. The as-received sample shows randomly distributed etch pits and scratches. Surfaces etched in a 1:1 HCl:$H_2O$ solution for 1 min were much smoother, and similar improvements were observed for surfaces etched in 1% Br-methanol for 1 min. Increasing the etch time to 5 min for 1:1 HCl:$H_2O$ resulted in etch pits, which are more densely distributed along the scratches.

Surfaces etched in 1% Br-methanol for 10 min, in 2:1 HCl:$H_2O$ for 5 min and in 1% Br-methanol for 30 min are also shown in Fig. 6.1. Etching with 2:1 HCl:$H_2O$ for 5 min, or etching for longer than 1 min in the bromine solutions resulted in the formation of inverted pyramids, with {111} side planes, suggesting anisotropic etching of InAs (111)

using these etchants. The formation of large hexagonal pits (up to 3 μm across) was observed after for 30 min in the 1% Br-methanol solution. Tarui*et al.* [85] studied the anisotropic etching of GaAs in a 1% to 6% Br-methanol system. They observed that the etch rate depended strongly on the planes where the etch rate of (111)As> (100) > (111)Ga for a given concentration. Several conclusions were drawn from this study:

i) The (111)A plane has the lowest etch rate, and
ii) The anisotropic etch ratio of (111)As/(111)Ga depends markedly on the bromine concentration.

In the present study, this suggests that the features observed after 1 min of etching contributed to the difference in the etch rates of (111)A and (111)B planes.

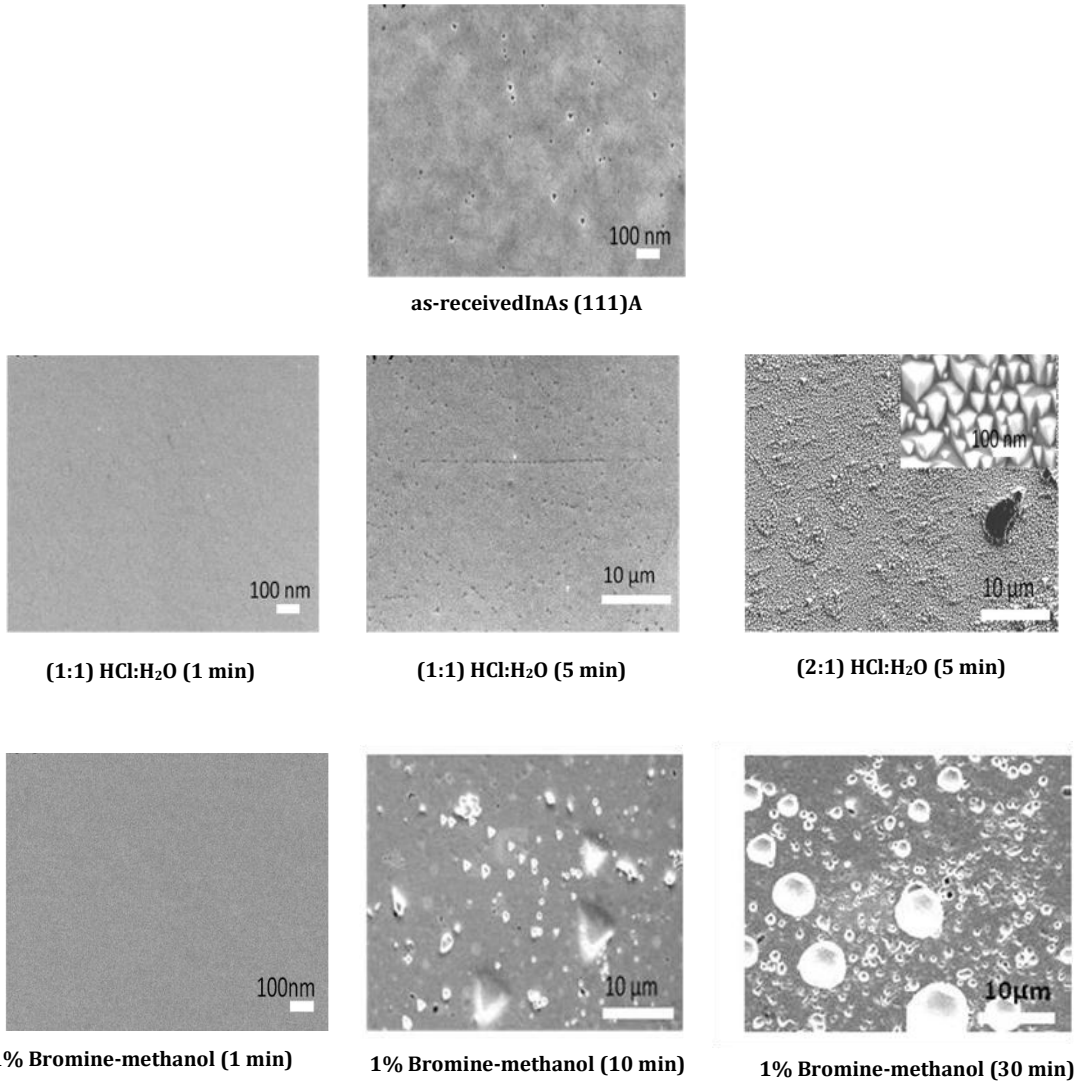


**Figure 6.1:** The effect of halogen-based etchants on the surface morphology of InAs (111)A.

## 6.2X-ray Photoelectron Spectroscopy

Figures 6.2 and 6.3 show XPS spectra of the In $3d_{3/2;5/2}$(a and e), As *3d* (b and f), O *1s* (c and g), Br $3d_{3/2;5/2}$ (d), and Cl$2p_{1/2;3/2}$ (h)core level signals for as-received and etched surfaces. The measured data is represented by squares, while the solid and thin lines represent Gaussian and Lorentzian functions employed to deconvolute the measured signals.Deconvolution of the In $3d_{3/2;5/2}$ core level spectra for the as-received sample (Fig. 6.2(a) and Fig. 6.3(e)) reveals the presence of two constituent compounds on the surface. The peaks observed at 444.1 eV and 451.6 eV are assigned to theIn-As chemical bond, while those at 445.1 eV and 452.7 eV correspond to $In_2O_3$.

The As*3d* core level spectra are shown in Fig. 6.2(b) and Fig.6.3(f). The In-As doublet is detected at ~40.5 eV and ~41.2 eV respectively.A broad signal between 44 eV and 46 eV, resulting from $As_2O_3$ and $As_2O_5$, is also observed.

Deconvolution of the O *1s* core level signal in Fig. 6.2(c) and Fig. 6.3(g) clearly shows that it consists of three contributions, with binding energies observed at 530.6 eV, 531.1 eV and 531.8 eV, and these are assigned to $In_2O_3$, $As_2O_3$ and $As_2O_5$, respectively.

Turning our attention to the etched samples, it is evident that etching in a 1% Br-methanol solution results in the complete removal of the native oxides (Fig. 6.2(a-c)). Systematic shifts to higher energies are observed for the In*3d* and As *3d* core level spectra in Fig. 6.2(a, b), and Fig. 6.2(d) shows the Brsignals at 68.8 eV ($3d_{3/2}$) and 69.8 eV ($3d_{5/2}$). The Br $3d_{3/2}$ and$3d_{5/2}$ signals are observed only after exposure to bromine for a period of 30 min.

Etching in a 1:1 HCl:$H_2O$solution also results in the complete removal of the native oxides (Fig. 6.3(a-c)), while evidence for arsenic oxide remaining on the surface after etching in a 2:1 HCl:$H_2O$ solution is evident in Fig. 6.3(c). The Cl spectra (Fig. 6.3(d)) reveal the presence of Cl on the etched surface in all cases, with the two peaks at 198.3 eV and 199.7 eV attributed to the chlorine $2p_{3/2}$ and $2p_{1/2}$ states of electrons, respectively. The peak at 204.3 eV is possibly due to contributions from Cl-O species (see Fig. 6.3 (g)).

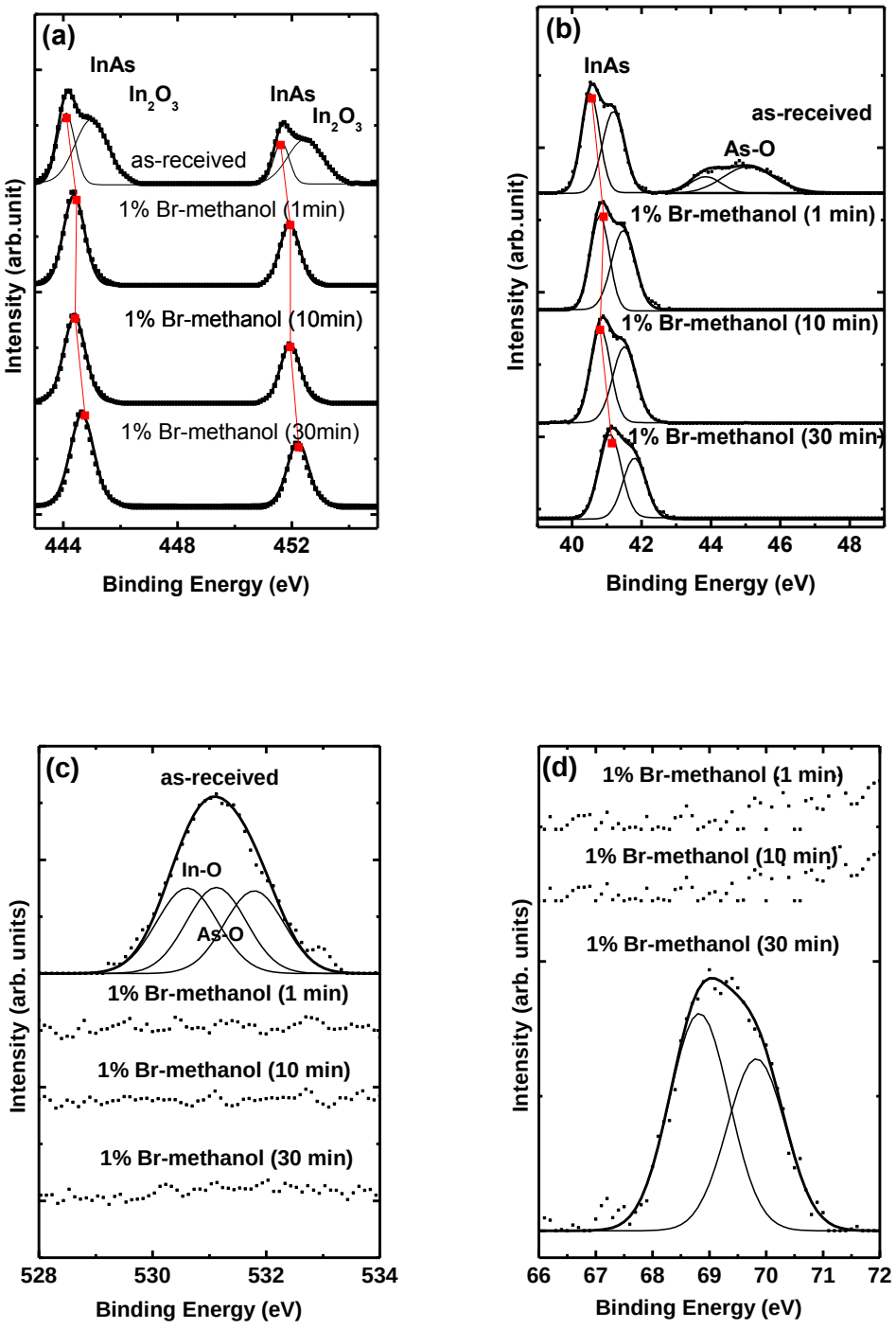


**Figure 6.2:** XPS spectra for samples etched in 1% bromine-methanol, obtained from the (a) In $3d_{3/2}$ and In $3d_{5/2}$, (b) As 3d, (c) O 1s, and (d) Br $3d_{3/2}$ and Br $3d_{5/2}$ core levels. The measured data is represented by squares, while the thin solid lines represent the fitted spectra.

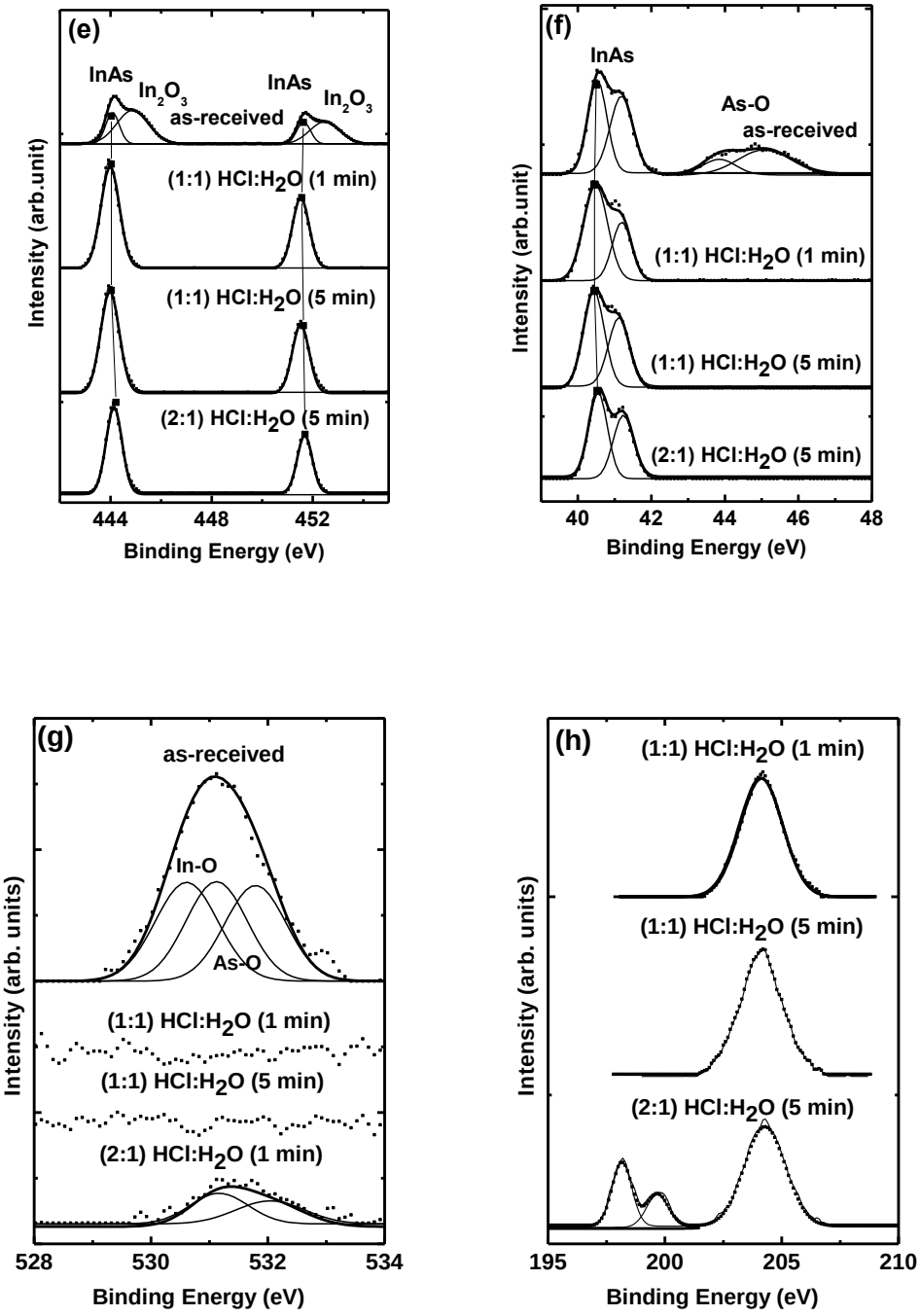


**Figure 6.3**: XPSspectra for samples etched in $HCl:H_2O$ obtained from the (e) In $3d_{3/2}$ and In $3d_{5/2}$, (f) As $3d$, (g) O $1s$, and (h) Cl$3d_{1/2}$ and Cl$3d_{3/2}$ core levels. The measured data is represented by squares, while the thin solid lines represent the fitted spectra.

The shifts in the In$3d_{3/2}$, In $3d_{5/2}$and As *3d* core level binding energies with etch time/concentration are ascribed to bromine and chlorine adsorption. The increase in binding energy is in accord with the progressive formation of In-Br, As-Br, In-Cl and As-Cl bonds when In-As bonds are broken in the presence of elemental bromine/chlorine. Similar effects were reported for halogen-etched III-V semiconductors [86, 87], in particular for bromine and chlorine adsorption onto GaAs(110) and (100) surfaces [88]. It has also been reported that the core level chemical shift increases linearly with the number of halogen atoms attached to the host atoms [51, 88], suggesting that in the present work the chemical shifts result from the formation of As-$Br_x$ , In-$Br_x$,As-$Cl_x$ and In-$Cl_x$compounds (x = 1, 2, 3). The formation of these compounds also explains the complete dissociation of the native oxides ($In_2O_3$, $As_2O_3$, $As_2O_5$), deduced from the disappearance of the O *1s* signal after etching or partial dissociation of As-O.

### 6.3 Raman Spectroscopy

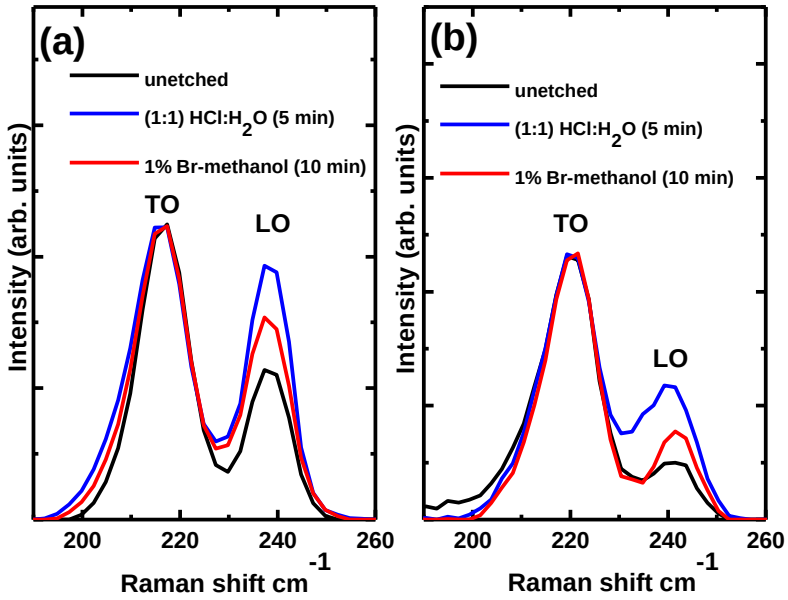


**Figure 6.4:** Raman spectra of InAs (111)A measured using an Ar ion laser before and after etching using (a) the 488 nm line and a laser power of 120 mW, and (b) the 514.5 nm line and a laser power of 40 mW.

Figure 6.4 compares the Raman spectra obtained before and after etching in the various solutions, using different wavelengths of the Ar ion laser: (a) 488 nm and (b) 514.5 nm.The spectra were normalised with respect to the intensity of the TO mode of the reference sample. The spectraillustrate that the LO/TO intensity ratio is larger in the case of excitation with 488 nm, i.e. for shallower penetration of the incident light, which enhances the role of the near-surface region in the Raman spectrum, irrespective of the sample treatment, confirming that the LO mode originates from the near-surface region and the TO mode from the bulk, in good agreement with the results reported by Geurts[9].

Figure 6.5 shows the measured integrated intensity ratios $I_{LO}/I_{TO}$, measured using the Raman spectra of as-receivedInAs (111)A and for the differently etched samples. The values of $I_{LO}/I_{TO}$ are used to qualitatively assess surface band bending, using the knowledge that the laser light scatters off the TO phonon in the bulk of the samples and off the LO phonon in the near-surface region.

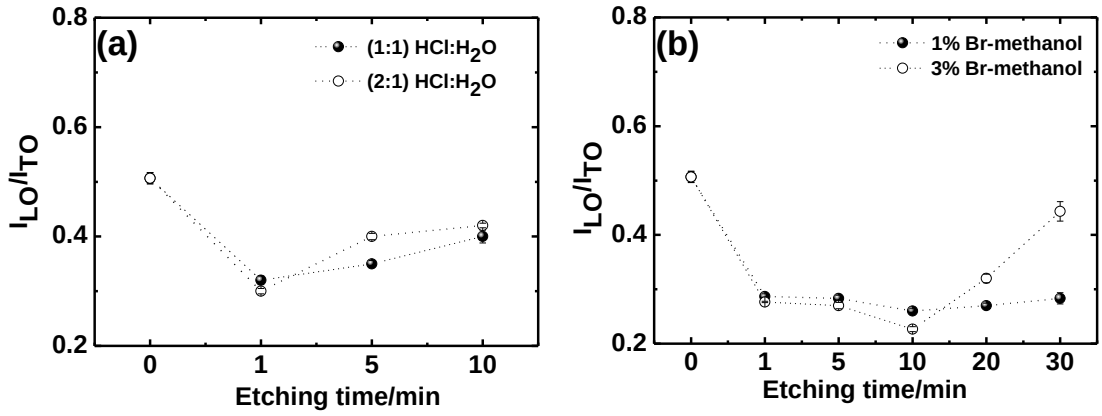


**Figure 6.5:**Measured intensity ratios $I_{LO}/I_{TO}$ from the Raman spectra as a function of etching time fordifferently etched InAs (111)A surfaces.

The results show that $I_{LO}/I_{TO}$ is most effectively reduced after a 1 min etch in (1:1)HCl:$H_2O$ and after 1-10 min etching in Br-methanol. The ratio increases upon a further increase in etch time and etchant concentration. The decrease in the $I_{LO}/I_{TO}$ intensity ratioafter chemical etching indicates a decrease in the LO phonon scattering

volume, which is expected for lower band bending compared to the reference sample. Increasing the etching time / etchant concentration probably increases the band bending due to the fact that more halogen atoms are adsorbed on the InAs surface. Furthermore, the adsorption of halogen atoms can introduce virtual gap states (VGSs), which can pin the Fermi level at the semiconductor surface, as suggested by Mönch*et al*. [33].It should be noted that an increase in the etchant concentrations and etch times also introduces morphological defects on the InAs surface, as seen by SEM (Fig. 6.1). These defects were observed to broaden the Raman lines due to inhomogeneous strain near the surface, which lowers the lattice symmetry, as reported by Evans [90].

## 6.4 Photoluminescence Spectroscopy

Fig. 6.6(a) shows PL spectra for the reference sample (A) and the samples etched in bromine-methanol solutions (B-D), while Fig. 6.6(b) compares the PL of the reference sample to that of the samples etched in HCl:$H_2O$ solutions (E-G). In all cases, the PL spectra contain the same five emission lines as pointed out in Chapter 5.

It is clear that HCl:$H_2O$ or bromine-methanol etching results in an increase in the PL intensity, with a gradual decrease in intensity observed for longer etch times. The reduction in PL intensity is more pronounced for prolonged etching in HCl:$H_2O$. The poor response for un-etched bulk InAs (111)A is attributed to the presence of an accumulation layer resulting from a high density of surface states. As before, it is again tempting to ascribe the enhancement in the PL intensity to the removal of the native oxides on the surface, which will reduce the surface state density and hence the accumulation layer width. Prolonged etching in Br-methanol or HCl:$H_2O$, however, gives rise to the adsorption of bromine or chlorine, which could introduce new surface states responsible for the observed drop in PL intensity after etching for more than 1 min. The significant degradation in PL intensity when etching with HCl:$H_2O$ contributed to adsorption of chlorine and oxygen atoms on the surface on the surface (see Fig. 6.3 (h) and Fig. 6.3(g)).

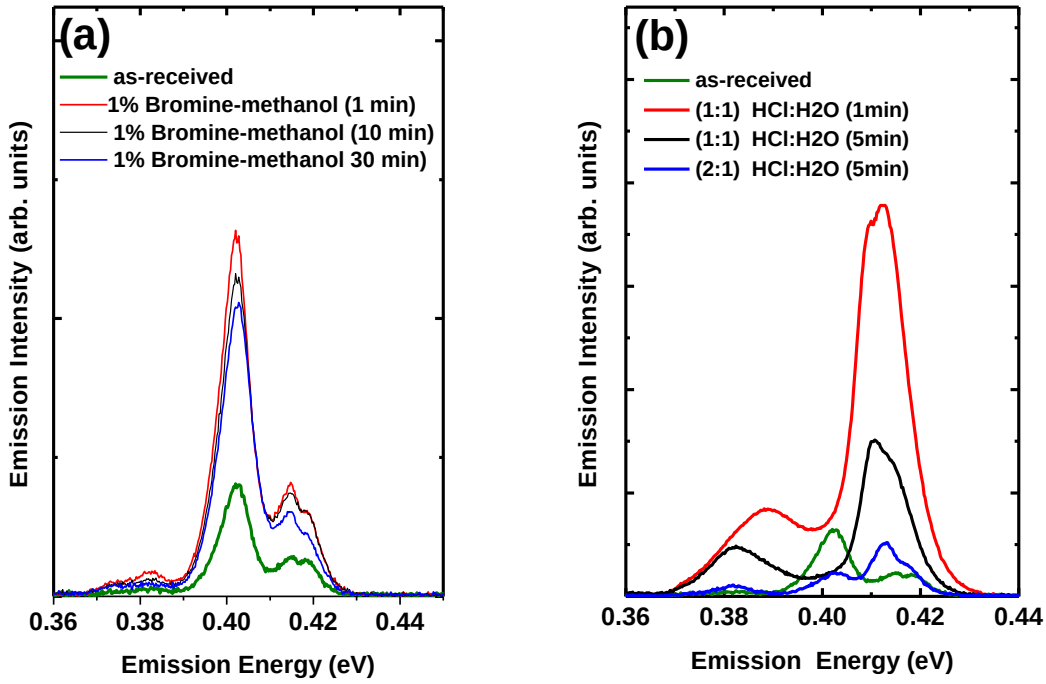


**Figure 6.6:** (a) Photoluminescence spectra at 3.5 K (laser power = 3 mW) for the reference sample (A) and bulk InAs (111)A samples etched in (a) bromine-methanol (B-D) and (b) HCl:$H_2O$ (E-G).

Figure 6.7(a) shows the Raman spectra obtained for samples A and B. For sample B, Raman spectra were also obtained as a function of exposure time to air. The spectra were normalised with respect to the TO mode at lower wave numbers. It is clear that the intensity of the LO phonon signal decreases following chemical treatment. As mentioned above, this is due to a decrease in the width of the accumulation layer, resulting in a smaller scattering volume for the LO phonon. Subsequent exposure to air results in an increase in the intensity of the LO phonon mode, and this suggests that the native oxide which results from exposure to air causes surface states. This may enhance the accumulation of charge on the surface, which will be accompanied by an increased depth of the accumulation region.

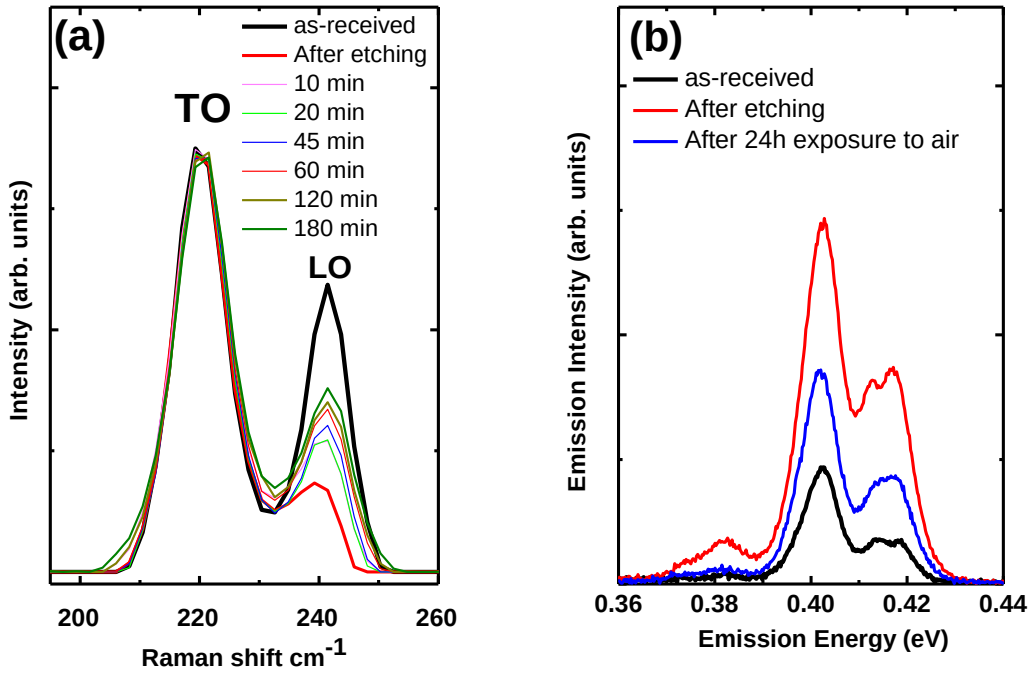


**Figure 6.7:** (a) Raman spectra obtained from the reference sample and the sample etched in 1% Br-methanol for 1 min. The Raman spectra obtained following exposure to air for different periods are also shown. (b) Low temperature PL response of the sample etched for 1 min, before and after exposure to air for a period of 24 hours. The spectrum from the reference sample is included for comparison.

In summary, both etchants show anisotropic etching of InAs (111)A surfaces. Raman scattering showed a significant reduction of the band bending after etching in 1:1 and 2:1 HCl:$H_2O$ (1 min), or in 1% and 3% Br-methanol (10 min). These concentrations and etch times also yielded relatively smooth and defect-free surfaces. On the other hand, longer exposure times and higher etchant concentrations increased band bending, also leading to strong anisotropic etching effects, which resulted in irregular surfaces with faceted pits.

The PL spectra of *n*-type InAs (111)A etched in a 1% Br-methanol and HCl:$H_2O$ solution have been studied. The removal of the native oxide on the InAs surface, as observed by XPS, resulted in a significant reduction in charge accumulation at the surface. This was accompanied by a significant enhancement in the PL intensity after a 1 min etch, and by a slight reduction in intensity for longer etch times. The enhancement is correlated with

the removal of native oxides from the surface for short etch times, while for longer etch times; bromine/chlorine adsorption probably leads to the formation of additional surface states, consequently quenching the photoluminescence. These results support the notion that native oxide-induced surface states and enhanced charge accumulation form at the (111)A surface of InAs.

# Chapter 7

## Thermal Oxidation of Bulk InAs (111)A and (100)

This chapter focuses on the characterisation of thermal oxide films formed after annealing between 350°C and 550°C for 45 min on both InAs (111)A and (100). The surface morphologies and photoluminescence of as-received and thermally oxidised surfaces were investigated using scanning electron microscopy (SEM) and photoluminescence (PL) spectroscopy. The compositions of the oxide film and the surface electronic structure for the oxide layer formed at 450°C were studied using X-ray photoelectron spectroscopy (XPS) and Raman spectroscopy.

### 7.1 Surface Morphology

Many attempts have been made to understand the fundamental processes underlying material oxidation and in developing device applications for the oxides. However, oxidised III-V surfaces are generally disordered [59,61] and the formation of high quality oxides remains a subject of continued research. The poor quality of the oxides on InAs has made it difficult to perform photoluminescence and electrical measurements on this material. As a result, there are very few reports available on photoluminescence measurements performed on thermally oxidisedInAs.

Figures 7.1 (A) and (E) show the surface morphologies of as-received InAs (111)A and InAs (100), respectively. InAs (111)A samples annealed in an oxygen ambient at different temperatures are shown in Fig. 7.1 (B-D), while the surfaces of InAs (100) samples annealed under the same conditions are shown in Fig. 7.1 (F-H). The reference samples in Fig. 7.1 (A and E) show randomly distributed etch pits and scratches. Relatively smooth surfaces were obtained for the samples annealed in $O_2$ at 350°C - 450°C for 45 min (B, C, F, G), indicative of the formation of a surface oxide layer. Increasing the annealing temperature to 550°C (D and H) resulted in the formation of

non-uniformly distributed poly-crystallites. These features could result from the out-diffusion of elemental arsenic from the InAs surface.

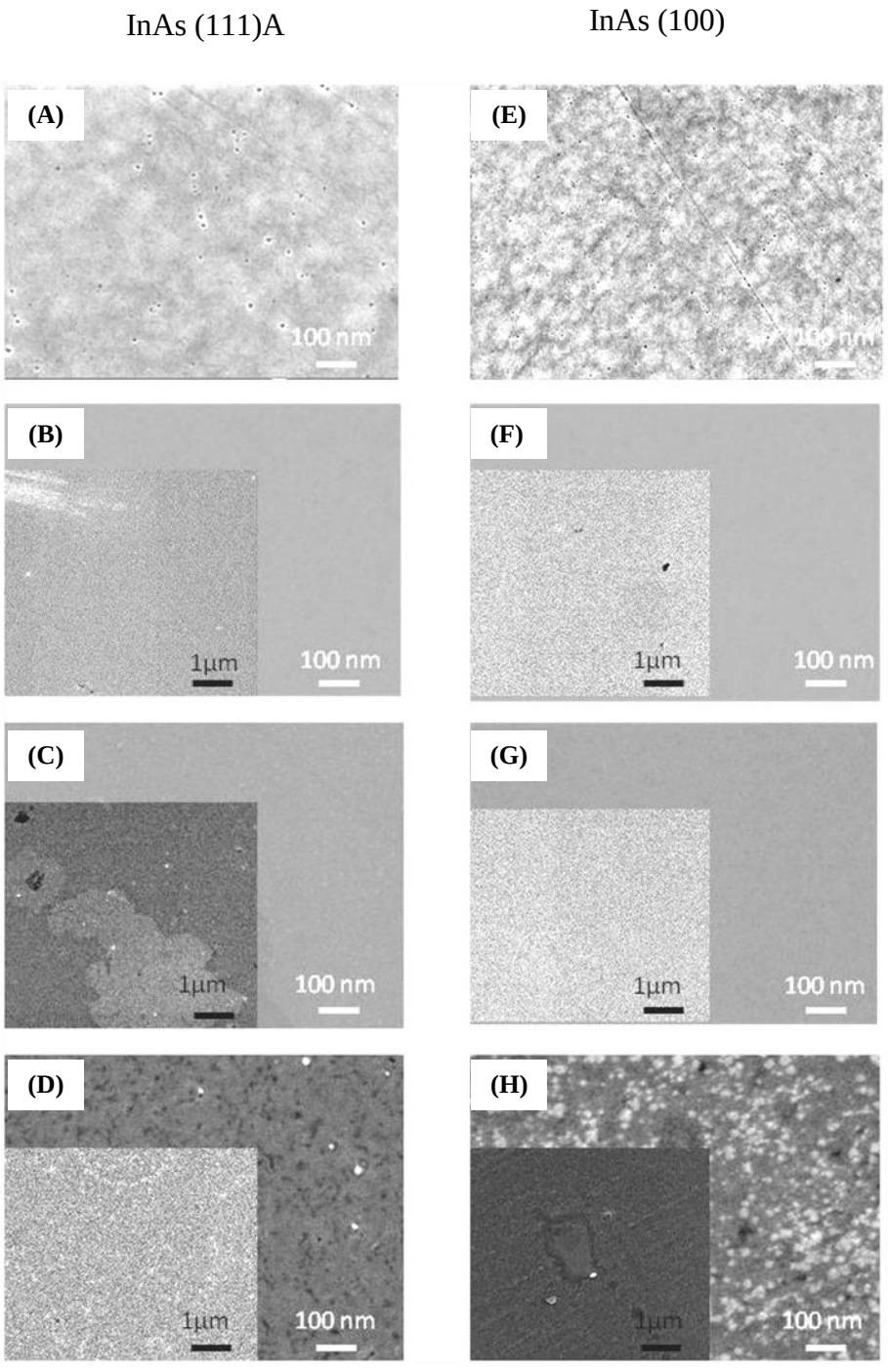


**Figure 7.1:** SEM micrographs of the as-received and thermally oxidised InAs (111)A and (100) surfaces: (A)and (E) are the as-received samples; the other samples were annealed in an oxygen ambient for 45 min at 350°C (B and F); at 450°C (C and G) and at 550°C (D and H).

## 7.2 Photoluminescence Spectroscopy

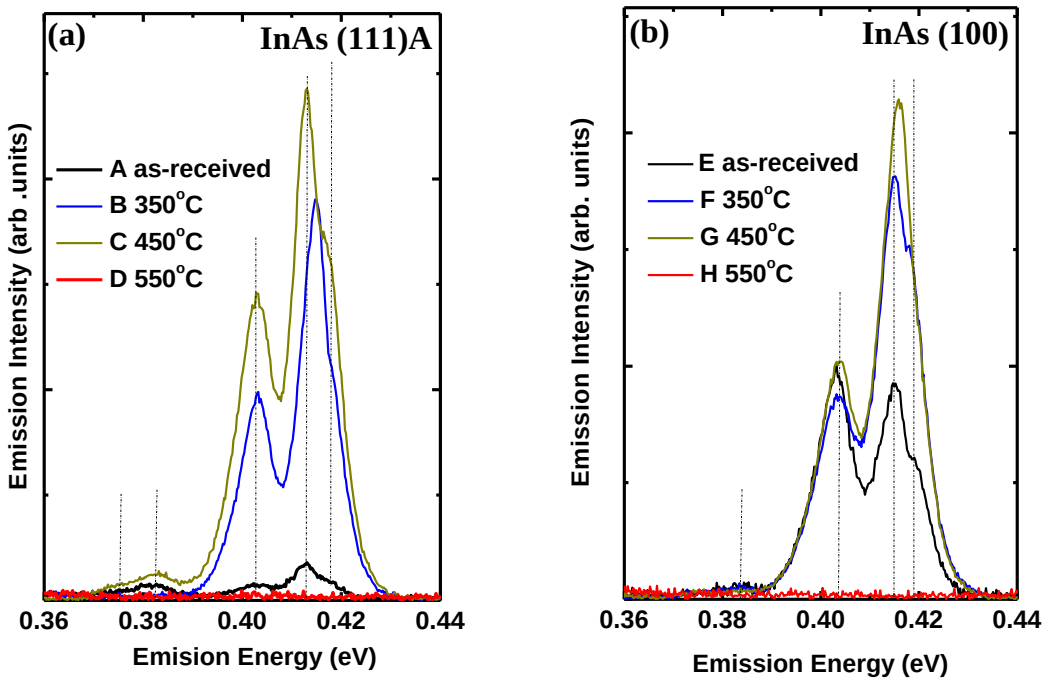


**Figure 7.2:**The PL spectra for as-received and annealed (a) InAs (111)A and b) InAs (100).

Figure 7.2(a) shows PL spectra for the as-received and annealed InAs (111)A, while Fig. 7.2(b) shows the PL spectra for the (100) samples. PL measurements were taken at 3.5 K using an excitation power of 3 mW. In all cases, the PL spectra contain the same five emission lines described earlier at 0.418 eV, 0.414 eV, 0.403 eV, 0.382 eV and 0.375 eV. It can be seen that annealing at 350°C and 450°C significantly increased the PL intensity for both surface orientations. The highest PL intensity (for both orientations) was observed for an annealing temperature of 450°C (C and G). No emission was observed for the samples annealed at 550 °C (D and H) due to surface degradation. The enhancement in PL intensity after annealing at 350°C and 450°C is ascribed to the formation of a well-ordered oxide layer. This result is in good agreement with Punkkinen*et al*. [64], who recently reported the formation of a well-ordered oxide on InAs at 400 °C.

## 7.3X-ray Photoelectron Spectroscopy

XPS measurements were performed to investigate the chemical composition of the near surface region before and after the thermal annealing treatments. Figure 7.3 shows narrow scan XPS spectra in the region of the In $3d_{3/2;5/2}$, As *3d*, and O*1s* core levels for as-received InAs (111)A (sample A), as-received InAs (100) (sample E), and samples annealed in oxygen at 450°C for 45 min (C and G). The measured data is represented by squares, and Gaussian and Lorentzian functions were employed to deconvolute the measured signals (solid lines). In each graph, the spectrum for the reference (as-received) surface appears at the top.

For the as-received samples, the peaks at 444.1 eV and 451.5 eV are ascribed to the In-As chemical bond, while the peaks at 445.0 eV and 452.4 eV correspond to $In_2O_3$. The As*3d* core level spectra for the reference samples indicate an In-As doublet at 40.5 eV and 41.2 eV and a broad signal between 44 eV and 46 eV, resulting from $As_2O_3$ and $As_2O_5$. Deconvolution of the O *1s* core level signals clearly show that it consists of three contributions, with binding energies observed at 530.3 eV, 531.4 eV and 531.8 eV, which are assigned to $In_2O_3$, $As_2O_3$ and $As_2O_5$, respectively.

In the samples that underwent thermal oxidation at 450°C for 45 min (C and G) the In-As related signal completely disappears for both surface orientations. A shift to higher energy by 0.55 eV was observed for the In $3d_{3/2;5/2}$ core level in $In_2O_3$ and by 0.55 eV for the As *3d* core level in arsenic oxide, while the O *1s* level blue-shifted by 1.1 eV. No evidence was detected for the presence of $As_2O_5$ after oxidation. The shifts in the In $3d_{3/2;5/2}$, As *3d* and O *1s* core level binding energies are ascribed to an increase in the number of adsorbed oxygen atoms, as seen in Table 7.1, where the amount of oxygen (atomic %) before and after thermal annealing is shown to increase after oxidation. Measured and reported binding energies, and possible chemical oxide components, from XPS core level data for thermally oxidised samples are presented in Table 7.2.

InAs (111)A

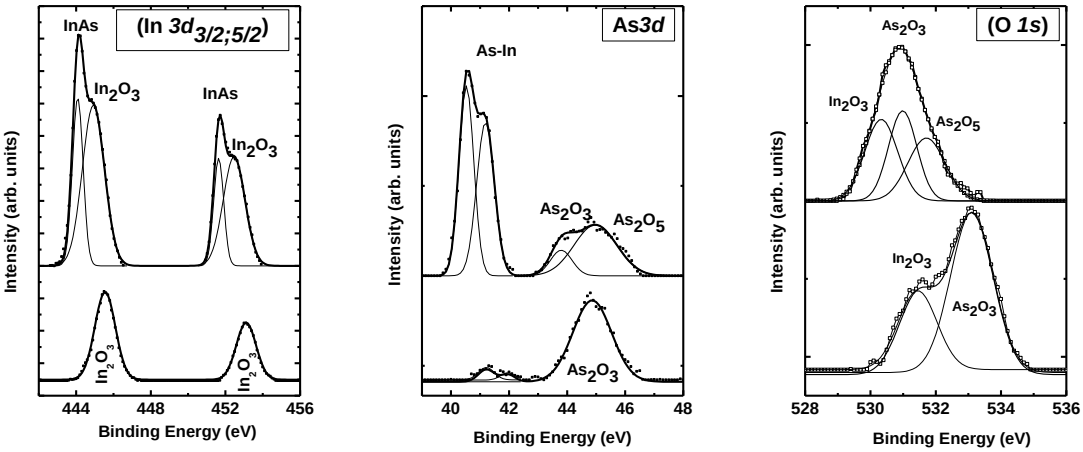


InAs (100)

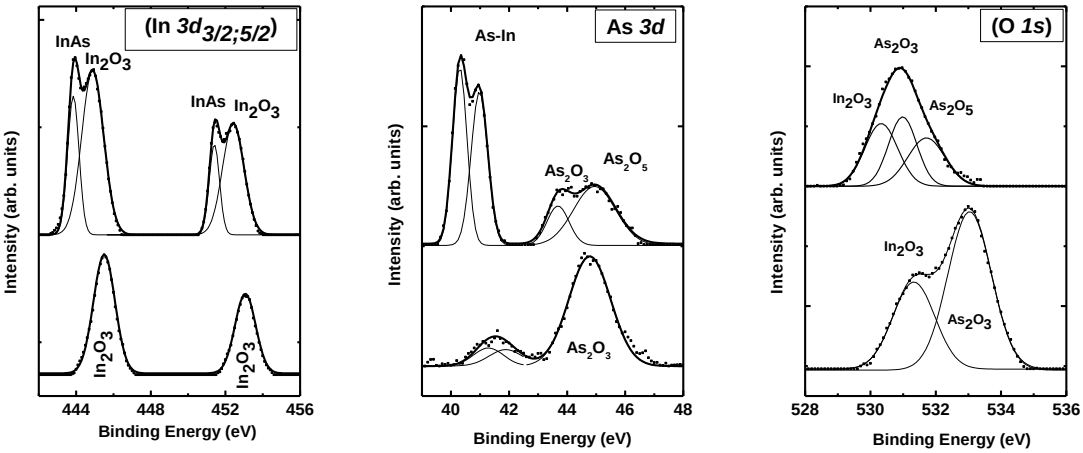


**Figure 7.3:** XPS spectra of InAs (111)A and (100) surfaces before and after thermal oxidation at 450°C, obtained from the In $3d_{3/2}$and In $3d_{5/2}$, As *3d* and O*1s* core levels. In all cases, the upper spectrum was measured from the as-received surface.

**Table 7-1:**Atomic concentration of oxygen, before and after annealing as obtained from XPS measurements.

| **Orientation** | **Oxygen concentration (Atomic %)** | |
|---|---|---|
| | **as-received** | **after thermal annealing** |
| InAs(111)A | 33 | 65 |
| InAs(100) | 38 | 68 |

**Table7-2:**Measured and reported binding energies, and possible chemical oxide components, from XPS core level data for thermally oxidised samples.

| | | Measured Binding Energy (eV) | Reported Binding Energy (eV) | Possible chemical oxide components |
|---|---|---|---|---|
| **In 3d** | $3d_{5/2}$ | 446.05 | 445.5 [59] | $In_2O_3$ |
| | $3d_{3/2}$ | 453.65 | | |
| | $3d_{5/2}$ | | 445.3 [59] | $InAsO_4$ |
| **As 3d** | $3d_{3/2}$ | 46.0 | 44.4 [95]; 45.2 [96]; 45.8 [97]; 46.0 [98] | $As_2O_3$ |
| | $3d_{3/2}$ | see Fig 7.3 | 46.4 [98]; 46.5 [51];46.6 [96] | $As_2O_5$ |
| | $3d_{3/2}$ | | 45.9 [60] | $InAsO_4$ |
| **O 1s** | O 1s | 531.9 | 530.2 [60] | $In_2O_3$ |
| | O 1s | 533.0 | 531.9 [60] | $As_2O_3$ |
| | O 1s | See Fig 7.3 | 532.4 [60] | $As_2O_5$ |
| | O 1s | | 531.2 [60] | $InAsO_4$ |

The interaction of oxygen with In and As was suggested by Schwartz *et al.*[91]:

$$3O_2 + 2InAs \rightarrow As_2O_3 + In_2O_3 \quad (0\text{-}1)$$

$$As_2O_3 + 2InAs \rightarrow In_2O_3 + 4As \quad (0\text{-}2)$$

**or**

$$4O_2 + 2InAs \rightarrow As_2O_5 + In_2O_3 \quad (0\text{-}3)$$

$$As_2O_3 + 2InAs \rightarrow In_2O_3 + 4As \quad (0\text{-}4)$$

**or**

$$2O_2 + InAs \rightarrow InAsO_4 \quad (0\text{-}5)$$

$$3InAsO_4 + 5InAs \rightarrow 4In_2O_3 + 8As \quad (0\text{-}6)$$

A schematic of the phase composition of the native oxide grown thermally on InAs, as suggested by these authors [91], is shown in Fig. 7.4. The different products resulting from the interaction of oxygen with In and As atoms was explained, and the nature of the produced oxide film was also described. Under conditions where no $As_2O_3$ and elemental arsenic diffuses from the film (i.e. no volatility losses), the film will be composed of $In_2O_3$, $As_2O_3$ or $InAsO_4$ (Fig. 7.4(a)). The film will consist only of $In_2O_3$ (Fig. 7.4(b)) in the case of total volatility losses of $As_2O_3$ and arsenic, whereas partial losses of both $As_2O_3$ and arsenic will result in $In_2O_3$, $In_2O_3$ and $As_2O_3$ or $In_2O_3$ and $InAsO_4$ as shown in Fig. 7.4(c) (*l, m* and *n* are the molar ratios).

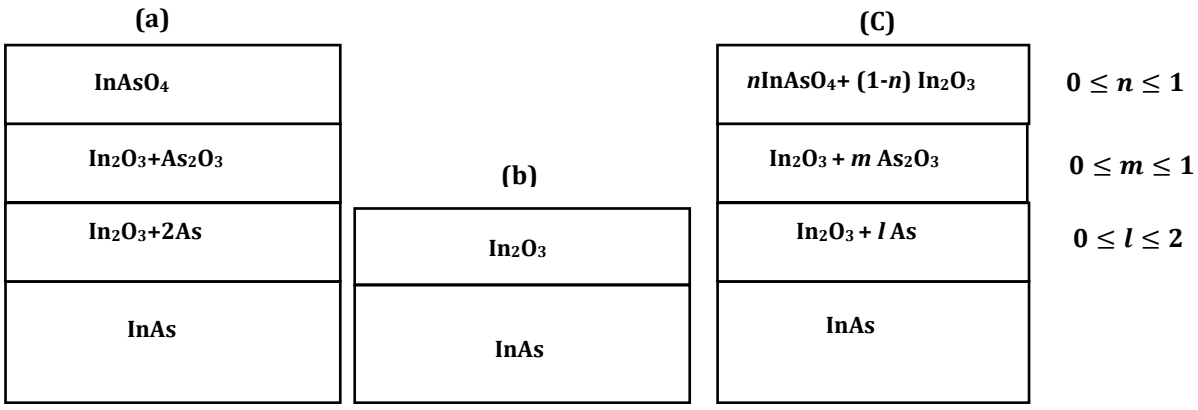


**Figure 7.4:** Phase composition of oxides on InAs under equilibrium growth conditions where (a) no volatility losses occur, (b) total volatility losses of $As_2O_3$ and arsenic occur and (c) partial losses of both $As_2O_3$ and arsenic occur [92].

In this thesis, the chemical reaction of oxygen with InAs at 450°C is suggested to follow the reaction path shown in equations (7-1) and (7-2), where either no or partial loss of $As_2O_3$ and elemental As occurs (compare Fig. 7.4 (a) and (c)). The resultant oxide films for both InAs (111)A and (100) are composed of $In_2O_3$ and $As_2O_3$, as seen in Fig. 7.3. Similar effects were reported previously for thermally oxidised III-V semiconductors [59, 93], particularly for InAs (100) [60] and (111)A surfaces [94]. The possible chemical oxide components of the thermally oxidised samples are listed in Table 7.2.

Figure 7.5 shows high resolution XPS spectra for samples C and G, annealed in oxygen at 450°C for 45 min. The spectra were obtained in the regions of the (a) In $3d_{3/2;5/2}$and (b) As *3d* core levels, before and after Ar-ion sputtering for different times. A 2 kV Ar-ion beam was used, giving a sputter rate of about 8.5 nm/min. It is observed that the oxide-related signal disappears after sputtering for a period of 7 min, indicating that the thickness of the $In_2O_3$ and $As_2O_3$ formed during the annealing treatment is ~ 70 nm. The recovery of the In-As signals (at ~41 eV, 444.1 eV and 451.5 eV) upon Ar-ion sputtering is obviously linked to the removal of the oxide layer formed during the annealing treatment. The apparent shift in the In 3*d* peaks is due to an increased contribution of the In-As signal to the overall peak with sputter time, i.e. the In-As signal increases while the In-O peak decreases as the oxide is removed from the surface. This is similarto what was observed for the As 3*d* signal, the only difference being that in the latter case the As-In and As-O signals are spectrally well-resolved.

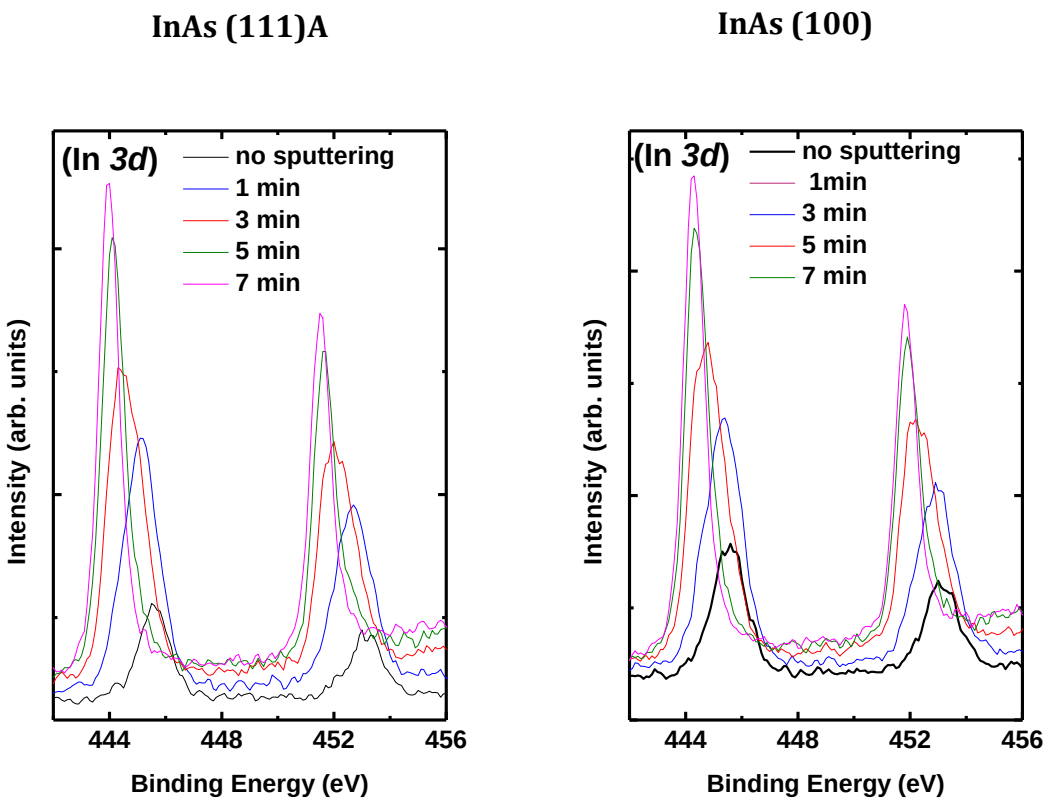

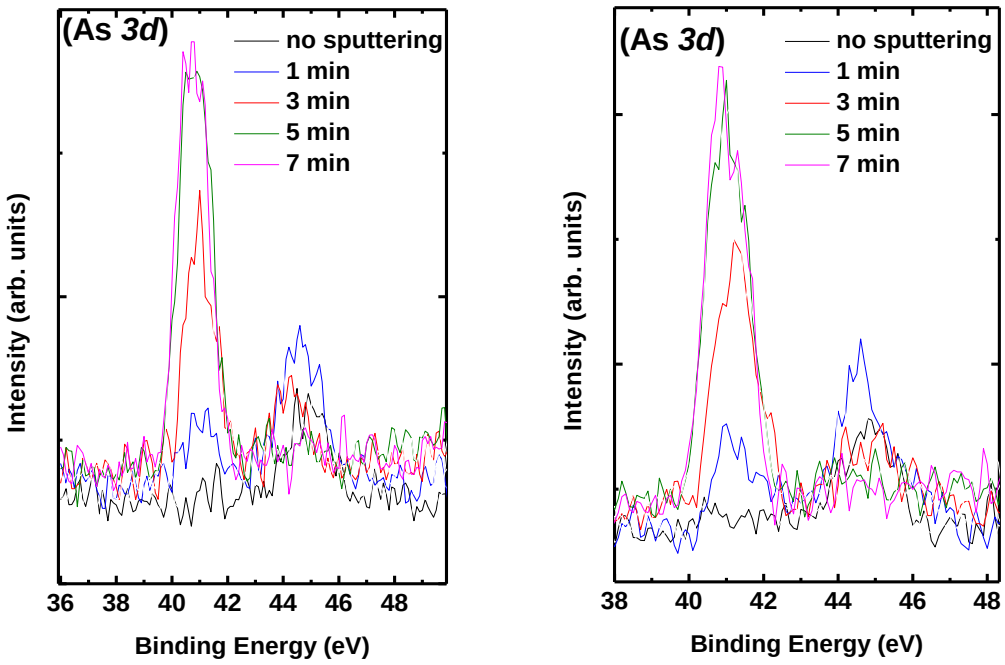


**Figure 7.5:** XPS spectra obtained from the In $3d_{3/2;\ 5/2}$ and As *3d* core levels for InAs (111)A (sample C) and InAs (100) (sample G) annealed at 450°C for 45 min as function of argon ion sputtering time.

## 7.4 Raman Spectroscopy

Figure 7.6 shows the Raman spectra obtained for the as-received InAs (111)A (sample A) and for the sample annealed at 450°Cfor 45 min (sample C). The spectra show two Raman modes: the low frequency TO phonon mode near 219 $cm^{-1}$and the unscreened LO phonon mode at ~ 239 $cm^{-1}$ [23]. It is clear that the intensity of the LO phonon signal decreases following the oxidation process. This reduction in the LO mode intensity indicates a decrease in the width of the accumulation layer.

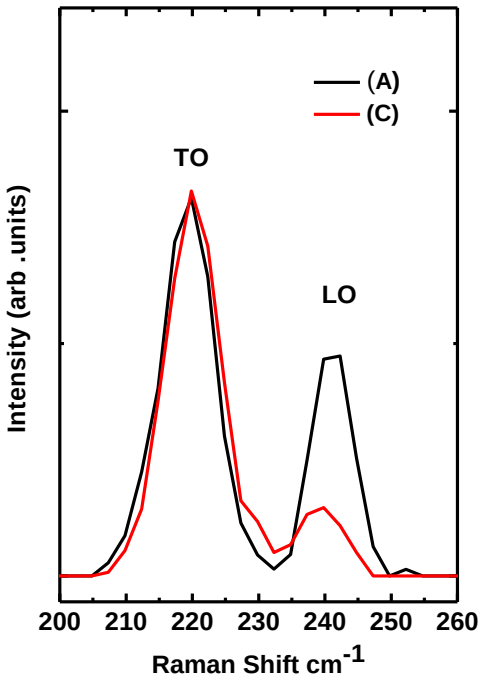


**Figure 7.6:** Raman spectra of InAs (111)A measured before and after thermal annealing at 450°Cfor 45 min.

In conclusion, thermally grown oxides were studied on both InAs (111)A and (100). Oxide "growth" took place when annealing in $O_2$at 350°C, 450°C and 550°C for 45 min. SEM images suggest that sample morphology improves with annealing temperature, with the best morphology obtained at a growth temperature of 450°C. At higher anneal temperatures, morphology deteriorated. The improved morphology (350°C and 450°C) was accompanied by a significant increase in PL intensity for both surface orientations. The highest PL intensity (both orientations) was observed for an annealing temperature of 450°C and is ascribed to the formation of a well-ordered oxide layer. The dramatic changes in the PL intensity at 550°C occurred as a result of the out-diffusion of elemental arsenic from the InAs surface. XPS suggests that the composition of the oxide film formed at 450°C is composed of a mixture of $In_2O_3$ and $As_2O_3$. The thickness of these oxides is suggested to be ~70 nm. The results presented in this chapter verify that the adsorption of oxygen onto both InAs (111)A and InAs(100) at 350°C and 450°C decreases the surface state density, as evidenced by an increase in the PL intensity and a reductionin the surface band bending.

# Chapter 8

## Laser Power and Temperature Dependent Photoluminescence of InAs (111)A

This chapter provides an overview of the optical transitions in bulk *n*-InAs (111)A. Variable laser power and temperature dependent PL measurements were used to identify some of the optical transitions and impurity-related emissions for chemically treated/oxidised samples.

### 8.1 Photoluminescence Spectroscopy

A considerable number of PL studies have been undertaken to try and understand the optical transitions in InAs. However, due to a lack of well-resolved PL spectra, the identification of the optical transitions and the activation energies of the related impurities/defects are not as well-established as for Si and other III-V compounds like GaAs and InP[99,101].

Band-to-band transitions have been observed in molecular beam epitaxy (MBE) grown InAsepilayers around 0.418 eV at 4.2 K [102]. Free exciton recombination is not commonly observed in InAsepilayers, and has never been observed in bulk InAs substrates. However,B-B transitionswere reported by Lacroix*et al.*[103] at around 0.415 eV (at 1.4 K) for InAs grown by metal organic chemical vapour deposition (MOCVD). The free exciton transition has also been reported by Tang *et al*. [104] for MBE grown InAs at around 0.417 eV (at 11 K). Two impurity-related transitions, a shallow and a deep donor bound exciton at 0.414 eV[104]and 0.403 eV [105], respectively, have been observed for MOCVD-grown ($n\sim5\times10^{15}cm^{-3}$) and MBE-grown($n\sim5\times10^{14}$ $cm^{-3}$) *n*-InAs. Note that the formation of excitons typically occurs for free electron concentrations below the Mott screening density ($\sim5\times10^{14}$ $cm^{-3}$) [14].Also, the effects of surface accumulation, defects and impurities often tend to dominate the emission spectra and prevent the formation of free excitons.

Figure 8.1 displays the dependence of the PL spectra on laser power for a sample etched for 1 min in 1% bromine-methanol. The PL spectra were obtained at 3.5 K with laser powers ranging from 3 mW to 12.3 mW.

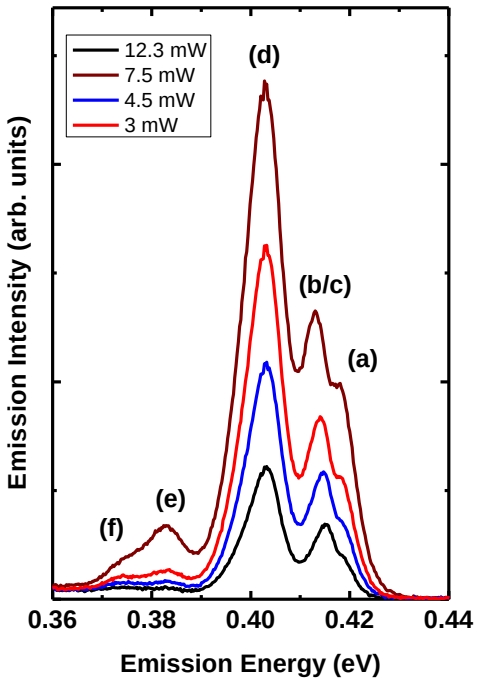


**Figure 8.1:** Laser power dependent photoluminescence spectra at 3.5 K for a sample etched for 1 min in 1% Br-methanol. The laser power ranged from 3 mW to 12.3 mW.

Figure 8.2 shows the temperature dependent PL spectra obtained using a laser power of 4.5 mW in the temperature range of (a) 3.5 K to 17 K and (b) 3.5 K to 38 K. The spectrain (c) were obtained with a laser power of 5 mW in the temperature range of 3.5 Kto 35 K. The PL spectra displayed in Fig. 8.2(a) and (b) were obtained from the same sample, while those in Fig. 8.2(c) were obtained from another sample treated similarly.

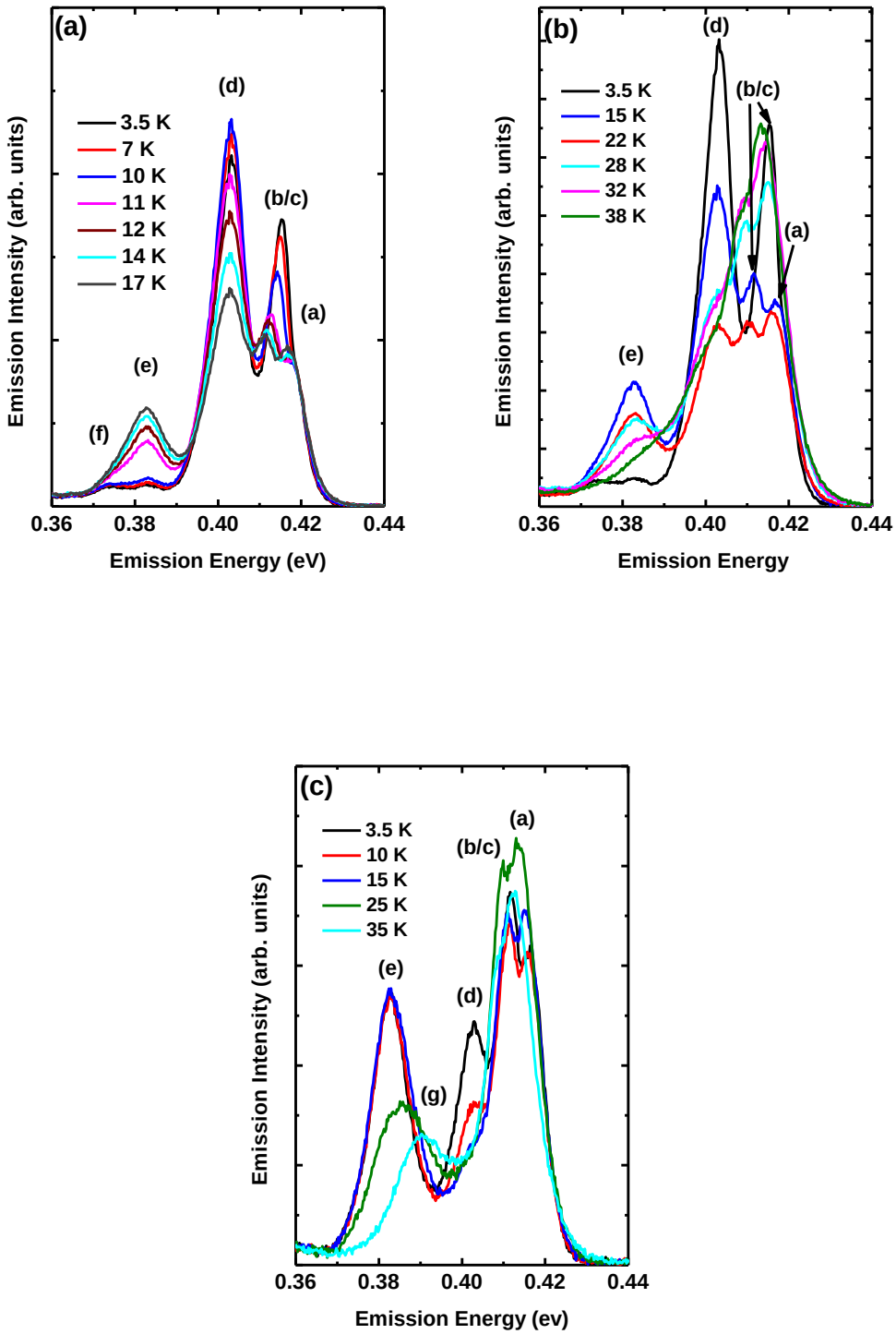


**Figure 8.2:** Temperature dependent PL spectra obtained with a laser power of 4.5 mW in the temperature range of (a) 3.5 K to 17 K and (b) 3.5K to 38 K. The spectra in (c) were obtained for a sample treated similarly to the one studied in (a) and (b), but using a laser power of 5 mW.

Several emission lines can be seen in the PL spectra in Figs. 8.1 and 8.2. These are labelled (a) through (g).The emission lines behave differently with differing laser powers and temperatures, which indicates that various mechanisms are responsible for the emission. The nature of the optical transitions will be discussed presently. The observed redshift of the signal at ~0.415 eV with excitation increase is ascribed to the presence of two unresolved lines in the range 0.410 eV to 0.416 eV (hence the label *(b/c)*). This would also explain the slight variationin the emission peak position in this energy range for different samples (see e.g. Fig. 5.11, Fig. 6.6 and Fig.7.2).

***i) Excitonic transitions***

Excitation power dependent PL is often used for evaluating the origin of light emission in semiconductors. It has been established that the PL intensity ($I$) depends on the excitation power of the laser ($L$): $I \propto L^k$. It was also shown that $1 < k < 2$ for exciton-related transitions [106].

Several features can be observed from Fig. 8.1. The emission intensities for all emission lines shown in Fig. 8.1 increase with excitation intensity. For lines *(b/c)* and *(d)* the intensity increases approximately linearly with excitation power. A redshift of ~3 meV is observed for line *(b/c)* when the excitation intensity is increased. Tang *et al.*[26] used magneto-absorption spectra measured at 4.2 K to identify the binding energy of the free exciton on MBE-grown *n*-InAs ($n \sim 5\times10^{14}$ cm$^{-3}$) as 1.0 meV. Since the formation of free excitons is not expected for carrier concentrations of $\sim2\times10^{16}$ cm$^{-3}$ (which is the background electron concentration in our bulk material), it seems likely that lines *(b/c)* and *(d)* arise from excitons trapped on neutral or ionised impurities/defects. The redshift observed for line *(b/c)* is ascribed to the saturation of the higher energy transition, causing a systematic shift to lower energies as the lower energy transition in this range starts to dominate.

The recombination giving rise to lines*(b/c)* and *(d)*in Fig. 8.2(a) decreases rather quickly upon increasing the temperature from 3.5 K to 17 K. This is seen in Fig. 8.3, which shows the PL intensity of line *(d)* in an Arrhenius plot for this temperature range.

The data was fitted with the following equation, yielding an activation energy $E_T$for the thermally induced quenching of approximately 7 meV:

$$I(T) = \frac{I_0(T=0)}{1 + Cexp\left(-\frac{E_T}{kT}\right)} \qquad (0\text{-}1)$$

Here $I_o$is the intensity as $T$ approaches 0 K and $C$ is a temperature-independent constant related to the Fermi level [68].

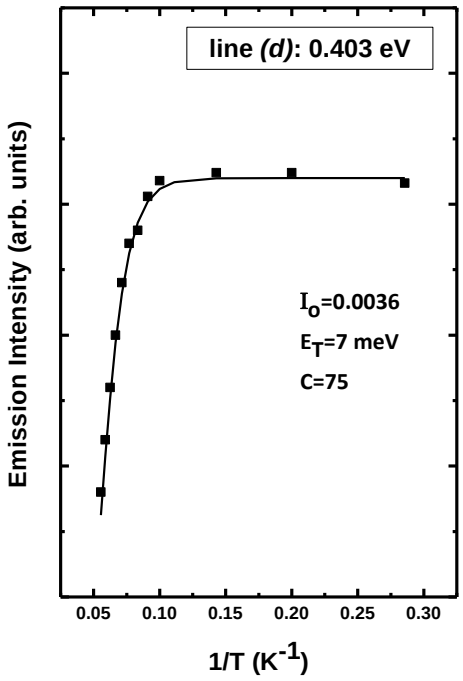


**Figure 8.3:** Measured temperature dependence (filled squares) of the intensity of line *(d)* (at 0.403 eV) and the simulated temperature dependence from equation (8-1) (solid line).

To determine the nature of a bound-exciton complex (i.e. whether an exciton is bound to a neutral or an ionised donor or acceptor), one has to compare the observed binding energy of the complex with the theoretical estimates for the four possible complexes.

The four cases and their binding energies are:

$$(D^o, X) = exciton\ bound\ to\ a\ neutral\ donor\ \approx E_X + 0.15E_d\ \sim 1.16\ meV \qquad (0\text{-}2)$$

$$(D^+, X) = exciton\ bound\ to\ a\ ionized\ donor\ \approx E_d + 1.1E_d \sim 2.22\ \text{meV} \qquad (0\text{-}3)$$

$$(A^o, X) = exciton\ bound\ to\ a\ neutral\ acceptor\ \approx E_X + 0.056E_a \sim 1.76\ \text{meV} \qquad (0\text{-}4)$$

$$(A^-, X) = exciton\ bound\ to\ a\ ionized\ acceptor\ \approx E_a + 2.1E_a \sim 53.1\ \text{meV} \qquad (0\text{-}5)$$

These values were estimated based on analogies between an exciton bound to a neutral donor and a hydrogen molecule. The estimated binding energies presented in equations (8-2) to (8-5) were obtained from the work of Scharma and Rodriguez [107], Skettrup*et al.* [108], Stebb and Munschy[109] and Scharma and Rodriguez [110]. From the effective mass argument, the donor ionisation energy $E_d$ is estimated by $(1+\sigma)Ex$ = 1.05 meV, and the acceptor ionisation energy $E_a = E_d/\sigma$= 21 meV, where $E_x$ is the free-exciton binding energy and $\sigma = m_e/m_h$ (=0.07 for InAs[24]). Based on the above binding energies, excitons bound to neutral and ionised hydrogenic donors and to neutral hydrogenic acceptors, will give rise to bound exciton luminescence in the range 0.410 eV– 0.416 eV.

Indeed, seven emission lines of excitons bound to neutral donors have been observed in the range 0.41523 eV to 0.41556 eV for MOCVD grown *n*-InAs with carrier concentrations of $\sim 5\times10^{14}$ cm$^{-3}$,while eight emission lines of excitons bound to neutral acceptors have been observed in the range 0.41316 eV to 0.41378 eV at 4.2 K [111]. This, together with the analysis in the preceding paragraph, suggests that the two unresolved transitions indicated as *(b/c)* in Fig. 8.1 and Fig. 8.2 may originate from excitons bound to shallow neutral/ionised donors or shallow neutral acceptors. However, the intensity of this emission was found to be strongly dependent on the oxygen and sulphur concentrations on the surface after chemical treatment, as will be discussed presently. It has also been pointed out that both oxygen and sulphur act as donors in InAs [8, 36], suggesting that these transitions might be due to excitons bound to oxygen and sulphur donors.

In principle, the dissociation energy of a bound exciton complex is defined as the energy required to remove an exciton from the complex. Experimentally, this dissociation energy ($D_0$) is commonly measured as the energy separation between the free-exciton peak and the bound exciton emission peak. Therefore, the expected dissociation energy for line *(d)* is estimated to be ~14 meV, which is significantly larger than the thermal activation energy of 7 meV obtained from the Arrhenius plot in Fig. 8.3.

Several dissociation paths are, however, available to ($D^+$, $X$) and ($D^o, X$)complexes [67]:

$$(D^+, X) \rightarrow D^o + h\,;\; D_0(D^o, h) \;\; = \; E_{XD^+} - E_d \; \sim 1.17\; meV \qquad (0\text{-}6)$$

$$(D^+, X) \rightarrow D^+ + X\,;\; D_0(D^+, X) = \; E_{XD^+} - E_X \; \sim 1.22\; meV \qquad (0\text{-}7)$$

$$(D^+, X) \rightarrow D^+ + e - h\,;\; D_0(D^+, e - h) = \; E_{XD^+} \; \sim 2.22\; meV \qquad (0\text{-}8)$$

$$(D^o, X) \rightarrow D^o + X\,;\; D_0(D^o, X) = \; E_{XD^o} - E_X \; \sim 0.16\; meV \qquad (0\text{-}9)$$

$$(D^o, X) \rightarrow (D^+ + X) + e\,;\; D_0(e) \qquad (0\text{-}10)$$
$$= E_X + D_0(D^o, X) - D_0(D^o, h) \; \sim \; 0 \; meV$$

$$(D^o, X) \rightarrow D^+ + e;\; D_0(Auger\; recombination) \sim ? \qquad (0\text{-}11)$$

These dissociation energies estimated for hydrogenic donor-bound exciton complexes are obviously significantly smaller than what is measured for line*(d)* (at 0.403 eV). However, using the relative dissociation energies for the various mechanisms as a guide, it is clear that there is one mechanism for each of the two types of complexes which yields a dissociation energy that is smaller than what would be expected for the dissociation of the complex into the donor (ionised or neutral) and a free exciton. These two dissociation paths are given in equations (8-6) and (8-10). The former involves the liberation of a hole from the ($D^+, X$) complex, while the latter involves the liberation of an electron from the ($D^o, X$) complex. It is worth noting at this point that the decrease in intensity of line *(d)* with increasingtemperature is accompanied by an increase in intensity of emission line *(e)* (identified as donor-acceptor pair (DAP) recombination

below). This is most clearly illustrated in Fig. 8.2(a). Since an acceptor is expected to be ionised in *n*-type material (in thermal equilibrium at least), any mechanism that supplies additional free holes will increase the probability of finding neutral acceptors, and hence enhance DAP emission as observed in Fig. 8.2(a). It is thus suggested that the bound exciton complex giving rise to line *(d)* is a $(D^+, X)$ complex and that the dissociation path responsible for its thermal quenching (Fig. 8.3) involves the liberation of a free hole as shown in equation (8-6).

The transition at 0.403 eV was observed for the first time by Fang *et al*. [104] and later also by Tang *et al*. [103]. Both groups assigned this line to an exciton bound to a deep donor. The peak around 0.373 eV (only visible at low temperatures) is ascribed to an LO phonon replica of the line at 0.403 eV (the unscreened LO phonon has an energy of 30.05 meV [111]).

***ii) Band-to-band transitions***

Line *(a)* at ~0.4185 eV in Fig. 8.1 and Fig. 8.2 starts as a shoulder on the high energy side of the spectra (at the lowest laser power and temperature), grows significantly with increasing excitation power and shifts towards lower energy as the temperature increases from 3.5 K to 38 K. The shape of the peak (at higher temperatures) shows clear characteristics of band-to-band transitions (B-B), where the intensity rises sharply and then drops off with a Boltzmann tail at higher energies [68].

***iii) Donor-Acceptor Pair Transitions***

The peak observed at 0.383 eV, line *(e),* has the characteristics of donor-acceptor pair (DAP) recombination [68]. The emission line undergoes a blue shift as the temperature is raised from 3.5 K to 38 K (see Fig. 8.2(b)). The energy shift is ascribed to the ionisation of the shallow level (presumably the donor) upon an increase in temperature, which enhances the probability of the free-to-bound recombination process *(g)* at 0.390 eV. This transition from DAP to free-to-bound is illustrated most clearly in Fig. 8.2(c). The binding energy for this acceptor giving rise to lines *(e)* and *(g)* is

estimated to be 28 meV. This is obtained from the peak position measured at 30 K and the band gap value at this temperature of 0.418 eV from equation (4-7).

## 8.2 Identification of Donors

A combination of PL and the atomic concentration of elements obtained from XPS measurements before and after the various treatments were used to identify the chemical nature of the impurities giving rise to bound exciton recombination in InAs (111)A. This was done by observing the changes in surface coverage resulting from various treatments and the corresponding changes in relative intensities of the transitions.

Figure 8.4 compares the PL spectra of an as-received sample and samples treated in either 1% Br bromine-methanol (a), $(NH_4)_2S$ + S or $[(NH_4)_2S$ / $(NH_4)_2SO_4]$ + S solutions (b), or annealed in oxygen (c).These spectra were all obtained at 3.5 K using an excitation power of 3 mW. Although the relative intensities of the various lines vary from sample to sample, the spectra display the same emission lines identified earlier and summarized in Table 8.1.

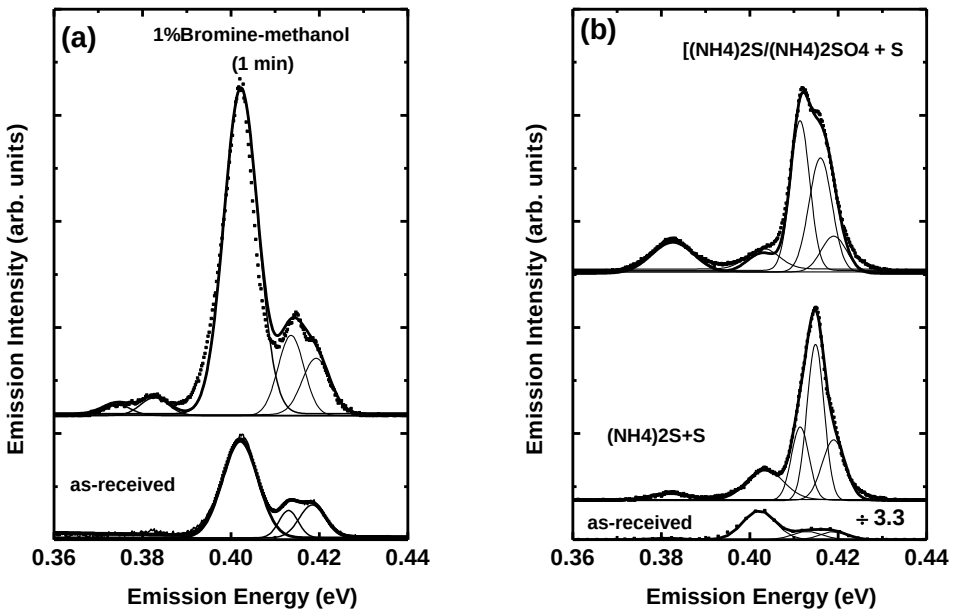

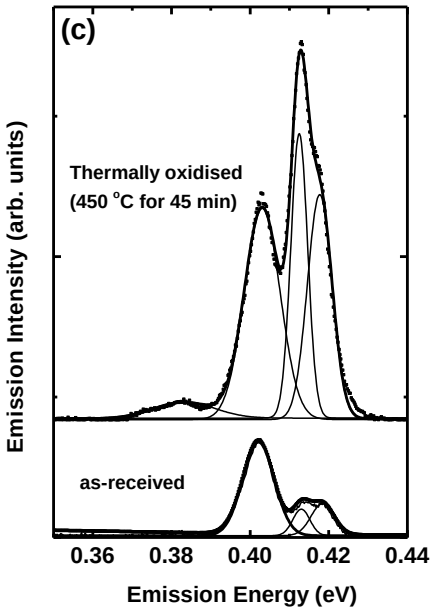


**Figure 8.4:** PL spectra at 3.5 K (laser power of 3mW) of the as-received sample and samples (a) etched in 1% Br-methanol for 1 min, (b) treated in $(NH_4)_2S$ + S or $[(NH_4)_2S/(NH_4)_2SO_4]$+ S solutions for 25 min and (c) annealed in $O_2$ at 450°C for 45 min.

**Table 8-1:** Photoluminescence peak (obtained at 3.5 K) and its assigned transition.

| **Peak Position (eV)** | **Transition Assignment** |
|---|---|
| 0.1485 | Band-to-Band (B-B) |
| 0.410 to 0.416 | Excitons bound to shallow donors $(D^{o/+}, X)$ |
| 0.403 | Excitons bound to deep donor $(D^{+}, X)$ |
| 0.383 | DAP |
| 0.390 | (e, $A^o$) |
| 0.373 | LO Phonon replica of transition at 0.403 eV |

Table 8.2 summarises the surface coverage and changes in PL transition intensities for the as-received surface relative to the treated/oxidised surfaces, which resulted from a chemical treatment or oxidation. Table 8.3 shows the atomic concentrations of elements before and after chemical treatment/oxidation. It can be seen from Table 8.2 that etching in 1% bromine-methanol for 1 min results in the removal of ~400 nm of InAs material. The native oxide is removed and the overall PL intensity increases by a factor of ~3 (Fig. 8.4 (a)). No significant changes in the relative intensities of lines (*a*), *(b/c),* or *(d)*are observed (Fig 8.4(a)). For samples treated in solutions of $(NH_4)_2S$ + S or [$(NH_4)_2S$ / $(NH_4)_2SO_4$] + S, it can be seen that, besides the enhancement in the PL intensity (Fig 8.4 (b)), the amount of oxygen detected is reduced (Table 8.3) and a sulphide layer is left on the surface (Table 8.2). In both cases the ($D^o$, *X*) transitions are more prominent than the ($D^+$, *X*) emission after treatment.

**Table 8-2:** Surface coverage (from XPS) and changes in the PL transition intensities for the treated/oxidised surfaces (denoted by *I*) relative to the corresponding transition in the as-received sample (denoted by $I_0$) from Fig. 8.4. The thickness of any residual layer after treatment was obtained by successive argon ion sputtering and either XPS or AES measurements.

| Treatment | Surface Coverage | Thickness (nm) | $\frac{I(a)}{I_0\,(a)}$ | $\frac{I(b/c)}{I_0(b/c)}$ | $\frac{I(d)}{I_0(d)}$ | $\frac{I(e)}{I_0(e)}$ |
|---|---|---|---|---|---|---|
| as-received | native oxide ($In_2O_3$,$As_2O_3$, $As_2O_5$) | ≥ 10 | | | | |
| 1% bromine –methanol (1 min) | Etched | ~ 400 | ~ 1.7 | ~ 2.8 | ~ 3.2 | ~ 2.7 |
| $(NH_4)_2S$ + S (25 min) | In-S | ≥ 15 | ~ 1.5 | ~ 6.1 | ~ 0.23 | ~ 1.3 |
| [$(NH_4)_2S$ / $(NH_4)_2SO_4$] + S (25 min) | In-S | ≥ 10 | ~ 1.1 | ~ 4.6 | ~ 0.23 | ~ 4 |
| Thermal oxidation (450°C for 45 min) | $In_2O_3$ and $A_2O_3$ | ≥ 70 | ~ 6.7 | ~ 10 | ~ 2.1 | ~ 2.3 |

**Table 8-3:** XPS atomic concentration of elements present on the surface before and after chemical treatment/oxidation.

| Treatment | Element Concentration (Atomic %) | | | | |
|---|---|---|---|---|---|
| | **O *1s*** | **C *1s*** | **In *3d*** | **As *3d*** | **S *2p*** |
| as-received | 34 | 32 | 24 | 10 | 0 |
| 1% bromine-methanol (1 min) | 10 | <1 | 65 | 23 | 0 |
| $(NH_4)_2S$ + S (25 min) | 11 | 11 | 49 | 15 | 24 |
| $[(NH_4)_2S$ / $(NH_4)_2SO_4]$ + S (25 min) | 5 | 10 | 58 | 20 | 17 |
| Thermal oxidation (450 for 45 min) | 77 | 8 | 9 | 6 | 0 |

The PL response of the sample annealed in oxygen at 450°C for 45 min is shown in Fig. 8.5(c). Thermal oxidation results in the formation of ~70 nm of $In_2O_3$ and $As_2O_3$ (Table 8.2). A considerable increase in PL intensity is observed after annealing, the effect being more pronounced for the ($D^o$, $X$) (line (*b/c*) and B-B (line (*a*)) transitions. For all treated samples, the DAP emission is enhanced as compared with the as-received sample.

The overall increase in PL intensity after treatment is ascribed to a reduction in band bending near the surface, as explained in previous chapters. The observation that treatment in a sulphur-containing solution or an oxygen environment enhances the relative intensity of lines (*b/*c) suggests that these lines are indeed related to sulphur and oxygen on the surface. It appears that the lower energy line is favoured when oxygen is present, either as part of the solution or in the annealing environment, while the higher energy line is favoured when only sulphur is present in the solution. Thus, it is tempting to conclude that the lower energy donor bound exciton in the range between 0.410 eV and 0.416 eV is due to trace amounts of atomic oxygen, while the higher energy line in this energy range is due to sulphur. It is not possible to conclude whether the donors binding the excitons in these cases are neutral or ionised. However, any residual band bending/electron accumulation near the surface will ensure that these donors remain neutral, which leads to the speculation that the two lines are shallow neutral donor bound excitons.

In conclusion, the overall increase in PL intensity after treatment/oxidation is ascribed to a reduction in band bending near the surface. This allows several well-defined peaks never observed for bulk InAs with a carrier concentration $n \sim 2 \times 10^{16}$ $cm^{-3}$ to be studied. A combination of PL and XPS measurements before and after the various treatments is used to identify some of the chemical nature of the impurities giving rise to bound exciton recombination in InAs (111). Band–to-band transitions have been observed at 0.4185 eV. In addition, two shallow neutral donor bound excitons have been observed in the range between 0.410 eV and 0.416 eV, and are due to trace amounts of atomic oxygen (at 0.412 eV), while the higher energy line in this energy range is due to sulphur (at 0.414 eV). Anexciton bound to deep ionised donor transitionswas observed at 0.403 eV and a free-to-bound transition (e, $A^o$) at 0.390 eV. Donor–acceptor pair (DAP) emission was observed at 0.382 eV and an LO phonon replica of the transition wasidentified at 0.373 eV.

# Chapter 9

## Summary of Results

In this thesis, the role of surface chemistry duringthe treatment of bulk InAs (111)A and (100) in sulphide and halogen-based solutions, and during thermal oxidation treatments, on surface modification was investigated. The changes observed in the optical properties and electronic structure resulting from the adsorption of sulphur, chlorine, bromine and oxygen are summarised below.

Treatment with ([$(NH_4)_2S$ / $(NH4)_2SO_4$] + S) resulted in significantly better surfacesthan other treatment procedures on the surface morphology of the as-received (111)AInAs surface. From AES depth profiles, the native oxide was estimated to be less than 8.5 nm thick, as a sputter rate of 8.5 nm/min resulted in its complete removal from the surface. Treatment of the material in all the chalcogen-based solutions employed in this study resulted in partial ($Na_2S.9H_2O$) or complete removal ([$(NH_4)_2S$] + S) and ([$(NH_4)_2S$ /$(NH4)_2SO_4$] + S) of the indium oxide from the surface with minimal surface degradation. Regarding the latter two treatments, an In-S layer “replaced” the In-O instead, suggesting that chemisorbed S atoms substituted O (in In-O) to form a thin In-S layer. Oxide removal seems to be most effective for samples treated with ([$(NH_4)_2S$ / $(NH_4)_2SO_4$] + S). Finally, the treated surfaces, assessed over a period of ten days, show poor short-term stability, with the lowest re-oxidation rate observed for ([$(NH_4)_2S$ / $(NH4)_2SO_4$] + S). The observed enhanced removal of the native oxide ($In_2O_3$) in the case of samples treated with ([$(NH_4)_2S$] +S) and ([$(NH_4)_2S$ / $(NH4)_2SO_4$] + S), is attributed to the availability of $H_3O^+$ through a hydrolysis reaction, while the efficient removal of As-O is accounted for by its higher solubility in the ([$(NH_4)_2S$ / $(NH4)_2SO_4$] + S) solution. From Raman scattering it could be deduced that these chemical changes on the surface result in a reduction in band bending near the surface. The improvement in both the electronic properties and the enhancement of the PL intensity after treatment correlates with the surface de-oxidation.

Chlorine and bromine solutions show anisotropic etching of InAs (111)A surfaces. Raman scattering showed a significant reduction in band bending after etching in 1:1 and 2:1 HCl:$H_2O$ (1 min) or 1% and 3% Br-methanol (10 min). These concentrations and etch times also yielded relatively smooth and defect-free surfaces. On the other hand, longer exposure and higher etchant concentrations increased the band bending, also leading to strong anisotropic etching effects, which resulted in irregular surfaces with faceted pits.

The photoluminescence spectra of *n*-type InAs (111)A etched in a 1% Br-methanol and HCl:$H_2O$ solution were also studied. The removal of the native oxide from the InAs surface, as observed by XPS, resulted in a significant reduction in charge accumulation on the surface. This was accompanied by a significant enhancement in the PL intensity after a 1 min etch, and by a slight reduction in intensity for longer etch times or etchant concentrations. The enhancement was correlated with the removal of native oxides from the surface for short etch times, while for longer etch times bromine/chlorine adsorption probably leads to the formation of additional surface states, consequently quenching the photoluminescence. The results obtained support the notion that native oxide-induced surface states are responsible for the charge accumulation on the InAs (111)A surface.

Thermally grown oxides were studied on both InAs (111)A and (100). Oxide "growth" was conducted when annealing at 350°C, 450°C and 550°C in $O_2$ for 45 min. SEM images suggest that the sample morphology improves with annealing temperature, with the best morphology obtained at an annealing temperature of 450°C, whereafter it deteriorated. The improved morphology (350°C and 450°C) was accompanied by a significant increase in the PL intensity for both surface orientations. The highest PL intensity (both orientations) was observed for an annealing temperature of 450°C and is ascribed to the formation of a well-ordered oxide layer. The dramatic deterioration in the PL intensity for the sample annealed at 550°C resulted from the out-diffusion of elemental arsenic from the InAs surface. XPS suggested that the oxide film formed at 450°C is composed of a mixture of $In_2O_3$ and $As_2O_3$. The thickness of the oxide film was ~70 nm. The results verified that the adsorption of oxygen onto both InAs (111)A and

InAs(100) at 350°C and 450°C decreases the surface state density, as evidenced by an increase in the PL intensity due to a reduction in the surface band bending.

The results presented in this thesis established a correlation between the degree of band bending and the surface oxygen concentration, with the largest band bending observed for the as-received sample (which also typically had the largest oxygen surface coverage). It was also observed that the native oxide which results from exposure to air causes an accumulation of excess charge on the surface, and increases the depth of the accumulation region. Oxides grown thermally in the temperature range 350°C to 450°C resulted in a significant increase in the PL intensity and a reduction in the band bending. This was ascribed to the formation of a well-ordered oxide layer. It may be concluded that the effect of adsorbed oxygen on the InAs surface depends strongly on the nature of the oxide. Reportedly, native oxides are amorphous, which explains the poor luminescence and electronic properties of as-received surfaces as compared to those exhibited by thermally oxidised surfaces.

Surface treatment/oxidisation was shown to significantly enhance the overall photoluminescence intensity relative to that of as received samples, due to a reduction in the surface state density upon de-oxidation or due to the formation of a well-ordered oxide layer on the surface in some cases. The overall increase in PL intensity after treatment was ascribed to a reduction in band bending near the surface. Several well-defined peaks (of which the origin is unknown), not previously observed for bulk InAs with a carrier concentration $n \sim 2\times10^{16}$ $cm^{-3}$, were detected andcan now be further pursued. A combination of PL and XPS measurements before and after the various treatments was used to identify the chemical nature of some of the impurities giving rise to bound exciton recombination in InAs (111).

A transition at 0.4185 eV has been identified as band-to-band recombination. Two shallow neutral donor bound excitons were observed in the range between 0.410 eV and 0.416 eV and were ascribed to trace amounts of atomic oxygen (at 0.412 eV) and sulphur (at0.414 eV). An exciton bound to a deep ionised donor gave rise to a PL line at 0.403 eV, while a free-to-bound transition (e, $A^o$) was observed at 0.390 eV and a donor-acceptor pair (DAP) emission at 0.382 eV.

*Recommendations for future work*

Concerns regarding the stability of the surface modifications on InAsremain. While ([$(NH_4)_2S$ / $(NH4)_2SO_4$] + S) seems to be a promising sulphide solution for InAs, the stability of the "passivation" effect requires further study.

In this work, the relative changes in intensity of different Raman modes were used to qualitatively evaluate the surface electronic properties (bend bending and accumulation layer thickness) of bulk InAs with a carrier concentration $n \sim 2 \times 10^{16}$ $cm^{-3}$. It would be useful to study samples with different carrier concentrations in order to quantify the thicknesses of the accumulation layers.

## Bibliography


[1] B.R. Bennet, R. Mango, J.B. Boss, W. Kruppa and M.G. Ancona, Solid State Electronics 49 (2005) 1875

[2] N. Li, E.S. Harmon, J. Hyland, D.B. Salzman, T.P. Ma, Y. Xuan, and P.D. Ye, Appl. Phys. Lett. 92 (2008) 143507

[3] B.R. Bennett, B.P. Tinkham, J.B. Boos, M.D. Lange and R. Tsai, J. Vac. Sci. Technol. 22 (2004) 688

[4] A. Kroemer, Physica E 20 (2004) 196

[5] M. Akazawa and H. Hasegawa, J. Cryst. Growth 301-302 (2007) 951

[6] A. Milnes, Materials Science and Engineering B 18 (1993) 237

[7] D.C. Tsui, Phys. Rev. B 4 (1971) 4438

[8] K. Smith, L. Koenders and W. Monch, J. Vac. Sci. Technol. B 7 (1989) 888

[9] J. Geurts, Surf. Sci. Reports 18 (1993) 1

[10] J.R. Weber, A. Janotti, and C.G. Van de Walle, Appl. Phys. Lett. 97 (2010) 192106

[11] R.J. Elliott, Phys. Rev. B 108 (1957) 1384

[12] F. Fuchs, K. Kheng, P. Koidl and K. Schwarz, Phys. Rev. B 48 (1993) 7884

[13] J.F. Fan, H. Oigawa and Y. Nannichi, Jpn. J. Appl. Phys. 27 (1988) L2125

[14] P.D. Wang, S.N. Holmes, Tan Le, R.A. Stradling, I.T. Ferguson and A.G. de Oliveira,Semicond. Sci.Technol. 7 (1992) 767

[15] T.H. Chiu and J.A. Ditzenberger, Appl. Phys. Lett. 56 (1990) 2219

[16] R.D. Grober, H.D. Drew, J.I. Chyi, S. Kalem and H. Morkoç, J. Appl. Phys. 65 (1989) 4079

[17] C. Kittel, Introduction to Solid State Physics(John Wiley & Sons) 1986

[18] B.Van Zeghbroeck, Principlesof Semiconductor Devices,http://ece-www.colorado.edu/~bart/book/, 2007

[19] O. Madelung, Semiconductor:Data Handbook (Springer, Berlin, 1996) 256

[20] M. Cardona, Phys. Rev. 121 (1961) 752

[21] J.R. Chelikowsky and M.L. Cohen, Phys. Rev. B 14 (1976) 556

[22] S. Mokkapati and C. Jagadish, Materials Today 12 (2009) 22

[23] O. Madelung, Semiconductor:Data Handbook (Springer, Berlin, 1996) 148

[24] L.M. Kanskaya, S.I. Kokhanovskii, R.P. Seisyan, Al. L. Efros and V.A. Yukish, Sov. Phys. Semicond. 17 (1983) 449

[25] Y. Varshni, Physica 34 (1967) 149

[26] Z.M. Fang, K.Y. Ma, D.H. Jaw, R.M. Cohen and G.B. Stringfellow, J. Appl. Phys. 67 (1990) 7034

[27] P.J.P. Tang, M.J. Pullin and C.C. Phillips, Phys. Rev. B 55 (1997) 4376

[28] M.I. Guseva, N.V. Zotova, A.V. Koval and D. N. Nasledov, Sov. Phys. Semicond. 8 (1974) 34

[29] M.I. Guseva, N.V. Zotova, A.V. Koval and D.N. Nasledov, Sov. Phys. 8 (1975) 1323

[30] A.J. Bard, R. Memming and B. Miller, Pure Appl. Chem. 63 (1991) 569

[31] W. Monch, Semiconductor Surface and Interface, Third Edition (Springer-Verlag, Berlin, Heidelberg, New York, 2001) 33

[32] R.O. Jones, Phys. Rev. Lett. 20 (1968) 992

[33] W. Mönch, J. Vac. Sci. Technol. B 4 (1986)1085

[34] A. Krier, M. Yin, V. Smirnov, P. Batty, P.J. Carrington, V. Solovev, V. Sherstnev, Phys. Status Solidi A 205 (2008) 129

[35] Y. Watanabe and F. Maeda, Appl. Surf. Sci. 117-118 (1997) 735

[36] M.J. Lowe, T.D. Veal, A.P. Mowbray and C.F. McConville, Surf.Sci. 544 (2003) 320

[37] S.O. Kasap, Principles of Electronic Materials and Devices, Second Edition, (McGraw-Hill, 2002) 128

[38] S. Adachi, Physical properties of III-V semiconductor compounds (John Wiley & Sons, 1992) 8-11

[39] C.B. Duke, Advances in Solid State Physics 33 (1993) 1

[40] K.S. Leandersson, PhD Thesis , Royal Instiute of Technology, Stockholm, 2010

[41] V.L. Berkovits, N. Witkowski and Y. Borensztein, Phys.Rev.B 63 (2001) 121314

[42] M. Sugiyama, S. Maeyama and M. Oshima, Phys. Rev. B 50 (1994) 4905

[43] B. Murphy, P. Moriarty, L. Roberts, T. Cafolla, G. Hughes, L. Koenders and P. Bailey, Surf.Sci. 317 (1994) 73

[44] N. Eassa, D.M. Murape, J.H. Neethling, R. Betz, E. Coetsee, H.C. Swart, A. Venter and J.R. Botha, Surf. Sci. 605 (2011) 994

[45] C.J. Sandroff, R.N. Nottenburg, J-C. Bischoff and R. Bhat, Appl. Phys. Lett.51 (1987) 33

[46] D.Y. Petrovykh, M.J. Yang and L.J. Whitman, Surf. Sci. 523 (2003) 231

[47] M.J. Jeng, H.T. Wang, L.B. Chang and R.M. Lin, Jpn. J. Appl. Phys. 40 (2001) 562

[48] L.A. Farrow, C.J. Sandroff and M.C. Tamargo, Appl. Phys. Lett. 51 (1987) 1931

[49] V.N. Bessolov and M.V. Lebedev, Semiconductors 32 (1998) 1141

[50] V.N. Bessolov, M. Lebedev, A. Ivankov, W. Bauhofer and D.T. Zahn, Appl. Surf.

Sci. 133(1998) 17

[51] T. Ishikawa and H. Ikoma, Jpn. J. Appl. Phys. 31 (1992) 3981

[52] W.C. Simpson and J.A. Yarmoff, Annu. Rev. Phys. Chem. 47 (1996) 527

[53] P.R. Varekamp, M.C. Håkansson, J. Kanski, B.J. Kowalski, L.Ö. Olsson, L. Ilver, Z.Q. He, J.A. Yarmoff and U.O. Karlsson, Surf. Sci. 352-354 (1996) 387

[54] W.K. Wang, W.C. Simpson andJ.A. Yarmoff, Phys. Rev. Lett.81 (1998) 1465

[55] W.C. Simpson, D.K. Shuh and J.A. Yarmoff, J. Vac. Sci. Technol. B 14 (1996) 2909

[56] D. Troost, L. Koenders and W. Monsh, Appl. Surf. Sci . 55-66 (1993) 619

[57] D. Troost, L. Koenders, Y.L. Fan and W. Mönch, J. Vac. Sci. Technol. B 5 (2009) 1119

[58] N.Eassa, D.M. Murape, R. Betz, J.H. Neethling, A. Venter and J.R. Botha, Physica B 407 (2012) 1591

[59] M.J. Graham, S. Moisa, G.I. Sproule, X. Wu, D. Landheer, A.J. SpringThorpe, P. Barrios, S. Kleber and P. Schmuki, Corrosion Science 49 (2007) 31

[60] G. Hollinger, R. Skheyta-kabbani and M. Gendry, Phys. Rev. B 49 (1994) 11159

[61] G.P.Schwartz, G.J. Gualtieri, J.E. Griffiths, C.D. Thurmond and B. Schwartz, J. Electrochem. Soc:Solid State Science and Technology 127 (1980) 2488

[62] M. Hong, J. Kwo, A.R. Kortan, J.P. Mannaerts and A.M. Sergent, Science 283

(1999)1897

[63] M.J. Hale, S.I. Yi, J.Z. Sexton, A.C. Kummel and M. Passlack, J. Chem. Phys. 119 (2003) 6719

[64] M.P.J. Punkkinen, P. Laukkanen, J. Lång, M. Kuzmin, M. Tuominen, V. Tuominen, J. Dahl, M. Pessa, M. Guina, K. Kokko, J. Sadowski, B. Johansson, I. J. Väyrynen, and L. Vitos, Phys. Rev. B 83 (2011) 195329-1

[65] T. H. Gfroerer, Encyclopedia of Analytical Chemistry , R.A. Meyers (Ed.) Copyright Ó John Wiley & Sons Ltd p. 9209–9231

[66] P. Dean, Prog.Crystal Growth Charact. 5 (1982) 89

[67] H.B. Bebb and E.W. Williams, Photoluminescence I: Theory, Semiconductors and Semimetals8, ed. by R.K. Willardson and A.C. Beer (Academic Press, 1972) 181–320

[68] E.W. Williams and H.B. Bebb in:Semiconductors and Semimetals 8, ed. by R. K. Willardson and A. C. Beer (Academic Press, New York, 1972), 321

[69] R.P. Griffiths and A.J. Haseth, Anal. Bioanal. Chem. 391 (2008) 2379

[70] A. Michelson and E. Morley, American Journal of Science 34 (1987) 333

[71] D. Mashigo, Magister Scientiae, Nelson Mandela Metropolitian University, South Africa, 2009

[72] J.F. Moulder, W.F. Stickle, P.E. Sobol and K.D. Bomben, Handbook of X-ray Photoelectron Spectroscopy (370ULVAC-PHI, Inc, Enzo, Chigasaki, 1995)253

[73] R. Egerton, Physical principles of electron microscopy: An introduction to TEM, SEM, and AEM. (Springer, New York, 2005)

[74] Y. Fukuda, Y. Suzuki, N. Sanada, M. Shimomura and S. Masuda, Phys. Rev. B 56 (1997) 1084

[75] L.R. Bailey, T.D. Veal, C.E. Kendrick, S.M. Durbin and C.F. McConville, Appl. Phys. Lett. 95 (2009) 192111

[76] J.C. Ho, A.C. Ford, Y.L. Chueh, P.W. Leu, O. Ergen, K. Takei, G. Smith, P. Majhi and J. Bennett, Appl. Phys. Lett.95 (2009) 072108

[77] J.W.J. Slavin, U. Jarori, D. Zemlyanovc and A. Ivanisevic, J. Electron. Spectrosc. Relat. Phenom. 172 (2009) 47

[78] D.Y. Petrovykh, J.M. Sullivan and L.J. Whitman, Surf. Interface Anal.37 (2005) 989

[79] W. Richter, R. Zeyher and M. Cardona, Phys. Rev. B 18(1976) 4312

[80] L. Ferrari, M. Fodonipi, M. Righini and S. Selci, Surface Science 331-333 (1995) 447

[81] Y. Kanemitsu and S. Okamoto, Phys. Rev.B 56 (1997) 1696

[82] R.R. Chang, R. Iyer and D.L. Lile, J. Appl. Phys. 61 (1987) 1995

[83] K. Mettler,Appl. Phys. 12 (1977) 75

[84] L. McGhee, I. Nicol, R.D. Peacock, M.I. Robertson, P.R. Stevenson and J.M. Winfield, J. Mater. Chem. 24 (1997) 217

[85] Y. Tarui, Y. Komiya and Y. Harada, J. Electrochem. Soc. 118 (1971) 118

[86] P.R. Varekamp, M.C. Håkansson, J. Kanski, D.K. Shuh, M. Björkqvist, M. Gothelid, W.C. Simpson, U.O. Karlsson and J.A. Yarmoff, Phys. Rev.B. 54 (1996) 2101

[87] F. Stepniak, D. Rioux and J.H. Weaver, Phys. Rev. B 50 (1994) 1929

[88] C. Gu, Y, Chen, T.R. Ohno and J.H. Weaver, Phys. Rev. B 46 (1992) 10197

[89] W.H. Hung, J. Phys, Chem. B 102 (1998) 1141

[90] D.J. Evans and S. Ushioda, Phys. Rev. B 9 (1973) 1638

[91] G.P. Schwartz, W.A. Sunder, J.E. Griffiths and G.J. Gualtieri, Thin Solid Films 94 (1982) 205

[92] G.P.Schwartz, J.E. Griffiths and G.J. Gualtieri, Thin solid Films 94 (1982) 213

[93] G. Landgren, R. Ludeke, Y. Jugnet, F. Morar and F.J. Himpsel, J. Vac. Sci. Technol. B2 (1984) 351

[94] D.H. Laughlin and C.W. Wilmsen, Thin Solid Films 70 (1980) 325

[95] G. Leonhardt, A. Berndtsson, J. Hedman, M. Klasson, R. Nilsson and C. Nordling, Phys. Status Solidi B 60 (1973) 241

[96] L.D. Hulett and T.A.Carlson, Appl. Spectrosc. 25 (1971) 33

[97] A.W. Czanderna, Methods of surface analysis (Elsevier, Amsterdam, 1975) 119

[98] W.J. Stec, W.E. Morgan, R.G. Albridge and J.R. van Wazer, Inorg. Chem. 11 (1972) 219

[99] E. HAL Bogardus and H. Barry Bebb, Phys. Rev. 176 (1968) 993

[100] W.T.Masselink, Y.C. Chang and H. Morkoc, Phys. Rev. B 28 (1983) 7373

[101] L.Pavesi and F. Piazza, Phys. Rev.B 44 (1991) 9052

[102] R.D. Grober and H.D. Drew, J. Appl. Phys.65 (1989) 4079

[103] Y. Lacroix, S.P. Watkins, C.A. Tran and M.LThewalt, Appl. Phys. Lett.66 (1994) 1101

[104] P.J. Tang , C.C. Phillips and R.A. Stradling, Semicond. Sci. Technol.8 (1993) 2135

[105] Z.M.Fang, K.Y. Ma, D.H. Jaw, R.M. Cohen and G.B. Stringfellow, J. Appl. Phys. 67 (1990) 7034

[165] T. Schmidt, K. Lischka and W. Zulehner, Phys. Rev. B 45 (1992) 8989

[107] R.R. Scharma and S. Rodriguez, Phys. Rev.159 (1976) 649

[108] T. Skettrup, M. Suffcznsk and W. Gorzkowski, Phys. Rev.4 (1971) 512

[109] B. Stbeb and G. Munschy, Phys. Stat. Sol. 88 (1978) 713

[110] R.R. Scharma and S. Rodriguez, Phys. Rev. 153 (1967) 649

[111] Y. Lacroix, PhD Thesis, Simon Fraser University, Canada, 1996.